

# Investigation into the Effect of Relaxed Static Stability on a Business Jet's Preliminary Design

D. Decloedt

Faculty of Aerospace Engineering



# INVESTIGATION INTO THE EFFECT OF RELAXED STATIC STABILITY ON A BUSINESS JET'S PRELIMINARY DESIGN

by

**D. Decloedt**

in partial fulfilment of the requirements for the degree of

**Master of Science**  
in Aerospace Engineering

at Delft University of Technology,  
to be defended publicly on Monday August 29, 2016 at 13:00

Student number:	4048571
Thesis registration number	086#16#MT#FPP
Supervisor:	Dr. Ir. M. Voskuijl
Thesis committee:	Prof. Dr. Ir. L.M. Veldhuis Dr. Ir. S. Hartjes

An electronic version of this thesis is available at <http://repository.tudelft.nl/>.

---

**Cover Image:** B. Trevelyan, Business Jets and BoldIQ, (2013), <http://sextantreadings.com/business-jets-boldiq/>



# ACKNOWLEDGEMENTS

This report marks the conclusion of my student career at Delft University of Technology and therefore some words of gratitude are in place. First of all, I would like to thank my supervisor M. Voskuijl, whose office was always open for an interesting discussion and whose excellent guidance was key in completing this project. Furthermore I would like to extend my gratitude to professor L.M. Veldhuis for his valuable input as well as S. Hartjes, for being part of my exam committee.

Furthermore I cannot thank my parents and family enough for their unconditional support and keeping me motivated. Also, this word of gratitude would not be complete without thanking all those who were part of my student life and made into a unforgettable experience. I would like the specifically mention the fellow students of "Kamertje 1" and the volunteers at Lambach Aircraft.

Dries Decloedt  
Delft, August 2016



# SUMMARY

In order to face the challenges faced by the European aviation industry, the Cleansky initiative was launched in 2008 and one of the initiatives within the programme is an increased collaboration between aircraft manufacturers, research institutes and universities. One technology that is investigated within this framework is the effect of relaxed static stability on the preliminary design of business jet aircraft. RSS aircraft have a neutral point located closer to or even in front of the aircraft's centre of gravity. As a consequence, the required trim force is reduced and thus the tail size may be reduced as well. Due to the infamous snowball-effect, it is anticipated that RSS can lead to significant weight loss and fuel savings. On the downside however, it is expected that RSS requires complex stability augmentation systems and reduces the elevator effectiveness. In this research it is quantified how RSS affects the mass of key aircraft components, as well as how RSS influences the handling qualities, by investigating its effect on the inertia tensor and stability & control derivatives.

For this research a preliminary design tool called the Initiator has been used. This tool is developed at the FPP-department at Delft University of Technology and was initially set-up for large conventional commercial aircraft. As part of this research, the capabilities of the Initiator were extended such that the tool can also be used to analyse the preliminary design of business jet aircraft. First, the class 2 weight estimation was overhauled by implementing the methods of Torenbeek and General Dynamics. Furthermore, an iteration loop was implemented, such that the Initiator now produces a converged weight estimate for the given aircraft configuration. Moreover, a correction factor to account for the use of composites in modern aircraft was implemented. The weight estimates obtained with the new methods and those obtained with the already implemented Raymer's method were then compared to weight data. As such, it was shown that within the Initiator, Torenbeek's method provides the most accurate weight estimate for business and commercial aircraft with a mean error of 1% and a maximum error of 11%.

Secondly the method for estimating the stability and control derivatives was updated based on the approach described by J. Roskam and it was shown that this module does a reasonable well job at predicting the longitudinal stability derivatives as well as the control derivatives. For example, a mean error of 3% in  $C_{L\alpha}$  was obtained for business jet aircraft over a range of three conditions. The directional and lateral control derivatives however, were estimated with larger errors. The main reason this error is believed to be caused by the fact that the module was validated by separating it from the Initiator. As a consequence no accurate estimate for the centre of gravity's x and y-position is available, which highly affects those derivatives.

Furthermore, the inertia estimation was updated such that it would also account for the contributions of the payload and fuel. The updated module was validated for the Fokker 100 and it was observed that although the module estimates the inertia tensor for the fully loaded aircraft reasonably well with a mean error of 3% and a maximum error of 13%, it has the tendency to underestimate the tensor of the empty aircraft by a considerably larger margin. This error is compensated for the fully loaded aircraft due to an over-estimation of the cargo's contribution to the inertia tensor. Based on the validation of the aforementioned modules it was concluded that these could be used to estimate the extend of the effects of relaxed static stability on the preliminary aircraft design and its handling qualities.

To assess the effect of RSS on business jet aircraft, a baseline aircraft based on the requirements of the Cessna Citation II was created. By shifting the wing forward, thus decreasing the static margin, it was observed that a decrease of 5% of MTOM could be achieved. Furthermore it was observed that although the MTOM decreased, the weight of the fuselage actually increased by 7%. This is a consequence of shifting the wing forward, and thus increasing the tail arm, which results in a heavier fuselage. Furthermore as anticipated, it was observed that the increased tail arm resulted in a smaller horizontal (14%) and vertical tail (16%). The most noticeable effect on the stability derivatives, was the change in  $C_{m\alpha}$  from -0.518 for the reference aircraft to -0.036 and a steady decrease in the pitch rate derivatives. Finally, it was rather surprisingly observed that although the elevator's size decreases, the elevator control power is almost unaffected by RSS. This is caused by the fact that in the chosen approach to obtain RSS, the horizontal tail volume remains constant.



# NOMENCLATURE

## Roman Symbols

A	Aspect ratio	[-]
b	Span	[m]
c	Chord	[m]
$\bar{c}$	Mean chord	[m]
e	Oswald factor	[-]
g	Gravitational acceleration	[m/s <sup>2</sup> ]
h	Height	[m]
k	Correction factor	[-]
L	Fuselage length	[m]
l	Length	[m]
$l_h$	Horizontal tail arm	[m]
$l_v$	Vertical tail arm	[m]
L	Lift	[N]
M	Mach number	[-]
$M_H$	Maximum Mach number at sea-level	[-]
$n_{ult}$	Ultimate load factor	[-]
$N_{cr}$	Number of crew (cockpit and cabin)	[-]
$N_e$	Number of engines	[-]
$N_t$	Number of tanks	[-]
$P_2$	Inlet dynamic pressure	[N/m <sup>2</sup> ]
q	Dynamic pressure	[N/m <sup>2</sup> ]
$\bar{q}_D$	Average dynamic dive pressure	[N/m <sup>2</sup> ]
R	Range	[km]
$\bar{R}_i$	Radius of gyration	[-]
S	Main Wing Area	[m <sup>2</sup> ]
$S_{fgs}$	Fuselage gross shell area [m <sup>2</sup> ]	
$S_{TO}$	Take-off distance	[m]
$t/c$	Thickness-to-chord ratio	[-]
T	Thrust	[N]
$U_1$	Free Stream Velocity	[m/s]
V	Airspeed	[m/s]
$V_D$	Dive speed	[m/s]
$V_{pax}$	Volume of the cabin used for passengers	[m <sup>3</sup> ]
w	Width	[m]
W	Weight	[N]
X	Wing quarter chord position on fuselage	[m]
$\bar{x}$	x-coordinate normalized w.r.t. MAC	[-]
$z_h$	z-distance from c.g. to horizontal tail	[m]

## Greek Symbols

$\alpha$	Angle of attack	[deg]
$\alpha_0$	Zero-lift angle of attack	[deg]
$\beta$	Sideslip angle	[deg]
$\beta$	Prandtl Glauert compressibility correction factor	[-]
$\epsilon$	Downwash angle	[deg]

$\eta$	Non-dimensional spanwise coordinate (y)	[-]
$\eta_c$	Ratio of canard to main wing dynamic pressure	[-]
$\eta_h$	Ratio of horizontal tail to main wing dynamic pressure	[-]
$\Delta f$	Flap deflection angle	[deg]
$\theta$	Pitch angle	[deg]
$\lambda$	Taper ratio	[-]
$\Lambda$	Sweep angle	[deg]
$\Lambda_{c/4}$	Quarter-chord sweep angle	[deg]
$\Lambda_{c/2}$	Mid-chord sweep angle	[deg]
$\xi$	Damping ratio	[-]
$\rho$	Air density	[kg/m <sup>3</sup> ]
$\omega_n$	Frequency	[Hz]

### Subscripts

ac	Aerodynamic centre
ai	Air induction system
api	Air-conditioning, pressurization, anti- & de-icing system
apu	Auxiliary Power Unit
$A-h$	Tailless aircraft contribution
c	Canard
cg	Centre of gravity
crew	Crew (cockpit and cabin)
e	Engines
ec	Engine controls
ess	Engine starting system
E	Empty
f	Fuselage
fc	Flight controls system
F	Fuel
feq	Fixed equipment
fur	Furnishing
h	Horizontal tail
hps	Hydraulic and pneumatic system
iae	Instrumentation, avionics & electronics
MZF	Zero Fuel Mass
np	Neutral point
ops	Operational items
ox	Oxygen system
p	Propulsion system
prop	Propeller
pt	Paint
pwr	Powerplant
PL	Payload
struct	Structure
tfo	Trapped fuel & oil
TO	Take-off
v	Vertical tail
w	Wing
wf	Wing fuselage combination
$\infty$	At infinity

## Stability & Control Derivatives

$C_{L1}$	Steady state lift coefficient	[-]
$C_{D1}$	Steady state drag coefficient	[-]
$C_{L\alpha}$	Lift-due-to-angle-of-attack derivative	[rad <sup>-1</sup> ]
$C_{D\alpha}$	Drag-due-to-angle-of-attack derivative	[rad <sup>-1</sup> ]
$C_{m\alpha}$	Pitching-moment-due-to-angle-of-attack derivative	[rad <sup>-1</sup> ]
$C_{y\beta}$	Sidelforce-due-to-sideslip derivative	[rad <sup>-1</sup> ]
$C_{l\beta}$	Rolling-moment-due-to-sideslip derivative	[rad <sup>-1</sup> ]
$C_{n\beta}$	Yawing-moment-due-to-sideslip derivative	[rad <sup>-1</sup> ]
$C_{yp}$	Sidelforce-due-to-roll-rate derivative	[rad <sup>-1</sup> ]
$C_{lp}$	Rolling-moment-due-to-roll-rate derivative	[rad <sup>-1</sup> ]
$C_{np}$	Yawing-moment-due-to-roll-rate derivative	[rad <sup>-1</sup> ]
$C_{Dq}$	Drag-due-to-pitch-rate derivative	[rad <sup>-1</sup> ]
$C_{Lq}$	Lift-due-to-pitch-rate derivative	[rad <sup>-1</sup> ]
$C_{mq}$	Pitching-moment-due-to-pitch-rate derivative	[rad <sup>-1</sup> ]
$C_{yr}$	Sidelforce-due-to-yaw-rate derivative	[rad <sup>-1</sup> ]
$C_{lr}$	Rolling-moment-due-to-yaw-rate derivative	[rad <sup>-1</sup> ]
$C_{nr}$	Yawing-moment-due-to-yaw-rate derivative	[rad <sup>-1</sup> ]
$C_{Le}$	Lift-due-to-elevator-deflection derivative	[rad <sup>-1</sup> ]
$C_{De}$	Drag-due-to-elevator-deflection derivative	[rad <sup>-1</sup> ]
$C_{me}$	Pitching-moment-due-to-elevator-deflection derivative	[rad <sup>-1</sup> ]
$C_{ya}$	Sidelforce-due-to-aileron-deflection derivative	[rad <sup>-1</sup> ]
$C_{la}$	Rolling-moment-due-to-aileron-deflection derivative	[rad <sup>-1</sup> ]
$C_{na}$	Yawing-moment-due-to-aileron-deflection derivative	[rad <sup>-1</sup> ]
$C_{yr}$	Sidelforce-due-to-rudder-deflection derivative	[rad <sup>-1</sup> ]
$C_{lr}$	Rolling-moment-due-to-rudder-deflection derivative	[rad <sup>-1</sup> ]
$C_{nr}$	Yawing-moment-due-to-rudder-deflection derivative	[rad <sup>-1</sup> ]



# LIST OF FIGURES

2.1	Moment equilibrium around the centre of gravity	4
2.2	Example of an X-plot	5
2.3	Comparison between the DC-10-30 (left) and the MD-11 (right)	6
2.4	Example of effect of the longitudinal wing position on the c.g. range	8
2.5	Example of the c.g. range graph overlayed with x-plot	9
2.6	The Initiator top level design process	12
3.1	Weight reduction factors for composite structures	16
3.2	Wing and Thrust Loading Diagram for the Cessna Citation II	17
3.3	Estimation of $C_{D1}$ from the Drag Polar	24
3.4	Example of cylindrical cross-section with distribution of lumped masses	29
3.5	Example of aerofoil cross-section with distribution of lumped masses	30
3.6	Chord-wise mass distribution of lifting surfaces	32
4.1	Flow Diagram for the Class 2 Weight Estimation Module	35
4.2	Flow Diagram for the component weight estimation	36
4.3	Flow Diagram for the Stability and Control Derivative Estimation Module	37
4.4	Flow Diagrams to estimate the angle-of-attack derivatives	38
4.5	Flow Diagram for the Inertia Estimation Module	39
4.6	Flow Diagram to estimate the passenger inertia	39
5.1	Validation of take-off constraint in Weight and Thrust Loading Diagram	41
5.2	Comparison of the original and the updated wing loading diagram for the Cessna Citation II	42
5.3	Comparison in geometry of the Cessna Citation II	43
5.4	Comparison in geometry of the Bombardier Learjet 45	44
5.5	Comparison in geometry of the Embraer Phenom 300	45
5.6	Comparison in geometry of the Gulfstream G650	46
5.7	Comparison in geometry of the Airbus A320-200	46
5.8	Comparison in geometry of the Fokker 100	47
5.9	Definition of Fuselage Stations	48
5.10	Inertia tensors calculated for the Fokker 100 (left) the Initiator Fokker 100 (right)	51
6.1	The Initiator-Citation	55
6.2	Overview of the design convergence for the Citation-Initiator	57
6.3	Definition of the wing shift	58
6.4	Change in wing, horizontal and vertical tail area as function of wing shift	59
6.5	Change in MTOM, EOM and fuel mass as function of wing shift	59
6.6	Change in lift-over-drag ratio as function of wing shift	60
6.7	Change in MTOM, EOM and fuel mass as function of wing shift	61
6.8	Comparison in geometry of Cessna Citation II with or without RSS	61
6.9	Comparison of the Inertia Tensors	63
B.1	Empennage rolling $K$ -factor	71
F.1	Flow Diagram for the Fokker Inertia tool	81
F.2	Overview of the aircraft-definition-file	82



# LIST OF TABLES

2.1	Comparison between the DC-10-30 and the MD-11 . . . . .	7
3.1	Overview of the calculated stability derivatives . . . . .	23
5.1	Comparison of the weight estimates for the Cessna Citation II . . . . .	44
5.2	Comparison of the weight estimates for the Bombardier Learjet 45 . . . . .	44
5.3	Comparison of the weight estimates for the Embraer Phenom 300 . . . . .	45
5.4	Comparison of the weight estimates for the Gulfstream G650 . . . . .	46
5.5	Comparison of the weight estimates for the Airbus A320-200 . . . . .	47
5.6	Comparison of the weight estimates for the Fokker 100 . . . . .	47
5.7	Conditions used for validating stability and control derivatives (Learjet 24) . . . . .	49
5.8	Conditions used for validating stability and control derivatives (Boeing 747-100) . . . . .	49
5.9	Validation of the Learjet 24's most important derivatives . . . . .	50
5.10	Validation of the Boeing 747-100's most important derivatives . . . . .	50
5.11	Comparison of the Fokker 100 and the Initiator-Fokker 100 most relevant parameters . . . . .	52
6.1	Comparison of the Citation and the Initiator-Citation's most relevant parameters . . . . .	56
6.2	Change in angle of attack derivatives versus wing shift . . . . .	62
6.3	Change in pitch rate derivatives versus wing shift . . . . .	62
6.4	Change in elevator control derivatives versus wing shift . . . . .	62
E.1	Overview of empty Fokker 100 Inertia tensor contributions for gear down and up . . . . .	81



# CONTENTS

<b>List of Figures</b>	<b>xi</b>
<b>List of Tables</b>	<b>xiii</b>
<b>1 Introduction</b>	<b>1</b>
<b>2 Background</b>	<b>3</b>
2.1 Tail Surfaces . . . . .	3
2.2 Longitudinal Stability and Control . . . . .	4
2.2.1 Longitudinal Stability . . . . .	4
2.2.2 Longitudinal Control. . . . .	5
2.3 Relaxed Static Stability . . . . .	6
2.4 Weight & Centre of Gravity Estimation . . . . .	7
2.5 Horizontal Tail Sizing . . . . .	8
2.6 Handling Qualities . . . . .	9
2.6.1 Inertia Estimation . . . . .	9
2.6.2 Stability and Control Derivative Estimation . . . . .	10
2.7 the Initiator . . . . .	11
2.8 Research Objective . . . . .	12
<b>3 Methodology</b>	<b>15</b>
3.1 Class I Weight Estimation and Sizing . . . . .	15
3.2 Class II Weight Estimation . . . . .	17
3.2.1 Structural Weight Estimation . . . . .	18
3.2.2 Powerplant Weight Estimation . . . . .	20
3.2.3 Fixed Equipment Weight Estimation . . . . .	21
3.3 Stability & Control Derivative Estimation . . . . .	23
3.3.1 Steady State Coefficients . . . . .	24
3.3.2 Angle of Attack Derivatives ( $C_{L\alpha}, C_{D\alpha}, C_{m\alpha}$ ) . . . . .	24
3.3.3 Sideslip Derivatives ( $C_{y\beta}, C_{l\beta}, C_{n\beta}$ ) . . . . .	25
3.3.4 Roll Rate Derivatives ( $C_{y_p}, C_{l_p}, C_{n_p}$ ) . . . . .	26
3.3.5 Pitch Rate Derivatives ( $C_{D_q}, C_{L_q}, C_{m_q}$ ) . . . . .	26
3.3.6 Yaw Rate Derivatives ( $C_{y_r}, C_{l_r}, C_{n_r}$ ) . . . . .	27
3.3.7 Control Derivatives . . . . .	27
3.4 Inertia Estimation. . . . .	28
3.4.1 Bodies of Revolution . . . . .	28
3.4.2 Lifting Surfaces . . . . .	30
3.4.3 Other Aircraft Parts. . . . .	33
<b>4 Technical Implementation of Methodology</b>	<b>35</b>
4.1 Class II Weight Estimation . . . . .	35
4.2 Stability & Control Derivative Estimation . . . . .	36
4.3 Inertia Estimation. . . . .	38
<b>5 Validation of Methodology</b>	<b>41</b>
5.1 Validation of Class I Weight Estimation and Sizing . . . . .	41
5.2 Validation of the Class II Weight Estimation. . . . .	43
5.3 Validation of the Stability and Control Derivative Estimation . . . . .	48
5.4 Validation of the Inertia Estimation . . . . .	51
5.5 Conclusions. . . . .	53

---

<b>6</b>	<b>Results &amp; Discussion</b>	<b>55</b>
6.1	Baseline aircraft . . . . .	55
6.2	Procedure for Relaxed Static Stability . . . . .	57
6.3	Effects of Relaxed Static Stability . . . . .	58
<b>7</b>	<b>Conclusions &amp; Recommendations</b>	<b>65</b>
7.1	Conclusions. . . . .	65
7.2	Recommendations . . . . .	66
<b>A</b>	<b>Class II Weight Estimation: Assumptions</b>	<b>69</b>
<b>B</b>	<b>DATCOM Figures</b>	<b>71</b>
<b>C</b>	<b>Class2WeightEstimation-module</b>	<b>73</b>
<b>D</b>	<b>Stability and Control Derivatives estimation functions</b>	<b>75</b>
<b>E</b>	<b>Detailed Inertia Estimation Functions</b>	<b>77</b>
<b>F</b>	<b>Fokker Inertia tool</b>	<b>81</b>
	<b>Bibliography</b>	<b>83</b>

# 1

## INTRODUCTION

In order to face the challenges faced by the European aviation industry, the Cleansky initiative was launched in 2008 and one of the initiatives within the programme is an increased collaboration between aircraft manufacturers, research institutes and universities. One technology that is investigated within this framework is the effect of relaxed static stability on the preliminary design of business jet aircraft. RSS aircraft have a neutral point located closer to or even in front of the aircraft's centre of gravity. As a consequence, the required trim force is reduced and thus the tail size may be reduced as well. Due to the infamous snowball-effect, it is anticipated that RSS can lead to significant weight loss and fuel savings. On the downside however, it is expected that RSS may require stability augmentation systems and reduce the elevator effectiveness. In this research it is quantified how RSS affects the mass of key aircraft components, as well as how RSS influences the handling qualities, by investigating its effect on the inertia tensor and stability & control derivatives.

One technology that will be investigated within this framework is the effect of relaxed static stability on the preliminary design of business jet aircraft. Aircraft with relaxed static stability have a neutral point that is located closer to or even just in front of the aircraft's centre of gravity. The concept was first explored for supersonic fighter aircraft as this provides them with larger agility in subsonic conditions. Furthermore in supersonic flight the neutral point shifts further aft, by using RSS however the balancing trim force can remain within bounds [1]. The same principle can also be advantageous for commercial and business aircraft. By employing relaxed static stability, the required trim force is reduced and thus the tail size of these aircraft can be reduced as well. Due to the infamous snowball-effect, RSS can lead to significant weight loss and fuel savings. By employing RSS however, it is anticipated that the elevator effectiveness reduces, posing a limit on the potential gains [2].

By means of a preliminary design study, it is investigated in this report how much can be gained in the design of business jet aircraft by using RSS. Furthermore, it is investigated to what extent these gains are limited by factors such as elevator effectiveness and handling qualities. Therefore, this report has been set-up in the following structure:

In chapter 2, a short introduction to various topics relevant to this research and their state-of-the-art are discussed. Topics that will be treated are tail surfaces, longitudinal stability & control, weight estimation, preliminary tail sizing and the assessment of handling qualities. Next, the approach used to assess the effect of relaxed static stability on the preliminary tail design is explained in chapter 3. During this research, mainly the effects on aircraft mass, mass moment of inertia and stability & control derivatives were investigated and each topic is discussed in a separate section. This methodology, was implemented in a preliminary design tool called the Initiator and the work flow of the updated modules is discussed in chapter 4. Now, before the Initiator could be used to assess the effect of relaxed static stability, the updates made to the various modules needed to be validated, which is described in chapter 5. The Initiator was then used to assess the effect of relaxed static stability on the preliminary design of business jet aircraft. The main findings with respect to aircraft mass, inertia tensors and the most relevant stability and control derivatives are described chapter 6. Finally, the main conclusions and recommendations to be taken away from this research, are summarized in chapter 7.



# 2

## BACKGROUND

In this chapter, the theoretical background relevant this research is explained and the state-of-the-art of various topics is discussed. As such, this chapter could be considered as an extended introduction. First, in section 2.1 the main functions of tail surfaces and the requirements imposed upon those are introduced. Next, the basic principles of longitudinal stability and control are discussed in section 2.2, after which the concept of relaxed static stability is introduced in section 2.3. In this section also the main advantages and disadvantages of RSS are discussed. Next, since the centre of gravity's longitudinal position highly influences the longitudinal stability and control, the basics of weight and centre of gravity estimation are explained in section 2.4. The background with respect to stability and control and centre of gravity estimation is then used in section 2.5 to introduce a widely accepted tail sizing methodology. Furthermore, within this research also the effects of RSS on the aircraft's handling qualities are investigated and a short introduction to this topic is given in section 2.6. Finally, the aforementioned sections serve as a build-up to the main research question and objectives of this research, which are described in section 2.8.

### 2.1. TAIL SURFACES

Before describing how aircraft tails are designed to meet the stability and control requirements, it is important to take a step back first and to shortly discuss the main functions performed by and the requirements imposed on the tail surfaces. Now, as described by Obert in reference [3], tail surfaces typically perform three main functions in the aircraft design, which are:

1. Provide static and dynamic stability
2. Enable aircraft control
3. Provide a state of equilibrium in each flight condition

Note that there is no requirement for an aircraft to have a tail, the aforementioned functions however should be accounted for somewhere in the aircraft's design. Also, it is allowed to design an inherently unstable aircraft, in that case however a stability augmentation system should be included to provide artificial stability [4]. When a tail is used however, it should adhere to the following design requirements [3]:

1. Tail surfaces shall provide a sufficiently large contribution to the static and dynamic stability in longitudinal, directional and sometimes lateral directions.
2. Tail surfaces shall provide sufficient control capability
3. Control shall be possible with acceptable control forces
4. Tail surfaces shall be able to cope with high tailplane angles of attack/sideslip
5. Tail surfaces shall be able to generate sufficiently large control forces to balance the total tail-off forces and moments so that static equilibrium is achieved in all flight conditions
6. The Mach number at which serious flow separation occurs at the tail surfaces shall lie above the design dive Mach number ( $M_D$ )

These requirements often conflict in terms of the preferred geometrical tail surface design. For instance, in order to meet the first requirement a large lift gradient is desirable. Therefore, a tail surface with large

aspect ratio and minimum sweep would be beneficial. The exact opposite however, would for instance be beneficial to meet the fourth requirement. In that case a stable vortex is formed at the leading edge of the tail surface creating so-called vortex lift, increasing the stabilizing force. Furthermore, this vortex would allow for flow to remain attached up to higher angles of attack ( $\alpha$ ) and sideslip ( $\beta$ ) [5]. Because of these conflicting requirements, the stabilizer often has a sweep angle around 5 degrees larger than the wing's and a chord section 1% to 2% thinner than the wing's tip chord. Aspect ratios typically range around 5, as higher aspect ratios would inflict a too large structural weight penalty. Smaller taper ratios then again are beneficial for the structural weight, excessive taper however may result in premature tip stall. Therefore taper ratios typically range between 0.3 to 0.5 for horizontal tails [3].

## 2.2. LONGITUDINAL STABILITY AND CONTROL

In the previous section it was explained that the horizontal tail surface should provide the aircraft with sufficient longitudinal stability and control. In section 2.2.1 the governing principles behind longitudinal stability are discussed, followed by a similar discussion for longitudinal control in section 2.2.2. These principles will later be used in section 2.5, when presenting a common horizontal tail sizing methodology.

### 2.2.1. LONGITUDINAL STABILITY

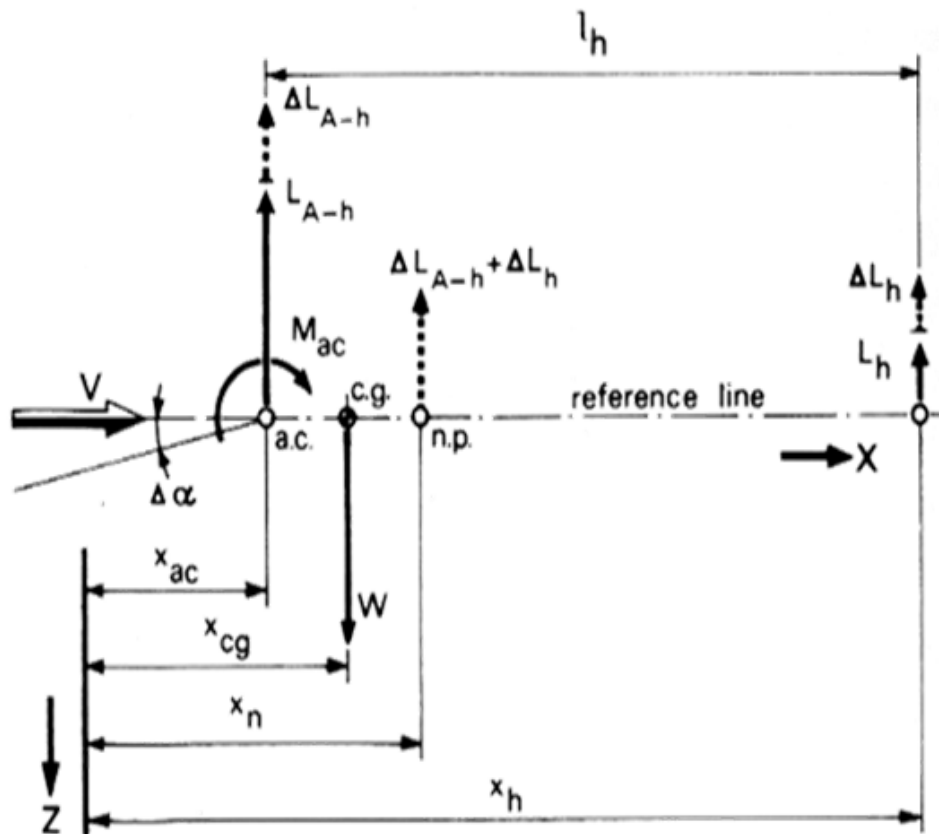


Figure 2.1: Moment equilibrium around the centre of gravity[6]

Duncan defines stability as: "the inherent quality of an aircraft to correct for conditions that may disturb its equilibrium and to return to or to continue on the original flight path" [7]. Note that in this research we mainly want to consider the aircraft's static longitudinal stability. The main requirement to be fulfilled in this case, is that any change in angle of attack ( $\alpha$ ) must result in a pitching moment returning the aircraft back to its original state. In Figure 2.1 the various forces contributing to this pitching moment are shown. Observe that in this model only the contributions of the wing and horizontal tailplane are taken into account, as these are considerably larger than for instance those of the fuselage. Also observe that, the change in lift caused by a perturbation ( $\Delta\alpha$ ) is indicated as well. Moreover, it is also shown that the resultant perturbing force acts through a single point, which is called the neutral point and by definition the moment change caused

by a perturbation around this point is zero. From this figure, equation 2.1 may be derived, describing the longitudinal position of the neutral point [6].

$$\bar{x}_{np} = \bar{x}_{ac} + \frac{C_{L\alpha_h}}{C_{L\alpha_{A-h}}} \left( 1 - \frac{d\varepsilon}{d\alpha} \right) \frac{S_h l_h}{S \bar{c}} \left( \frac{V_h}{V} \right)^2 \quad (2.1)$$

From Figure 2.1 it can also be deduced that to achieve longitudinal static stability, the aircraft's centre of gravity has to lie in front of the neutral point. In other words, the neutral point is the c.g.'s most aft-location before the aircraft becomes unstable [8]. Furthermore, the distance between the c.g. and the n.p. normalized with the MAC is called the static margin (S.M.). Hence, the maximum allowable aft position of the aircraft's centre of gravity (equation 2.2) can be determined by inserting the definition of the S.M. in equation 2.1 [6].

$$\bar{x}_{cg} = \bar{x}_{ac} + \frac{C_{L\alpha_h}}{C_{L\alpha_{A-h}}} \left( 1 - \frac{d\varepsilon}{d\alpha} \right) \frac{S_h l_h}{S \bar{c}} \left( \frac{V_h}{V} \right)^2 - S.M. \quad (2.2)$$

$$S.M. = \bar{x}_{cg} - \bar{x}_{np} \quad (2.3)$$

### 2.2.2. LONGITUDINAL CONTROL

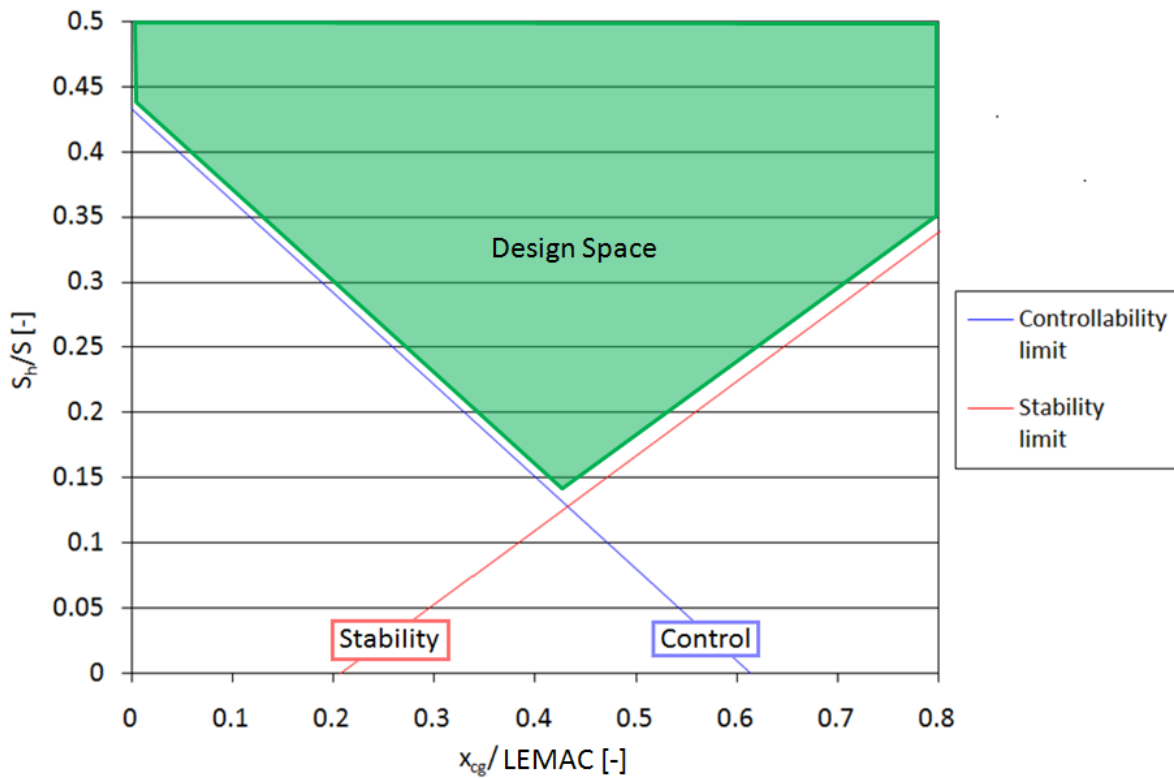


Figure 2.2: Example of an X-plot[9]

In essence, longitudinal control is a matter of controlling the aircraft's pitching moment around its centre of gravity. First, it should be possible to trim the aircraft or in other words to balance the moments around the c.g. such that the total pitching moment equals zero. Secondly, it must be possible to change this pitching moment such that manoeuvres such as take-off rotation, 2.5g pull-up and the landing flare can be executed. Now, when imposing the trim requirement, it can be shown that the most forward c.g. position allowing longitudinal control can be expressed as in equation 2.4 [6]. Again, note that to derive this equation, only the contributions of the wing and tail have been taken into account.

$$\bar{x}_{cg} = \bar{x}_{ac} - \frac{C_{m_{ac}}}{C_{L_{A-h}}} + \frac{C_{L_h}}{C_{L_{A-h}}} \frac{S_h l_h}{S \bar{c}} \left( \frac{V_h}{V} \right)^2 \quad (2.4)$$

An important consequence of trimming the aircraft is the so-called trim drag, which can be expressed as shown in equation 2.5.

$$D_{trim} = q \left( \frac{Vh}{V} \right)^2 S_h \frac{C_{L_h}^2}{\pi A_h e} \quad (2.5)$$

Finally, by combining equations 2.2 & 2.4 it is possible to create a so-called x-plot, which shows the design space available for the horizontal tail design. An example of such a plot is shown in Figure 2.2.

### 2.3. RELAXED STATIC STABILITY

In section 2.2 the concept of static margin was introduced, which for most conventional transport aircraft ranges between 5 to 10 % for the most aft c.g. position. Now, an aircraft is said to have relaxed static stability if the S.M. is less or even negative [8]. This concept was first explored for supersonic fighter aircraft as this provides them with larger agility in subsonic conditions. Furthermore in supersonic conditions, where the neutral point shifts further aft, the balancing trim force then remains within bounds [1]. The same principle can also be advantageous for commercial and business jet aircraft. By employing RSS, the required trim force is reduced and thus the tail size of these aircraft can be reduced as well. Due to the infamous snowball-effect, RSS can lead to significant weight loss, drag reductions and fuel savings.

Furthermore, from equation 2.5 it becomes apparent that reducing the horizontal tail-plane's lift coefficient ( $C_{L_h}$ ) and size are the most effective measures to reduce the aircraft's trim drag. Now, as explained in the previous paragraph, RSS aims at reducing the required tail lift by reducing the static margin. RSS thus not only results in a smaller and lighter tail, but it also reduces the associated trim drag. Note that for a smaller horizontal tail to achieve a similar change in tail lift coefficient, for instance to rotate the aircraft during the take-off roll, it is anticipated that larger control surface deflections are required. For instance, in reference [2] it was shown by using RSS in an MDO-framework for a medium range conventional aircraft that the required elevator deflection for take-off increased from 6.9 to 11.14 degrees. The required elevator deflection for other manoeuvres saw a similar, but smaller increase. Either way, this clearly demonstrates that the minimum horizontal tail size is limited by the elevator control power, because at a certain deflection, the control surfaces will stall and at this point the aircraft can no longer be controlled.

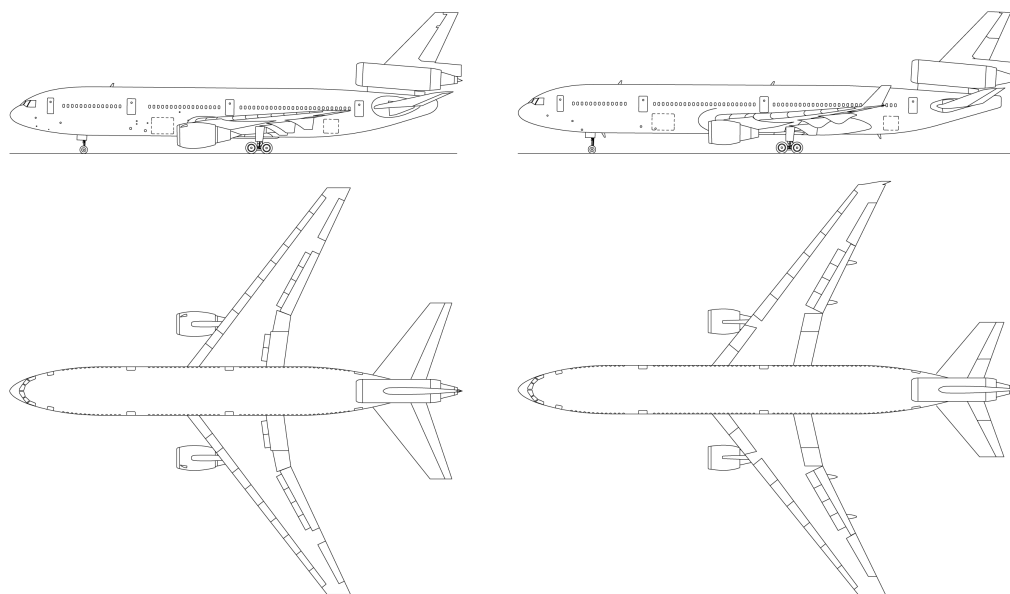


Figure 2.3: Comparison between the DC-10-30 (left) and the MD-11 (right)

A practical example of a commercial passenger aircraft designed with RSS is the McDonnell Douglas MD-11. This aircraft was designed in the late 1980's as the successor of the Douglas DC-10. Just like its predecessor, the MD-11 was a trijet, but it had redesigned wings (including winglets), a substantially longer fuselage and a smaller horizontal tailplane. Furthermore, the aircraft was also equipped with a longitudinal stability augmentation system, which included a ballast fuel tank in the vertical tail [10]. Figure 2.3<sup>1</sup> shows a comparison between the two aircraft designs, clearly demonstrating the aforementioned differences. Also, some interesting data of both aircraft is summarized in Table 2.1 [11]. From these figures it can be deduced that while the MD-11 has a capacity and range that are approximately 15 % larger than its predecessor, its MTOM and maximum fuel weight are only around 5% larger. It should be noted that the extent to which RSS contributes to the performance increase remains unclear, since other factors such as aerodynamic and structural improvements also have a beneficial effect on the MD-11's performance.

Table 2.1: Comparison between the DC-10-30 and the MD-11

Parameter	DC-10-30	MD-11	Units
Typical Seating Capacity (2-class)	285	323	[-]
MTOW	$259.5 \cdot 10^3$	$273.3 \cdot 10^3$	[kg]
MLW	$182.7 \cdot 10^3$	$200 \cdot 10^3$	[kg]
Wing Area, $S$	367.7	338.9	[m <sup>2</sup> ]
Wing Span, $b$	50.4	51.66	[m]
Tail Area, $S_h$	124.3	85.5	[m <sup>2</sup> ]
Fuselage Length	51.97	58.65	[m]
Maximum Fuel Weight	$111.5 \cdot 10^3$	$117.5 \cdot 10^3$	[kg]
Harmonic Range	10622	12450	[km]
Take-off run on MTOW	2847	3100	[m]
Landing speed on MLW	76.6	78.7	[m/s]

Incorporating RSS in the aircraft design also comes at a cost, for instance a complex stability augmentation system had to be included in the design [12]. Even with this system, the MD-11 did face issues caused by the reduction in stability. For instance, with an approach speed of 78.7 m/s the MD-11's landing speed is substantially larger than the 70 m/s of the Boeing 777-200, which is comparable in size and weight [13]. The higher approach speed reduces the reaction time pilots have to correct the aircraft during approach and landing. Moreover due to the geometric design of the MD-11, with a relative aft centre of gravity and main gear position, pilots experienced difficulties recognizing and properly correcting bouncy landings. Failure to do so in combination with the reduced elevator effectiveness, has led to at least three accidents. These crashes caused aviation authorities to recommend special landing trainings and upgrades to the stability augmentation system [14] [15] [16].

## 2.4. WEIGHT & CENTRE OF GRAVITY ESTIMATION

From equations 2.2 and 2.4, it should become apparent that to determine the stability and control characteristics of the aircraft, it is important to know the aircraft's centre of gravity position. In reality, the c.g. is not a fixed point, but it will shift during flight due to fuel being burned. Furthermore the initial c.g.-position is different each flight due to differences in aircraft loading. Therefore it is necessary to estimate the centre of gravity's range that may be anticipated during operations. To estimate this range, the weights and c.g.'s of all the aircraft components have to be estimated first. To this purpose, references [17] and [18] can be used, which describe various Class I and Class II weight estimation methods. With the estimated component weights and their associated position, the aircraft's c.g. for the OEM-condition can be determined. Note that the OEM is defined as the weight of the aircraft without fuel and payload.

Next, the maximum centre of gravity range for a variety of loading conditions can be estimated, for which it is recommended to set-up so-called loading or potato diagrams (see [6]). These diagrams show the shift in centre of gravity for the given aircraft configuration when loading the aircraft with payload and fuel. Now, to estimate the effect of the wing's longitudinal position, it is suggested to generate three loading diagrams

<sup>1</sup>CC-BY J. Scavini

corresponding to three different wing positions (forward, mid and aft) [6]. The results can then be collected in a single diagram as shown in Figure 2.4. In this particular example, the initial wing position was at 35% ( $X_{LEMAC}/X_{fus}$ ) while the most forward and most aft position were 25% and 45% respectively.

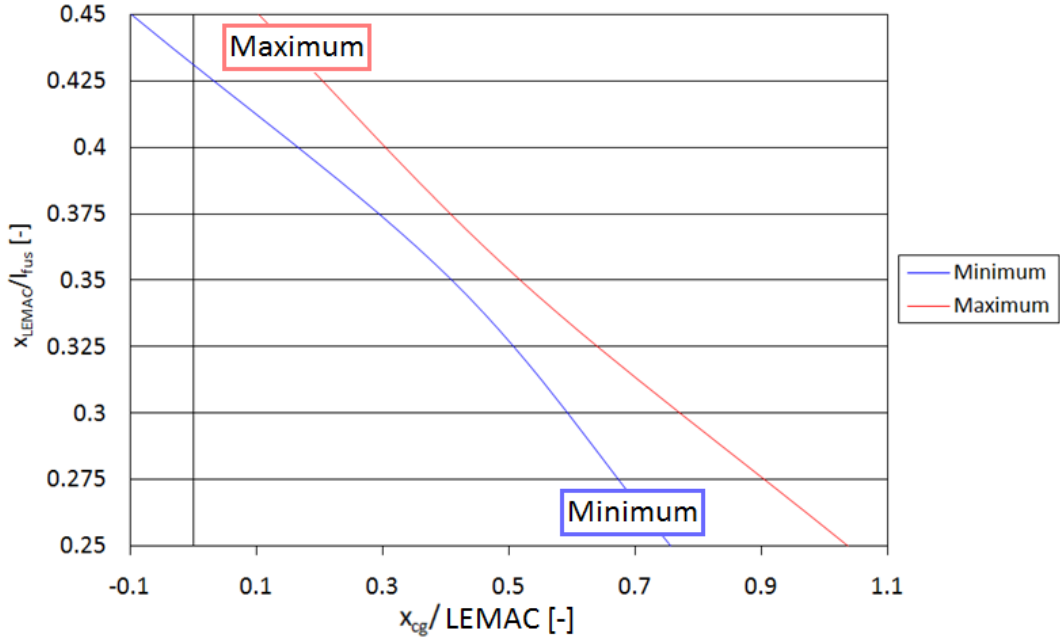


Figure 2.4: Example of effect of the longitudinal wing position on the c.g. range [9]

## 2.5. HORIZONTAL TAIL SIZING

A first estimate for the horizontal tail area is often obtained with the method described by Roskam in reference [19]. This approach uses the so-called tail volume coefficient, which is defined by equation 2.6 for the horizontal tail. For aircraft of a similar type it may be assumed that they have a similar tail volume coefficient. Furthermore, in reference [19] the tail volume coefficients for eight types of aircraft can be found. The horizontal tail area is then determined by choosing a tail volume coefficient of a similar aircraft and substituting the remaining parameters, which should already be known at the moment where the tail has to be sized, in equation 2.6. A similar approach can also be used to size the vertical tail, in this case the vertical tail volume is given by equation 2.7.

$$\tilde{V}_h = l_h S_h / S \bar{c} \quad (2.6)$$

$$\tilde{V}_v = l_v S_v / S b \quad (2.7)$$

Generally speaking, the estimate for the horizontal tail area is further refined by combining the results of the sections 2.2 and 2.4. As such, it can be verified whether the estimated tail area is sufficient to meet the stability and control requirements for the given aircraft configuration and centre of gravity range. In practical terms, this is done by overlaying x-plot with the centre of gravity range diagram as shown in Figure 2.5. When overlaying these figures, care should be taken that the axes are properly aligned. This means that the figures should be shifted vertically such that the line connecting the intersection points of minimum c.g. position line with the controllability limit and the maximum c.g. position line with the stability limit, is perfectly horizontal. Next, the optimal longitudinal wing position ( $X_{LEMAC}^{opt}/l_{fus}$ ) can be read of the red vertical axis. It can be seen in Figure 2.5, that in the case of this example an optimal position of 0.395 is obtained. In other words, the leading edge of the mean aerodynamic chord may be found at 39.5% of the total fuselage length. Moreover, from the black vertical axis in Figure 2.5 it may also be deduced that the optimal tail ratio is 0.21 or in other words, the horizontal tail area is 21% of the main wing's area.

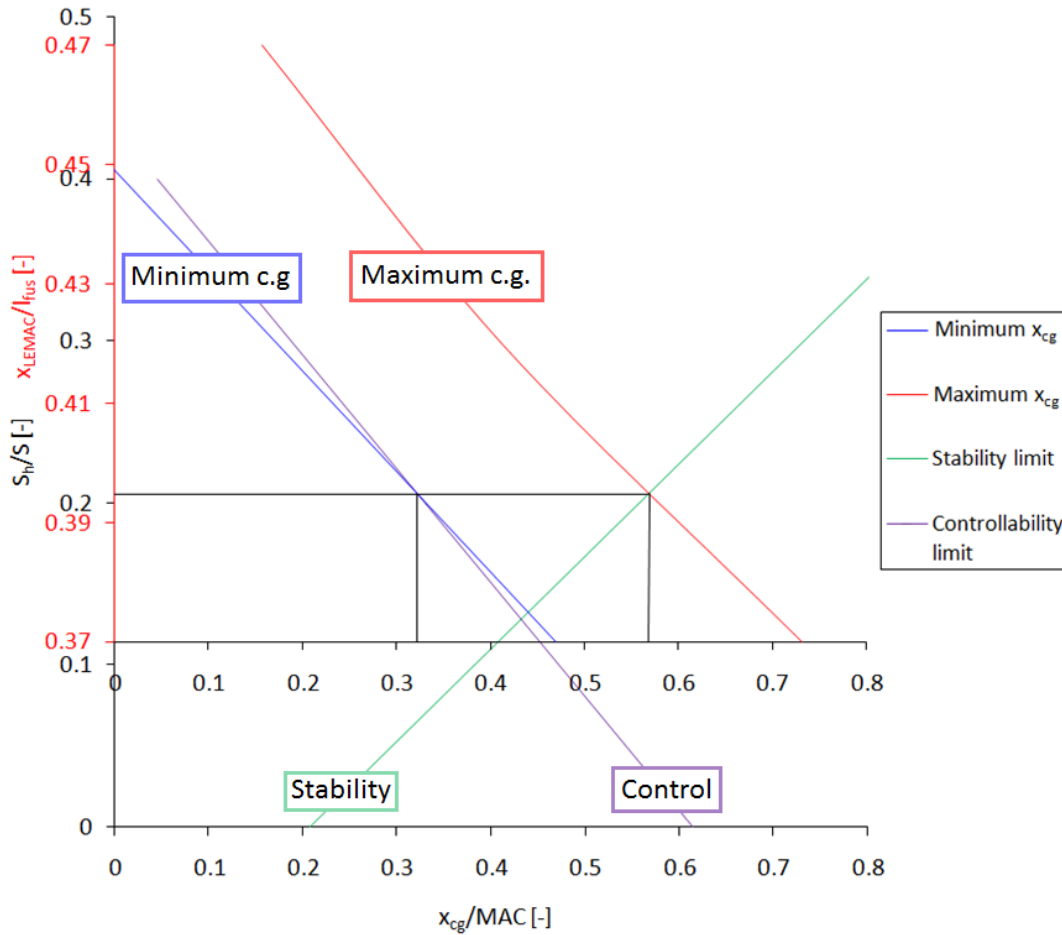


Figure 2.5: Example of the c.g. range graph overlaid with x-plot [9]

## 2.6. HANDLING QUALITIES

One of the aspects anticipated to be affected by incorporating relaxed static stability in the design of business jet aircraft, is a change in the handling qualities of the aircraft. Now, to assess these handling qualities in essence two properties need to be known, being the aircraft's mass moment of inertia matrix and its stability & control derivatives. A short introduction to these topics is given in sections 2.6.1 and 2.6.2 respectively.

### 2.6.1. INERTIA ESTIMATION

The mass moment of inertia, in essence dictates the resistance an object offers with respect to angular acceleration in the same way that mass does for acceleration. Generally speaking, the procedure to estimate a body's mass moment of inertia around a random axis, is to estimate the two contributions as shown in equation 2.8. The first term indicates the body's mass moment of inertia around an axis symmetrical to the random axis and through its own centre of gravity. The second contribution is the so-called Steiner-term and consists of the object's mass times the distance to the random axis squared.

$$I = I_0 + mr^2 \quad (2.8)$$

From this equation, it should also become apparent that the mass moment of inertia is different depending on the axis around which it is determined. Now, the general procedure is to calculate the mass moment of inertia around the body axis system and store the results in a 3x3 inertia tensor matrix as shown by equation 2.9. In this matrix, the symmetrical inertia components are put on the diagonal axis (from top left to bottom right).

$$I = \begin{bmatrix} I_{xx} & I_{xy} & I_{xz} \\ I_{yx} & I_{yy} & I_{yz} \\ I_{zx} & I_{zy} & I_{zz} \end{bmatrix} \quad (2.9)$$

A simple method to estimate an aircraft's the inertia tensor is shown in reference [18]. In this approach, the non-dimensional radii of gyration are estimated first based on statistical data. The radii of gyration for business jet aircraft can be estimated with equations 2.10 to 2.11. These estimates have been obtained by averaging the raddii of gyration for the various business jet aircraft as shown in Appendix B of reference [18].

$$\bar{R}_x \approx 0.3 \quad (2.10)$$

$$\bar{R}_y \approx 0.35 \quad (2.11)$$

$$\bar{R}_z \approx 0.45 \quad (2.12)$$

Next, the inertia tensor can be estimated with the matrix as shown in equation 2.13. As can be observed in this equation, the inertia contributions in this approach are a function of wing span ( $b$ ), aircraft length ( $L$ ), the radii of gyration ( $\bar{R}_i$ ) and the gravitational acceleration ( $g$ ). Furthermore, note that in this approach it is assumed that the asymmetrical inertia contributions are equal to zero. This is assumption is often made and is generally true for conventional aircraft as these are almost perfectly symmetrical around their body's x-axis. Finally, note that with this approach only a rough estimate for the inertia tensor is obtained and that the method used in this research to further refine this inertia tensor estimate is explained in chapter 3.

$$I = \begin{bmatrix} \frac{b^2 W (\bar{R}_x)^2}{4g} & 0 & 0 \\ 0 & \frac{L^2 W (\bar{R}_y)^2}{4g} & 0 \\ 0 & 0 & \frac{\left(\frac{b+L}{2}\right)^2 W (\bar{R}_z)^2}{4g} \end{bmatrix} \quad (2.13)$$

### 2.6.2. STABILITY AND CONTROL DERIVATIVE ESTIMATION

As mentioned before, the stability & control derivatives are together with the inertia tensor required to estimate the dynamic behaviour of aircraft [20]. Now, the total of aerodynamic forces and moment acting on an aircraft can be modelled with these derivatives as shown by the equations 2.14 and 2.15. Note that in equation 2.14 the longitudinal forces and moments are shown, whereas in equation 2.15 the lateral forces and moments are shown. Furthermore, observe that in these equations the derivative is indicated by the subscript, e.g.  $C_{L_\alpha}$  is the derivative of the lift force with angle of attack. Furthermore, the 1-subscript denotes the steady state coefficients, in other words the conditions at which these derivatives have been determined. It should also be mentioned that all derivatives in these equations are taken with respect to the stability reference frame, which can be converted into the body reference frame by a single rotation over the aircraft's angle of attack ( $\alpha$ ).

$$\begin{bmatrix} \frac{F_{ax}}{\bar{q}S} \\ \frac{F_{az}}{\bar{q}S} \\ \frac{m_a}{\bar{q}S} \end{bmatrix} = \begin{bmatrix} -(C_{D_u} + 2C_{D_1}) & -(C_{D_\alpha} + 2C_{L_1}) & -C_{D_q} & -C_{D_{\delta_e}} \\ -(C_{L_u} + 2C_{L_1}) & -(C_{L_\alpha} + 2C_{D_1}) & -C_{L_q} & -C_{L_{\delta_e}} \\ -(C_{m_u} + 2C_{m_1}) & -C_{m_\alpha} & -C_{m_q} & -C_{m_{\delta_e}} \end{bmatrix} \begin{bmatrix} \frac{u}{U_1} \\ \alpha \\ \frac{q\dot{c}}{2U_1} \\ \delta_e \end{bmatrix} \quad (2.14)$$

$$\begin{bmatrix} \frac{F_{ay}}{\bar{q}S} \\ \frac{l_a}{\bar{q}Sb} \\ \frac{n_a}{\bar{q}Sb} \end{bmatrix} = \begin{bmatrix} C_{y_\beta} & C_{y_p} & C_{y_r} & C_{y_{\delta_a}} & C_{y_{\delta_r}} \\ C_{l_\beta} & C_{l_p} & C_{l_r} & C_{l_{\delta_a}} & C_{l_{\delta_r}} \\ C_{n_\beta} & C_{n_p} & C_{n_r} & C_{n_{\delta_a}} & C_{n_{\delta_r}} \end{bmatrix} \begin{bmatrix} \beta \\ \frac{pb}{2U_1} \\ \frac{rb}{2U_1} \\ \delta_a \\ \delta_r \end{bmatrix} \quad (2.15)$$

As previously mentioned, these derivatives may be used to verify the longitudinal and lateral dynamic stability of an aircraft. With respect to the longitudinal stability, there are two so-called eigenmotions of importance to be considered, being the short period and the phugoid. To assess whether these two eigenmotions are stable, the eigen frequency and damping ratio should be estimated. The approach suggested in reference [21] may be used to determine these properties. Note that this model only estimates the natural frequency and damping ratio for the fixed-controls case. Furthermore, it is assumed that an irreversible control system can maintain the elevator in position when the pilot doesn't hold the stick.

$$\omega_{np} = \frac{1.411g}{U_1} \quad (2.16)$$

$$\xi_p = \frac{g}{2C_{L_1} U_1 \omega_{np}} \left( C_{D_u} + 2C_{D_1} - C_{T_{x_u}} - 2C_{T_{x_1}} \right) \quad (2.17)$$

$$\omega_{n_{SP}} = \sqrt{\frac{Z_\alpha M_q}{U_1} - M_\alpha} \quad (2.18)$$

$$\xi_{SP} = -\frac{M_q + (Z_\alpha / U_1) + M_{\dot{\alpha}}}{2\omega_{n_{SP}}} \quad (2.19)$$

Finally the eigen frequency and damping ratio should be compared to the requirements. Now, the phugoid's eigen frequency is primarily affected by the flight speed and there is no requirement for it. The requirements for the short period's eigen frequency and damping ratio depend on the aircraft type (Class I to IV) and flight conditions (A to C) and can be found in Appendix B of reference [21].

## 2.7. THE INITIATOR

The previous sections focused on the theoretical background concerning relaxed static stability and the factors anticipated to be affected by incorporating this concept in the preliminary design process of business jet aircraft. In this section, the Initiator tool is introduced, which will be used to predict how the preliminary design of business jet aircraft is affected by RSS. The Initiator is a conceptual/preliminary design tool, developed by TU Delft's Flight Performance and Propulsion Department (FPP), which synthesises the preliminary design of subsonic transport aircraft from a set of top-level requirements [22], [23]. The tool was originally set-up in 2011 for conventional and box-wing/Prandtl aircraft [24] and its capabilities were gradually extended, allowing for instance to design three-surface [25], [11] and blended-wing-body configurations [26], [27].

The Initiator is written in MATLAB and is set-up in a class-based programming style. XML is used for all its in- and output files, while for reading and writing XML-files the open-source TIXI library [28] is used. At the core of the program is the controller, which is connection between the aircraft object and the various modules. Its main purpose is to handle the program flow, i.e. to keep track of which modules have been completed as well as the dependencies between modules. The aircraft object is defined by using high level primitives called parts. All parts generate a geometry which is used to drive the analysis modules and visualisation of the aircraft. Currently, the Initiator can be started from two different starting points. First, it is possible to start an Initiator-run by defining a set of top-level requirements and the desired aircraft configuration. In this case the Initiator works as preliminary sizing and analysis tool and in the following paragraphs it will be described how the Initiator works in that case. Secondly one can also use the geometry of an existing aircraft as input. In that case the sizing modules are skipped and the existing geometry can be analysed immediately.

Figure 2.6 shows the N2 chart of the design process used by the Initiator when starting it from a set of top-level requirements. These requirements are used together with the Initiator's internal database to estimate the aircraft's MTOM with the *Class1WeightEstimation*-module. The Initiator database contains reference data for a large set of conventional commercial, turboprop and business jet aircraft as well as data of common engines and APU's. The majority of this data has been obtained from references as [29] and [30]. Next, based on the requirements and the predicted MTOM, a wing-thrust-loading diagram is constructed after which the most optimal design point is selected by the Initiator. The design point together with the MTOM-estimate is used by *GeometryEstimation*-module to size the aircraft model accordingly. The geometry is then together with the estimates for MTOM and fuel fraction, used by the *Class2WeightEstimation*-module to obtain a new estimate for the aircraft's EOM. This EOM is fed back each iteration to the *Class1WeightEstimation*-module, together with the output of the drag modules and the engine model, which provide the Initiator with updated estimates for the drag polar and the specific fuel consumption. This is the so-called Class 2 Loop and is indicated by the orange line in Figure 2.6. The Class 2 loop is repeated until the MTOM estimated by the *Class1WeightEstimation*- and *Class2WeightEstimation*-module converge to a predefined error margin.

Once the Class 2 loop is completed, the *MissionAnalyis*-module is run, which simulates an entire aircraft mission from take-off to landing, including a diversion. This module takes the range requirement, the drag polar and the specific fuel consumption as inputs and calculates a new MTOM based on the updated fuel fraction.

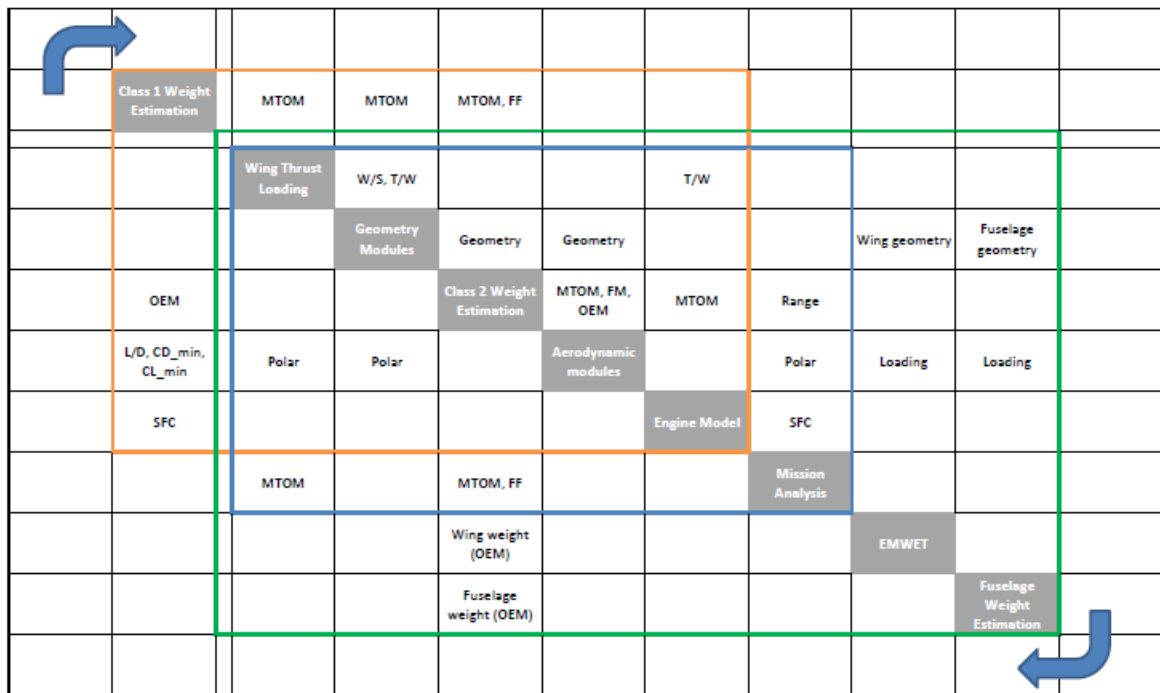


Figure 2.6: The Initiator top level design process

The *MissionAnalysis*-module's output is fed back to the *WingThrustLoading*-module until the MTOM predicted by the *Class2WeightEstimation*-module converges with the *MissionAnalysis*-module's estimate. This loop is referred to as the Mission Analysis loop and is indicated with the blue line in Figure 2.6. Finally, once the Mission Analysis loop has been completed, the wing and fuselage's geometry together with estimates for the loads acting upon these aircraft parts are fed into the *EMWETWeight*- and *FuselageWeight*-modules. These modules update the weight estimates for these parts and feeds these back into the *Class2WeightEstimation*-module. Again a loop is started until the MTOM estimate converges, which is called the Class 2.5 loop and is indicated by the green line in Figure 2.6.

## 2.8. RESEARCH OBJECTIVE

In the previous sections, the basic background concerning longitudinal stability and control was discussed. It was shown that the aircraft's centre of gravity, the wing/horizontal tail position as well as the horizontal tail size have the largest influence on the stability and control characteristics of the aircraft. Also, it was shown that by "relaxing" the requirements on stability, potential gains could be achieved with respect to aircraft drag and weight. Finally, the Initiator tool has been introduced, which will be used to assess the extent these effects. With this background information it is now possible to formulate a research question and objective:

### Research Question:

*What is the effect of implementing relaxed static stability on the design of a business jet aircraft in terms of its mass and key stability and control characteristics?*

### Research Objective:

*Investigate and quantify the effects of using relaxed static stability on the design of a business jet aircraft on a preliminary design phase level, by updating the weight, inertia and stability & control estimation methods within the Initiator*

This research objective entails that the capabilities of the Initiator will need to be extended first, such that the tool can complete the preliminary design of business jet aircraft based on a set of top level requirements. More specifically, as it is anticipated that relaxed static stability will lead to weight savings, the Class I and II

weight estimation methods within the Initiator will have to be updated, such that the total and component weight of business jet can be estimated with a preliminary design level of accuracy. In practical terms, this means that the databases used by the empirical methods in the Initiator's Class I weight estimation and sizing need to be updated first. Furthermore, the validity of these methods for business jet aircraft will need to be verified and alternative methods will need to be implemented where necessary. Next, the Class II weight estimation methods of Torenbeek and General Dynamics as described in [18] will be implemented in an iterative weight estimation loop, such that the snowball effect of reducing the tail size on the aircraft and component weight can be assessed.

Secondly, as it is anticipated that relaxed static stability will affect the aircraft's dynamic behaviour, the methods to estimate the inertia tensor as well the stability and control derivatives need to be updated as well. In this research, the inertia tensor will be estimated with the approach as first described in reference [31]. This method is in essence a combination of the Anemaat's lumped mass methods as described in [32] and [33] and the DATCOM method as described in [34]. Furthermore this method will also be expanded, such that it can also estimate the contributions of the fuel and payload to the inertia tensors, for which again a lumped mass method will be developed. Finally, in order to quickly estimate the stability and control derivatives, the empirical approach as described by Roskam in reference [20] will be used, which is in essence a simplified version of the DATCOM-method as can be found in reference [34].

Finally, with the updated Initiator a baseline business jet aircraft will be created based on the requirements of the Cessna Citation II. Next, the wing will be shifted forward in order to reduce the static margin and the methods described in the previous paragraphs will be used to quantify the effects of relaxed static stability on the preliminary design of business jet aircraft. As a concluding remark, observe that the majority of methods and updates that will be made to the Initiator are mainly based on empirical methods. This is in compliance with the goal to estimate the effects of relaxed static stability on a preliminary design level.



# 3

## METHODOLOGY

In this chapter the methodology to reach the research goals formulated in chapter 2 is described. Recall that the first research goal was to quantify the effect of relaxed static stability on the business jet aircraft's weight with a preliminary design level of accuracy. Therefore, the modules dealing with the Class I & II weight estimation and sizing were updated first. In summary, the Initiator's database was extended with business jet aircraft data and a new relation for the take-off constraint was implemented. These updates are described in section 3.1. Furthermore, to estimate the component weight of business jet aircraft more accurately, Torenbeek's and General Dynamics's empirical methods were added to the Initiator's Class II weight estimation. These methods are described in more detail in section 3.2. Next, to estimate the stability and control derivatives, the empirical method as described by Roskam [20], was implemented in the Initiator, which is described in section 3.3. Finally, to estimate the aircraft's inertia tensor, a combination of lumped mass methods and empirical methods were used, which is explained in more detail in section 3.4.

### 3.1. CLASS I WEIGHT ESTIMATION AND SIZING

The purpose of the Class I weight estimation and sizing is to provide the Initiator with a first estimate for the aircraft weight and geometry. To do this, purely statistical methods are employed as these are very fast and should provide a reasonably accurate first estimate for conventional aircraft types [23]. In this section it is described which the updates were made during this research to these methods, such that the Initiator can predict the MTOM, wing loading (W/S) and thrust loading (T/W) for a business jet more accurate on a Class I level.

First, as the Class I weight estimation and sizing methods rely heavily on statistical data, the first update to the Initiator was to create a dedicated database of business jet aircraft and their key performance parameters. The data was primarily obtained from references [29] and [30] and included parameters such as:

- MTOM
- OEM
- Payload mass
- Range
- Wing and Thrust Loading
- Landing and Take-Off Distance

Furthermore, it has been an ongoing trend in aviation to move from traditional aluminium structures to structures with more composite materials [35]. Now, in order to account for the effect of composites on the OEM, table 2.16 of reference [17] has been used, which is shown in Figure 3.1. It should be mentioned that the correction factors shown in this figure assume changing from a full aluminium to a full composite structure. Also note that these correction factors are to be applied on a part-level, which is not available at the Class I Weight Estimation level yet. Therefore, it was assumed, based on data provided in reference [6], that the wing and fuselage each account for approximately 25% of the OEM, whereas the empennage only contributes up to 3%. No correction factors to landing gears and any secondary structures have been applied, as

**Table 2.16 Weight Reduction Data for Composite**  
=====

<b>Construction</b> =====	
<b>Structural Component</b>	<b><math>W_{comp}/W_{metal}</math></b>
<b><u>Primary Structure</u></b>	
Fuselage	<b>0.85</b>
Wing, Vertical Tail, Canard or Horizontal Tail	<b>0.75</b>
Landing Gear	<b>0.88</b>
<b><u>Secondary Structure</u></b>	
Flaps, Slats, Access Panels, Fairings	<b>0.60</b>
Interior Furnishings	<b>0.50</b>
Air Induction System	<b>0.70 - 0.80</b>

Figure 3.1: Weight reduction factors for composite structures [17]

it is anticipated that their effect on the Class I Weight estimate is minimal. Finally, note that the same correction factors were applied in the Class II Weight Estimation as well (see chapter 3.2).

Secondly, the module handling the estimation of the design point in the wing thrust loading diagram also required an update. This update was necessary, because the module had the tendency to underestimate the thrust loading for business jet aircraft. As a consequence, the modelled engines were underpowered, resulting in an under prediction of the OEM and fuel mass. This also resulted in problems with the mission analysis module: since the engines were underpowered, a frequently encountered issue was that business jet aircraft could not climb up to cruise altitude. This caused the Initiator to end the design convergence at that point, hence no converged design was obtained.

Now, in Figure 3.2 an example of the original wing and thrust loading diagram for a Cessna Citation II is shown, with the chosen design point indicated by the red dot. Note that the black dots in this diagram indicate the 10 reference aircraft in the Initiator's database which have a MTOM closest to the MTOM-estimate obtained with the Class I weight estimation module. Also, the blue square in this diagram indicates the Cessna Citation II's actual design point. The black dots and blue square clearly demonstrate that the thrust loading is underestimated. It may also be observed in this figure that the Citation II's wing loading is relatively low compared to that of the reference aircraft, which is caused by the active landing constraint. The estimate for the wing loading obtained with this diagram ( $2155 N/m^2$ ) however, lies quite close to the actual wing loading of  $2195 N/m^2$  [30].

The wing and thrust loading module uses the empirical method as described by Roskam in reference [17] to estimate the constraints in Figure 3.2. The constraint for the take-off distance is an exception however, and is based on an unpublished relation derived by Torenbeek (see equation 3.1) [23]. In this relation, the thrust at  $V_2$ -speed ( $T_{V_2}$ ) is a function of the aircraft weight ( $W$ ), the number of Engines ( $N_e$ ), the wing span ( $b$ ), air density at take-off altitude ( $\rho_{TO}$ ), gravitational acceleration ( $g$ ) and the take off distance requirement ( $S_{TO}$ ). The advantage of this equation compared to the method as proposed by J. Roskam is that it does not take the  $(C_{L_{max}})_{TO}$  into account, which at the point of the Class I sizing is nothing more than an educated guess.

$$\frac{T_{V_2}}{W} = 1.10 \sqrt{\frac{N_e}{N_e - 1} \frac{W/b^2}{\rho_{TO} g S_{TO}}} \quad (3.1)$$

Equation 3.1, was validated for a set of 45 commercial aircraft and it was shown that for a given take-off length an error margin of approximately 10% was obtained [23]. The problem with applying this equation to business jet aircraft however, is that these aircraft quite often have a much larger thrust loading than predicted with this relation. Therefore, equation 3.2 was derived, which in essence is the same as equation 3.1, but with an additional correction factor based on the reference data of 70 business jet aircraft.

$$\frac{T_{V_2}}{W} = 1.50 \sqrt{\frac{N_e}{N_e - 1} \frac{W/b^2}{\rho_{TO} g S_{TO}}} \quad (3.2)$$

Finally note that this updated relation can only be applied to estimate the take-off constraint of business jet aircraft with multiple engines. This does not impose a real limit, because except for a couple of notable exceptions such as for instance the Cirrus SF50 [36], most business jet aircraft have two or more engines.

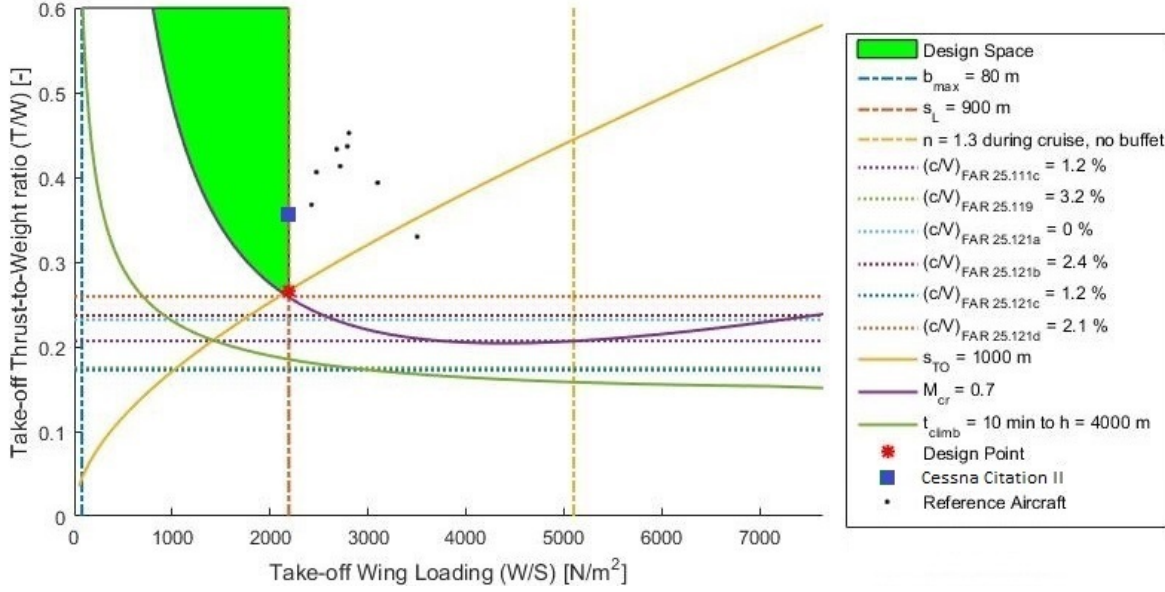


Figure 3.2: Wing and Thrust Loading Diagram for the Cessna Citation II

### 3.2. CLASS II WEIGHT ESTIMATION

As previously mentioned, an important goal of this research, is to assess the effect of RSS on the overall aircraft mass on a preliminary design level (Class II). Therefore the *Class2WeightEstimation*-module of the Initiator has been updated, in order to make it more robust. Originally, the Class II Weight Estimation within The Initiator's was done with Raymer's component weight estimation method [8]. The landing gear weight however, is determined with a shortened version of the methodology developed by Heerens[37]. It should be mentioned that Raymer only distinguishes 3 aircraft categories, being Fighter/Attack, Cargo/Transport and General Aviation and that within the Initiator, the Cargo/Transport-category is used to estimate the aircraft component weight. Now, as can be deduced from the category's name, this method was developed for large cargo/transport aircraft. As such it may not be ideally suited to accurately estimate the weight break-down for business jet-type aircraft. Therefore it was decided to expand the *Class2WeightEstimation*-module with the GD-method and Torenbeek's method as described in Airplane Design Part V [18].

Both methods estimate the aircraft's take-off mass ( $W_{TO}$ ), by estimating the separate contributions of equations 3.3 & 3.4. Now, the payload mass ( $W_{PL}$ ) in equation 3.3 is a given requirement, while the crew mass ( $W_{crew}$ ) directly follows from the regulations for that given payload [17]. The fuel weight  $W_F$  can be assumed to be identical to Class I fuel mass, or can be recalculated by assuming that the fuel fraction remains constant. For the trapped fuel ( $W_{PL}$ ) it may be assumed that this contributes to 0.5% of the take-off mass. The empty weight ( $W_E$ ) as determined with equation 3.4, consists of the contributions of the structure ( $W_{struct}$ ), powerplant ( $W_{pwr}$ ) and the fixed equipment ( $W_{feq}$ ).

$$W_{TO} = W_E + W_F + W_{PL} + W_{tfo} + W_{crew} \quad (3.3)$$

$$W_E = W_{struct} + W_{pwr} + W_{feq} \quad (3.4)$$

The approach used to determine the contributions to the structure weight is described in section 3.2.1. Next, it is explained in section 3.2.2 how the contributions to the powerplant weight are estimated. Finally, in section 3.2.2, it is described which items contribute to the fixed equipment weight and how their mass can be estimated. Before moving on to the details of the weight estimation approach, two important notes should be made first. First it should be noted that the Class II weight estimation is an iterative process. I.e. the weight of the aircraft ( $W_{TO}$ ) is estimated based on an initial estimate and thus the process should be iterated until the error between two estimates converges within 0.5% [18]. Secondly, note that based on assumptions made, the correction factors in some of the presented equations in the following sections have already been substituted. This will be indicated in the respective sections, but for clarity also a complete overview of the assumptions made is given in Appendix A.

### 3.2.1. STRUCTURAL WEIGHT ESTIMATION

The methodology to determine the structural weight ( $W_{struct}$ ) of the aircraft has been taken from chapter 5 in reference [18]. As such, the structural weight can be determined by estimating the contributions of the wing ( $W_w$ ), empennage ( $W_{emp}$ ), fuselage ( $W_f$ ), nacelles ( $W_n$ ) and landing gear ( $W_g$ ) as shown by equation 3.5. The equations used to determine these contributions will be outlined in the following paragraphs. Furthermore, it is very important to stress that all parameters in the equations presented in this section (and all of the following sections concerning weight estimation) should be substituted with the imperial unit system. Again it should be stressed that the estimation of the landing gear weight is done with an alternative method developed and described by Heerens [37].

$$W_{struct} = W_w + W_{emp} + W_f + W_n + W_g \quad (3.5)$$

Finally, an additional correction factor ( $K_{comp}$ ) can be applied to weight estimations of the wing, fuselage and empennage to account for the use of composites in these parts. The correction factor is identical to the one used in the Class I Weight Estimation and can thus be determined from figure 3.1. Again it should be stressed that this correction factor assumes going from a full metal to a full composite construction.

#### WING WEIGHT

As described in reference [18], the wing weight estimate can be obtained with the GD-method, using equation 3.6, or with Torenbeek's method as shown in equation 3.7. Note that the  $W_{MZF}$ -term in Torenbeek's method, denotes the maximum zero fuel weight. Additionally, correction factors based on the assumptions made (see Appendix A) are applied to both methods in order to account for the effect of:

- Spoilers and speed brakes
- Bending relief due to wing mounted engines
- Added weight due to flaps
- Mounting of landing gear

Note that in case more than one of these effects is applicable to the aircraft design, the corresponding correction factors should be multiplied in order to obtain the total correction factor.

#### GD-Method:

$$W_w = \frac{\{0.00428 (S^{0.48}) (A) (M_H)^{0.43} (W_{TO} n_{ult})^{0.84} (\lambda)^{0.14}\}}{[\{100(t/c)_m\}^{0.76} (\cos \Lambda_{1/2})^{1.54}]} \quad (3.6)$$

#### Torenbeek's Method:

$$W_w = 0.0017 \cdot W_{MZF} \cdot (b / \cos \Lambda_{1/2})^{0.75} \left[ 1 + \sqrt{6.3 \cdot \cos \Lambda_{1/2} / b} \right] \cdot (n_{ult})^{0.55} \cdot \{bS / [(t/c) \cdot W_{MZF} \cdot \cos \Lambda_{1/2}]\}^{0.3} \quad (3.7)$$

**EMPENNAGE WEIGHT**

Depending on the aircraft configuration, the empennage weight is obtained by adding the contributions of the horizontal tail, vertical tail and canard [18]. Equations 3.8 and 3.9 show how these contributions are estimated in the GD-method. Also, with this method the weight of the canard can be estimated by substituting its parameters into equation 3.8. Next, in equation 3.10 it is shown how the horizontal tail weight is estimated with Torenbeek's method. Note that in Torenbeek's method both the weight of the vertical tail and the canard can be estimated by substituting their parameters into equation 3.10. Finally, the  $K_h$ -factor depends on the tail type and can be determined as described in Appendix A.

**GD-Method:**

$$W_h = 0.0034 \{ (W_{TO} n_{ult})^{0.813} (S_h)^{0.584} (b_h / (t/c)_h)^{0.033} (\bar{c} / l_h)^{0.28} \}^{0.915} \quad (3.8)$$

$$W_v = 0.19 \left\{ \begin{array}{l} \sqrt{1 + z_h / b_v} (W_{TO} n_{ult})^{0.363} (S_v)^{1.089} (M_H)^{0.601} \\ (l_v)^{-0.726} (1 + S_f / S_v)^{0.217} (A_v)^{0.337} (1 + \lambda_v)^{0.363} \\ (\cos \Lambda_{1/4_v})^{-0.484} \end{array} \right\}^{1.014} \quad (3.9)$$

**Torenbeek's Method:**

$$W_h = K_h S_h \left[ 3.81 \{ (S_h)^{0.2} V_D \} / \left\{ 1000 \sqrt{\cos \Lambda_{1/2_h}} \right\} - 0.287 \right] \quad (3.10)$$

**FUSELAGE WEIGHT**

As described in reference [18], the fuselage weight estimate may be obtained with the GD-method as shown in equation 3.11. Note that in case of an aircraft with inlets in the fuselage or a buried engine, an additional correction factor  $K_{inl}$  of 1.25 should be taken into account. Furthermore, in equation 3.12 it is shown how the weight of the fuselage can be estimated, by using Torenbeek's method. Also here additional correction factors should be applied for a pressurized fuselage ( $K_f = 1.08$ ), attachment of the gear to the fuselage ( $K_f = 1.07$ ) and a top cargo floor ( $K_f = 1.1$ ). Note that these correction factors should be multiplied, for the total effect. Also, it should be clarified that the  $S_{fgs}$ -term denotes the fuselage gross shell area in feet squared.

**GD-Method:**

$$W_f = 20.86 (K_{inl})^{1.42} (\bar{q}_D / 1000)^{0.283} (W_{TO} / 1000)^{0.95} (l_f / h_f)^{0.71} \quad (3.11)$$

**Torenbeek's Method:**

$$W_f = K_f \sqrt{(V_D l_h) / (w_f + h_f)} (S_{fgs})^{1.2} \quad (3.12)$$

**NACELLE WEIGHT**

The nacelle weight estimated with the GD- and Torenbeek's method is assumed to consist of the structural weight of the external ducts and cowls as well as the pylon [18]. The weight of any other engine component is included in the powerplant weight estimation, which is described in section 3.2.2. As such, the nacelle weight of turbofan engines can be estimated with GD-method, using with equation 3.13. In Torenbeek's method the nacelle weight depends on the by-pass ratio of the engine (BPR). For engines with a low BPR, the nacelle weight may be estimated using equation 3.14, while equation 3.15 should be used for high BPR engines. Finally, note that all these equations account for the nacelle weight of all engines.

**GD-Method:**

$$W_n = 7.435 (N_{inl}) \left\{ \sqrt{A_{inl}} (l_n) (P_2) \right\}^{0.731} \quad (3.13)$$

**Torenbeek's Method:**

$$W_n = 0.055 T_{TO} \quad (3.14)$$

$$W_n = 0.065 T_{TO} \quad (3.15)$$

### 3.2.2. POWERPLANT WEIGHT ESTIMATION

As described in chapter 6 of reference [18], the powerplant weight estimate is obtained by adding the contributions of the engines ( $W_e$ ), the air induction system ( $W_{ai}$ ), fuel system ( $W_{fs}$ ) and propulsion system ( $W_p$ ) as shown in equation 3.16. In the following paragraphs it will be described how the weight of these components may be estimated using the GD- and Torenbeek's method. Also note that for business jet aircraft the weight of the propeller ( $W_{prop}$ ) can simply be omitted.

$$W_{pwr} = W_e + W_{ai} + W_{prop} + W_{fs} + W_p \quad (3.16)$$

#### ENGINES AND AIR INDUCTION SYSTEM

The equations to estimate the weight of the engines, using the GD- and Torenbeek's method can be found in chapter 6.1 of reference [18]. For this research however, it was decided to use the engine weight estimation already implemented in the Initiator. In this method the engine weight is estimated as a function the required on the required power/thrust obtained from the wing and thrust loading module. More specifically, the engine weight is estimated from a linear trend-line, relating the required power/thrust to the engine weight based on the data of 122 turbojet and turbofan engines.

In both the GD- and Torenbeek's method, the air-induction system is considered to be a part of the nacelle for podded engines [18]. Therefore their contributions are included in the nacelle weigh as calculated with equation 3.13 and 3.14 or 3.15. Note that this method cannot be applied for engines that are buried within the fuselage or wing. This type of inlets however, are considered to be outside of this research's scope.

#### FUEL SYSTEM

For both the GD- and Torenbeek's method, the fuel system's weight estimate highly depends on the type of fuel tank used [18]. Now, for this research it was assumed that integral fuel tanks or a so-called wet wing is used. This is generally true for most commercial and business jet aircraft and has as additional advantage that equation 3.17 may be used for both GD and Torenbeek. For the assumptions made when implementing this equation in the Initiator, Appendix A should be consulted.

#### GD- and Torenbeek's Method:

$$W_{fs} = 80(N_e + N_t - 1) + 15\sqrt{N_t}(W_f/K_{fsp})^{0.333} \quad (3.17)$$

#### PROPULSION SYSTEM

According to the GD method, the propulsion system consists of the engine controls, engine starting system and the propeller controls [18]. Note that in this research the weight of the propeller controls are neglected and therefore the weight of the propulsion system can be estimated with equation 3.18. Furthermore, note that equation 3.19 is only valid for rear-fuselage-mounted engines, which are the most common for business jet aircraft. A similar relation for wing-mounted engines can be found in reference [18]. Both equations were implemented within the Initiator, such that the updated Class II weight estimation module can also be used for large conventional aircraft.

In order to estimate the weight of the propulsion system for turbofan and turbojet engines with Torenbeek's method, equation 3.21 should be used, which includes the contributions of the starting systems, accessory drives, controls, starting and ignition systems [18]. Note that in Torenbeek's method, the weight contribution of the thrust reversers is included in the nacelle weight.

#### GD-method:

$$W_p = W_{ec} + W_{ess} \quad (3.18)$$

$$W_{ec} = K_{ec}(l_f N_e)^{0.792} \quad (3.19)$$

$$W_{ess} = 9.33(W_e/1000)^{1.078} \quad (3.20)$$

#### Torenbeek's method:

$$W_p = 36N_e(dW_f/dt)_{TO} \quad (3.21)$$

### 3.2.3. FIXED EQUIPMENT WEIGHT ESTIMATION

As described in chapter 7 of reference [18], the fixed equipment highly depends on the aircraft type and its nominal mission. For this research it is assumed that the fixed equipment for commercial and business jet aircraft consists of the following components:

- Flight controls ( $W_{fc}$ )
- Hydraulic and pneumatic system ( $W_{hps}$ )
- Instrumentation, avionics & electronics ( $W_{iae}$ )
- Air-conditioning, pressurization, anti- & de-icing system ( $W_{api}$ )
- Oxygen system ( $W_{ox}$ )
- Auxiliary Power Unit ( $W_{apu}$ )
- Furnishing ( $W_{fur}$ )
- Operational items ( $W_{ops}$ )
- Paint ( $W_{pt}$ )

In the following paragraphs the relations are given to estimate these weight contributions with the GD- and Torenbeek's method. Again, note that for the majority of these equations, the correction factors are already substituted based on the assumptions which can be found in Appendix A.

#### FLIGHT CONTROLS

As shown in chapter 7.1 of reference [18], the weight of the flight control system can be estimated with equation 3.22. The weight contribution of the flight controls can also be estimated with Torenbeek's method, for which equation 3.23 should be used. Note that the contributions of the hydraulic and pneumatic systems, which are used to drive the flight control system, are also taken into account by these relations. Finally, it should also be mentioned that these equations do not account for the added weight in the control system due to relaxed static stability. For instance, it is not unthinkable that a stability augmentation system is required, which would increase the control system's weight. To solve this issue, a correction factor may be applied to the obtained result, accounting for the increase in flight controls weight.

#### GD-method:

$$W_{fc} = 56.01 \{ (W_{TO}) (\bar{q}_D) / 100000 \}^{0.576} \quad (3.22)$$

#### Torenbeek's method:

$$W_{fc} = 0.64 (W_{TO})^{2/3} \quad (3.23)$$

#### ELECTRICAL SYSTEM

Equation 3.24 shows how the weight of the electrical system can be estimated with the GD-method [18]. Observe that in this method, the weight of the electrical system is dependent on the weight of the fuel system and the weight contributions of the instruments/avionics. The weight of the electrical system can also be estimated using Torenbeek's method and in this case, equation 3.25 should be used. Note that this equation is only valid for jet aircraft. Also, from this equation it can be observed that in Torenbeek's method the weight of the electrical system, mainly depends on the volume of the passenger cabin [18].

#### GD-method:

$$W_{els} = 1163 \{ (W_{fs} + W_{iae}) / 1000 \}^{0.506} \quad (3.24)$$

#### Torenbeek's method:

$$W_{els} = 10.8 (V_{pax})^{0.7} \{ 1 - 0.018 (V_{pax})^{0.35} \} \quad (3.25)$$

#### INSTRUMENTATION, AVIONICS AND ELECTRONICS

The weight of the instrumentation can be estimated with the modified GD-method, as shown in equation 3.26. The first term in this equation accounts for the flight instruments and is thus dependent on the amount of pilots ( $N_{pil}$ ). The second term accounts for the engine instruments while the two final terms are used to

estimate the mass of the remaining instruments [18]. Secondly, the instruments' weight may also be estimated with Torenbeek's method, using equation 3.27 or 3.28. Note that the first relation is valid for regional transport aircraft, while the second should be applied to jet transport aircraft, both have been implemented within the Initiator. Finally, note that most modern aircraft make use of so-called "glass cockpits" and thus the weight predicted with these methods will be a rather conservative estimate.

**GD-method:**

$$W_i = N_{pil} \{1 + 0.032 (W_{TO}/1000)\} + N_e \{5 + 0.006 (W_{TO}/1000)\} + 0.15 (W_{TO}/1000) + 0.012 W_{TO} \quad (3.26)$$

**Torenbeek's method:**

$$W_{iae} = 120 + 20N_e + 0.006 W_{TO} \quad (3.27)$$

$$W_{iae} = 0.575 (W_E)^{0.556} (R)^{0.25} \quad (3.28)$$

### AIR CONDITIONING, PRESSURIZATION AND DE-ICING

As described in chapter 7.5 of reference [18] the weight contribution of the air conditioning, pressurization and de-icing system combined may be estimated using equation 3.29 or 3.30. Note, that in the Torenbeek relation, the  $l_{pax}$ -term is the length of passenger cabin and that these relations are only valid for pressurized aircraft.

**GD-method:**

$$W_{api} = 469 \{V_{pax} (N_{cr} + N_{pax}) / 1000\}^{0.419} \quad (3.29)$$

**Torenbeek's method:**

$$W_{api} = 6.75 (l_{pax})^{1.28} \quad (3.30)$$

### OXYGEN SYSTEM

Rather surprisingly, the weight of the oxygen system is not included in the contribution of the pressurization system. Equation 3.31 shows how this system's weight may be estimated with the GD-method. Torenbeek's method is slightly more complex and makes the distinction between regional and long range aircraft as indicated by equations 3.32 and 3.33. Note that Torenbeek's method also includes a third relation for general aviation aircraft cruising below 25000ft. This type of aircraft however cannot be analysed by the Initiator and thus this relation was not included in the updated *Class2WeightEstimation*-module

**GD-method:**

$$W_{ox} = 7 (N_{cr} + N_{pax})^{0.702} \quad (3.31)$$

**Torenbeek's method:**

$$W_{ox} = 30 + 1.2 N_{pax} \quad (3.32)$$

$$W_{ox} = 40 + 2.4 N_{pax} \quad (3.33)$$

### FURNISHING WEIGHT

The method to estimate the furnishing weight with the GD- and Torenbeek's method has been taken from chapter 7.8 in reference [17]. Note that these equations also account for the weight of operational items such as food, potable water, drink, china and lavatory supplies.

**GD-method:**

$$W_{fur} = N_{fdc} + 32N_{pax} + 15N_{cc} + 3.9(N_{pax})^{1.33} + 1.02(N_{pax})^{1.12} + 109\{(N_{pax}(1 + P_c))/100\}^{0.505} + 0.771(W_{TO}/1000) \quad (3.34)$$

**Torenbeek's method:**

$$W_{fur} = 0.211(W_{TO} - W_F)^{0.91} \quad (3.35)$$

**OTHER ITEMS**

Finally, there are some minor contributions that still need to be added to the fixed equipment. For this research, only the contributions of the the APU and the aircraft paint are taken into account. There is no separate GD- or Torenbeek method to estimate weight of these component, their weight is simply set to be the following ratio of the take-off weight [18]:

$$W_{apu} = 0.008W_{TO} \quad (3.36)$$

$$W_{paint} = 0.0045W_{TO} \quad (3.37)$$

**3.3. STABILITY & CONTROL DERIVATIVE ESTIMATION**

Table 3.1: Overview of the calculated stability derivatives

Derivative	Explanation	Section
$C_{L\alpha}$	Lift-due-to-angle-of-attack derivative	3.3.2
$C_{D\alpha}$	Drag-due-to-angle-of-attack derivative	3.3.2
$C_{m\alpha}$	Pitching-moment-due-to-angle-of-attack derivative	3.3.2
$C_{y\beta}$	Sideforce-due-to-sideslip derivative	3.3.3
$C_{l\beta}$	Rolling-moment-due-to-sideslip derivative	3.3.3
$C_{n\beta}$	Yawing-moment-due-to-sideslip derivative	3.3.3
$C_{yp}$	Sideforce-due-to-roll-rate derivative	3.3.4
$C_{lp}$	Rolling-moment-due-to-roll-rate derivative	3.3.4
$C_{np}$	Yawing-moment-due-to-roll-rate derivative	3.3.4
$C_{Dq}$	Drag-due-to-pitch-rate derivative	3.3.5
$C_{Lq}$	Lift-due-to-pitch-rate derivative	3.3.5
$C_{mq}$	Pitching-moment-due-to-pitch-rate derivative	3.3.5
$C_{yr}$	Sideforce-due-to-yaw-rate derivative	3.3.6
$C_{lr}$	Rolling-moment-due-to-yaw-rate derivative	3.3.6
$C_{nr}$	Yawing-moment-due-to-yaw-rate derivative	3.3.6

The stability and control derivatives are required to estimate the static and dynamic stability as well as the handling qualities of aircraft on a preliminary level. Therefore, to estimate these derivatives, the methodology as described in reference [20] has been used, which is in essence a simplified version of the DATCOM methodology (see reference [34]). This approach was chosen as it is a purely empirical method, allowing for quick estimation of the stability and control derivatives. The downside of this method however, is that it is less accurate than for instance vortex-lattice based methods (see reference [38]) and as a consequence correction factors to obtain the correct derivative may be required [39]. Furthermore, a couple of comments need to be made with respect to the validity of the presented method:

- Aero-elastic effects are not taken into account, hence rigid aircraft are assumed.
- Although the speed regime for which the selected method is valid depends from derivative to derivative, the selected approach should not be used for aircraft with a cruise speed higher than  $M = 0.9$
- All the derivatives estimated with this are calculated in ( $rad^{-1}$ ) and are derived with respect to the stability axes system.
- All parameters in the equations presented in the following paragraphs should be substituted in imperial units.

Now, because business jet aircraft are relatively small and have for instance a small to almost non-existing wing flex, the first comment does not really impose a limit on the use of the selected approach for this type of aircraft. If the derivatives of a larger aircraft with larger wingflex need to be determined however, the results obtained should be critically reviewed. Furthermore, quite often in flight mechanics, the derivatives are required to be calculated with respect to the body-axis reference frame. The derivatives obtained with this approach can be converted to this reference frame by a simple rotation matrix transformation over the aircraft's angle of attack. Finally, Table 3.1 shows an overview of the stability derivatives estimated as part of this research, as well as the section in which the method of estimation is described in more detail.

### 3.3.1. STEADY STATE COEFFICIENTS

Before estimating an aircraft's stability and control characteristics, the steady state conditions of the aircraft have to be determined first, as it is around these conditions that the derivatives will be estimated. For this research only two steady state coefficients are estimated, being the steady state lift coefficient ( $C_{L_1}$ ) and the steady state drag coefficient ( $C_{D_1}$ ). Now, the method to estimate the steady state lift coefficient is straightforward and is given by equation 3.38 [20]. Note that the  $n$ -factor in this equation denotes the aircraft load factor, which is equal to one in steady symmetric flight. The drag coefficient is directly obtained from the lift-drag polar as shown in equation 3.39 and in Figure 3.3. In this research, the drag polar is directly obtained from the Initiator's drag estimation module, which uses the drag prediction methods of [6] and [20] to calculate the drag polar in clean, take-off and landing conditions.

$$C_{L_1} = \frac{nW}{\bar{q}S} \quad (3.38)$$

$$C_{D_1} = f(C_{L_1}) \quad (3.39)$$

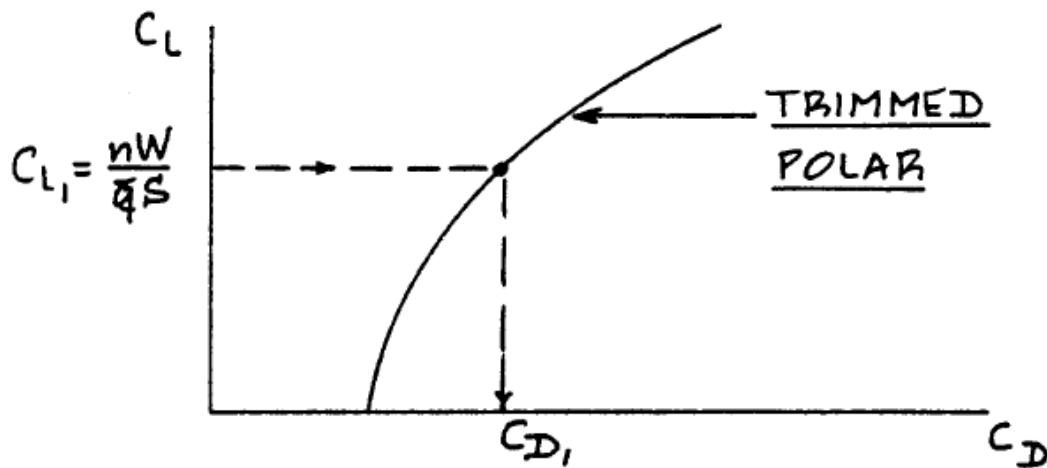


Figure 3.3: Estimation of  $C_{D_1}$  from the Drag Polar [20]

### 3.3.2. ANGLE OF ATTACK DERIVATIVES ( $C_{L_\alpha}$ , $C_{D_\alpha}$ , $C_{m_\alpha}$ )

As described in reference [20], before any angle of attack derivative can be estimated, the 3D lift curve slope of all lifting surfaces ( $C_{L_{\alpha_s}}$ ) should be estimated first. To this purpose equation 3.40 is used, which transforms the 2D lift curve slope by taking the effects of aspect ratio ( $A$ ), mid-chord sweep angle ( $\Delta_{c/2}$ ) and the ratio of the aerofoil lift slope to the theoretical flat plate slope ( $k$ ) into account. Also, observe that compressibility is taken in account by the  $\beta$ -term, denoting the Prandtl-Glauert compressibility correction factor.

$$C_{L_{\alpha_s}} = \frac{2\pi A}{2\sqrt{(A^2\beta^2/k^2)(1 + \tan^2(\Lambda_{c/2})/\beta^2) + 4}} \quad (3.40)$$

Next, the aircraft's lift curve slope ( $C_{L_\alpha}$ ) is estimated by adding the contributions of the wing-fuselage combination ( $C_{L_{\alpha_{wf}}}$ ), the horizontal tail ( $C_{L_{\alpha_h}}$ ) and the canard ( $C_{L_{\alpha_c}}$ ), as shown in equation 3.41. Moreover, it can be observed in this equation that the wing's contribution to  $C_{L_\alpha}$  is corrected with a wing-fuselage interference factor ( $K_{wf}$ ) in order to obtain the wing-fuselage combination's contribution. Next, the horizontal tail and the canard's contributions are calculated, by correcting with the dynamic pressure ratio ( $\eta_h$ ), the ratio of the tail's surface over the main wing's surface ( $S_h/S$ ) and the downwash/upwash gradient ( $d\varepsilon/d\alpha$ ). Note that the methods to determine these correction factors are described in more detail in chapter 8 of reference [20].

$$C_{L_\alpha} = K_{wf}C_{L_{\alpha_w}} + C_{L_{\alpha_h}}\eta_h(S_h/S)(1 - d\varepsilon/d\alpha) + C_{L_{\alpha_c}}\eta_c(S_c/S)(1 + d\varepsilon/d\alpha) \quad (3.41)$$

Next, to determine  $C_{D_\alpha}$ , it is assumed that the drag polar is parabolic and therefore equation 3.42 holds. Note that the  $C_{L_1}$ -term in this equation is the steady state lift coefficient, which was already determined with equation 3.38.

$$C_{D_\alpha} = \left(\frac{2C_{L_1}}{\pi Ae}\right)C_{L_\alpha} \quad (3.42)$$

To determine the aircraft's pitching-moment-due-to-angle-of-attack derivative, the variation of aircraft pitching moment with lift coefficient has to be estimated first. As shown by equation 3.43, this is done by estimating the distance between the aircraft's centre of gravity and the aircraft aerodynamic centre, both normalized with respect to the mean aerodynamic chord. Just like the lift curve slope, the aerodynamic centre is calculated by taking the contributions of wing-fuselage combination, horizontal tail and canard into account and correcting them with the same factors as mentioned before.  $C_{m_\alpha}$  can then be estimated with equation 3.44

$$(dC_m/dC_L) = \bar{x}_{ref} - \bar{x}_{ac} \quad (3.43)$$

$$C_{m_\alpha} = (dC_m/dC_L)C_{L_\alpha} \quad (3.44)$$

Finally, when implementing this methodology in the Initiator, it was discovered that the method proposed by Roskam has the tendency to over-estimate the forward shift in the aircraft's aerodynamic centre due to the fuselage considerably. Therefore, it was decided to estimate this effect with another approach, which is shown by equation 3.45. This equation relates the shift in aerodynamic centre to the fuselage length ( $L$ ) and the longitudinal position of the wing's quarter chord on the fuselage ( $X$ ) and is based on an empirical fit to wind tunnel test data [40]. It should be emphasized that this equation may only be used for swept-back wings, because it is unable to predict the rearward shift in aerodynamic centre due to forward-swept wings.

$$\Delta x_{ac} = -0.148 \frac{X}{L} \quad (3.45)$$

### 3.3.3. SIDESLIP DERIVATIVES ( $C_{y_\beta}, C_{l_\beta}, C_{n_\beta}$ )

The first angle of sideslip derivative to be estimated, is the sideforce-due-to-sideslip ( $C_{y_\beta}$ ). As shown in equation 3.46, this derivative consists of the contributions of the wing, fuselage and vertical tail. The wing contribution is negative and a function of the dihedral angle ( $\Gamma$ ). The fuselage's contribution is also negative and depends on a correction factor ( $K_i$ ), the wing area ( $S$ ) and the fuselage cross-sectional area at the point where the flow ceases to be potential ( $S_0$ ). Note that the  $K_i$  correction factor is dependent on the fuselage's diameter and the vertical wing position. The vertical tail's contribution ( $C_{y_{\beta_v}}$ ) is determined in an analogue manner as the horizontal tail's contribution to  $C_{L_\alpha}$ . The only difference is an empirical correction factor  $k_v$ , dependent on the fuselage depth ( $2r_1$ ) and vertical tail span ( $b_v$ ). Note that twin vertical tails have not been taken into account. Also note that the methods to estimate the aforementioned correction factors are described in more detail in chapter 10 of reference [21].

$$C_{y_\beta} = C_{y_{\beta_w}} + C_{y_{\beta_f}} + C_{y_{\beta_v}} \quad (3.46)$$

Next,  $C_{l_\beta}$  or the dihedral effect, consists of the contributions of the wing-fuselage combination, the horizontal tail and the vertical tail (see equation 3.47). The wing-fuselage combination's contribution depends amongst other variables on the wing-fuselage lift coefficient ( $C_{L_{wf}}$ ), wing & fuselage geometry, and correction factors for compressibility ( $K_M$ ) and fuselage induced effect on the wing height ( $\Delta C_{l_\beta}/\Gamma$ ). The horizontal tail's contribution is calculated in an analogue way, with an additional correction for the ratio of the horizontal tail's size over the main wing's size ( $S_h b_h/Sb$ ). The vertical tail's contribution is estimated by correcting  $C_{y_{\beta_v}}$  for the horizontal and vertical tail arms ( $l_v$  and  $z_v$ ),  $\alpha$  and the main wing span ( $b$ ).

$$C_{l_\beta} = C_{l_{\beta_{wf}}} + C_{l_{\beta_h}} + C_{l_{\beta_v}} \quad (3.47)$$

$C_{n_\beta}$  or the static directional stability consists of the contributions of the main wing, fuselage and vertical tail as shown in equation 3.48. The wing's contribution is only important at high angles of attack and therefore assumed to be zero. The fuselage's contribution is determined purely empirical, with important contributions of the fuselage length ( $l$ ) and side area ( $S_{b_s}$ ). The vertical tail's contribution is determined in an analogue way as for  $C_{l_\beta}$ .

$$C_{n_\beta} = C_{n_{\beta_w}} + C_{n_{\beta_f}} + C_{n_{\beta_v}} \quad (3.48)$$

### 3.3.4. ROLL RATE DERIVATIVES ( $C_{y_p}$ , $C_{l_p}$ , $C_{n_p}$ )

Before explaining how the roll rate derivatives are estimated, it should be specifically mentioned that the method presented here is only applicable to the subsonic speed regime. For other speed regimes, it is suggested to use the DATCOM method [34]. That being said, the first derivative to be calculated with respect to roll rate is the sideforce-due-to-roll-rate or  $C_{y_p}$ . As shown by equation 3.49, this derivative is primarily influenced by the vertical tail. Furthermore it may be also be observed from this equation that this derivative also depends on the rolling-moment-due-to-roll-rate derivative for zero lift and dihedral.

$$C_{y_p} = 2C_{y_{\beta_v}} (z_v \cos \alpha - l_v \sin \alpha - z_v) / b + 3 \sin \Gamma [1 - (4z/b) \sin \Gamma] \left( C_{l_p} \right)_{C_L=0, \Gamma=0} \quad (3.49)$$

As shown in equation 3.50,  $C_{l_p}$  or the roll damping derivative consist of the main wing's, horizontal tail's and vertical tail's contributions. Note that the fuselage's contribution to this derivative can be neglected. The main wing's contribution is determined by taking the roll damping parameter ( $\beta C_{l_p}/\kappa$ ), the wing lift curve slope ( $C_{L_{\alpha_w}}$ ), the dihedral effect, the wing drag contribution into account. The horizontal tail's contribution is calculated in a similar way as the main wing's and then corrected for some geometrical parameters such as the tail surface and span. The vertical tail's contributions consists of the vertical tail contribution to  $C_{y_\beta}$ , corrected for  $\alpha$  and the horizontal and vertical tail arms.

$$C_{l_p} = C_{l_{pw}} + C_{l_{ph}} + C_{l_{pv}} \quad (3.50)$$

The final roll rate derivative ( $C_{n_p}$ ), consists of the contributions of main wing and vertical tail as shown by equation 3.51. The wing's contributions consists of contributions due to the main wing lift ( $C_{L_w}$ ), the main twist ( $\epsilon$ ) and the flap deflection ( $\delta_f$ ). The main wing lift contribution is corrected for geometrical parameters such as aspect ratio, quarter-chord sweep and compressibility. The wing twist contribution is using look-up tables produced with the DATCOM method [34]. The flap contribution depends on the  $\Delta C_l$  caused by the flap, the clean aerofoil lift slope ( $C_{l_\alpha}$ ) and the flap deflection itself. It should be stressed that in the stability and control derivative estimation module, in which this method was implemented, only the  $\Delta C_l$  for plain flaps was implemented. As a consequence, the results obtained with this module for aircraft with other flap types should be critically reviewed. Finally, the vertical tail contribution exists of  $C_{y_{\beta_v}}$ , corrected for the main wing span and the horizontal and vertical tail arms.

$$C_{n_p} = C_{n_{pw}} + C_{n_{pv}} \quad (3.51)$$

### 3.3.5. PITCH RATE DERIVATIVES ( $C_{D_q}$ , $C_{L_q}$ , $C_{m_q}$ )

Similar to the roll rate derivatives, it should be noted that the method presented here is only applicable to the subsonic speed regime. For higher speeds, the DATCOM method should be consulted [34]. Furthermore, the first derivative to be estimated with respect to pitch is  $C_{D_q}$ , which negligible for most aircraft.

The lift-due-to-pitch rate is thus the first derivative to be estimated in this category and consists of the contributions of the main wing, horizontal tail and canard as shown in equation 3.52. The wing's contribution should be estimated at zero Mach first and then be corrected for aspect ratio, quarter chord-sweep and compressibility. The contribution at zero Mach mainly depends on the main wing's lift slope and the static margin. The horizontal tail's contribution mainly depends on the horizontal tail's lift slope, dynamic pressure ratio with respect to the wing and the tail volume coefficient. The canard's contribution is estimated in the same way. Again note that a more detailed explanation on how to estimate these contributions can be found in chapter 10 of reference [20].

$$C_{l_q} = C_{l_{qw}} + C_{l_{qh}} + C_{l_{qc}} \quad (3.52)$$

$C_{m_q}$  or the pitch damping derivative consists of the same contributions as  $C_{L_q}$ , see equation 3.53. The wing contribution to the pitching moment should again be estimated at zero Mach first and then be corrected for the main wing's geometrical properties. The horizontal tail and canard contribution are estimated in a similar fashion as for  $C_{L_q}$ , but should be multiplied by their respective tail arms.

$$C_{m_q} = C_{m_{qw}} + C_{m_{qh}} + C_{m_{qc}} \quad (3.53)$$

### 3.3.6. YAW RATE DERIVATIVES ( $C_{y_r}, C_{l_r}, C_{n_r}$ )

The final set of stability derivatives estimated in this research are those with respect to yaw rate and the first estimated derivative in this group is the sideforce-due-to-yaw-rate derivative or  $C_{y_r}$ . This derivative is primarily influenced by the vertical tail and for subsonic speeds (see sections 3.3.4 & 3.3.5), it may be estimated using equation 3.54.

$$C_{y_r} = -2 \left( C_{y_{\beta_v}} \right) (l_v \cos \alpha + z_v \sin \alpha) / b \quad (3.54)$$

As can be seen in equation 3.55, the rolling-moment-due-to-yaw-rate depends on the contributions of wing and vertical tail. Just as  $C_{n_{pw}}, C_{l_{rw}}$  depends on the contributions of the wing to the rolling moment, the wing twist and the flap deflection. Now, however is that here the dihedral effect should be taken into account as well. The vertical tail's contribution estimated by correcting  $C_{y_{\beta_v}}$  for  $b, l_v, z_v$  and  $\alpha$ .

$$C_{l_r} = C_{l_{rw}} + C_{l_{rv}} \quad (3.55)$$

Finally, the yaw-damping derivative or  $C_{n_r}$  depends on the contributions of the wing and vertical tail as shown in equation 3.56. The wing's contribution is a function of the lifting effect, the wing lift coefficient, the drag effect and the wing's zero lift drag. The vertical tail's contribution is again a function of  $C_{y_{\beta_v}}, b, l_v, z_v$  and  $\alpha$ .

$$C_{n_r} = C_{n_{rw}} + C_{n_{rv}} \quad (3.56)$$

### 3.3.7. CONTROL DERIVATIVES

Roskam's empirical approach is also used to determine the control derivatives and is described in chapter 10.3 of reference [20]. In this research, only the control derivatives of the elevator, ailerons and rudder are estimated. Note that modern aircraft also use other control surfaces, such as for instance spoilers or flaperons for roll-control. The estimation of these surfaces' control derivatives however, is considered to be outside of the scope of this research.

To estimate the elevator control derivatives, the horizontal tail's lift, drag and pitching moment contributions need to be estimated first. The stabilizer's drag may be estimated from equation 3.57, note that all terms without the h-subscript refer to the wing. The stabilizer's lift due to incidence can then be estimated from the horizontal tail's lift-due-to-angle-of-attack derivative using equation 3.58. Finally, also the stabilizer's pitching moment may be estimated from equation 3.59. Note that an analogue approach may be used to also estimate the lift, drag and pitching moment contributions of a canard.

$$C_{D_{i_h}} = 2 [C_L / \pi A e] (C_{L_h}) \eta_h (S_h / S) \quad (3.57)$$

$$C_{L_{i_h}} = \eta_h (S_h / S) C_{L_{\alpha_h}} \quad (3.58)$$

$$C_{m_{i_h}} = - (C_{L_{\alpha_h}}) \eta_h \tilde{V}_h \quad (3.59)$$

Now, the control surfaces are considered to be plain flaps which cause a change in local angle of attack. The derivative of angle of attack with respect to the elevator deflection ( $\alpha_{\delta_e}$ ) can be estimated with equation 3.60. In this equation  $K_b$  is the elevator span factor,  $(c_{l_\delta} / (c_{l_\delta})_{theory})$  is a correction factor for plain flaps,  $(c_{l_\delta})_{theory}$  is the theoretical elevator effectiveness,  $k'$  is a correction factor accounting for non-linear flap (elevator) behaviour and  $\{(\alpha_\delta)_{C_L}\} / \{(\alpha_\delta)_{C_l}\}$  accounts for the effect of aspect ratio and chord ratio on the elevator effectiveness. All these correction factors may be found with the methods presented in chapter 8 of reference [20].

$$\alpha_{\delta_e} = K_b \left\{ (c_{l_\delta} / (c_{l_\delta})_{theory}) \right\} (c_{l_\delta})_{theory} (k' / C_{L_{\alpha_h}}) [\{(\alpha_\delta)_{C_L}\} / \{(\alpha_\delta)_{C_l}\}] \quad (3.60)$$

The elevator control derivatives may then be estimated by multiplying the change in local angle of attack with the stabilizer control derivatives, as shown in equations 3.61 to 3.63. Finally, note that similar procedures were used to estimate the rudder and aileron control derivatives.

$$C_{D_{\delta_e}} = (\alpha_{\delta_e}) C_{D_{i_h}} \quad (3.61)$$

$$C_{L_{\delta_e}} = (\alpha_{\delta_e}) C_{L_{i_h}} \quad (3.62)$$

$$C_{m_{\delta_e}} = (\alpha_{\delta_e}) C_{m_{i_h}} \quad (3.63)$$

### 3.4. INERTIA ESTIMATION

As mentioned in chapter 2, the general procedure to estimate a body's mass moment of inertia around a random axis, is to estimate the two contributions as shown in equation 3.64. Recall that the first term indicates the body's mass moment of inertia around an axis symmetrical to the random axis and through its own centroid. The second contribution is the so-called Steiner-term and consists of the object's mass times the distance to the random axis squared.

$$I = I_0 + mr^2 \quad (3.64)$$

Now, for this research we are interested in estimating the aircraft's mass moment of inertia tensor around the body axis system. To this purpose, the method described in reference [31] is used, which relies heavily on the work of the DARcorporation, as described in [32] and [33]. In this method, four types of aircraft parts are distinguished and for each type, a different approach is used to estimate their contributions to the mass moment of inertia tensor. Firstly, there are the bodies of revolution (cylindrical objects), for which the inertia tensor is estimated with a lumped mass method described in section 3.4.1. Next, there are the lifting surfaces, for which two separate methods are used: one for the main wing and another for the tail surfaces. For the main wing also a lumped mass method is used, based on the results of the Initiator's EMWET module. For all other lifting surfaces the DATCOM method is used and both methods are explained in section 3.4.2. Finally, all other aircraft parts are assumed to be point masses and the method used to determine their contributions to the inertia tensor is discussed in section 3.4.3.

#### 3.4.1. BODIES OF REVOLUTION

To estimate the contributions of cylindrical objects to the inertia tensor, the method as described in reference [32] is used. As such, with this approach an estimate for the inertia contributions of the fuselage as well as the nacelles (not the engines!) can be obtained. In this approach, the cylindrical object is divided first into longitudinal stations, such that cross-sections as shown in Figure 3.4 are obtained. The mass of the cylinder is then divided over the cross-sectional stations by using equation 3.65. Next, the mass per station is divided

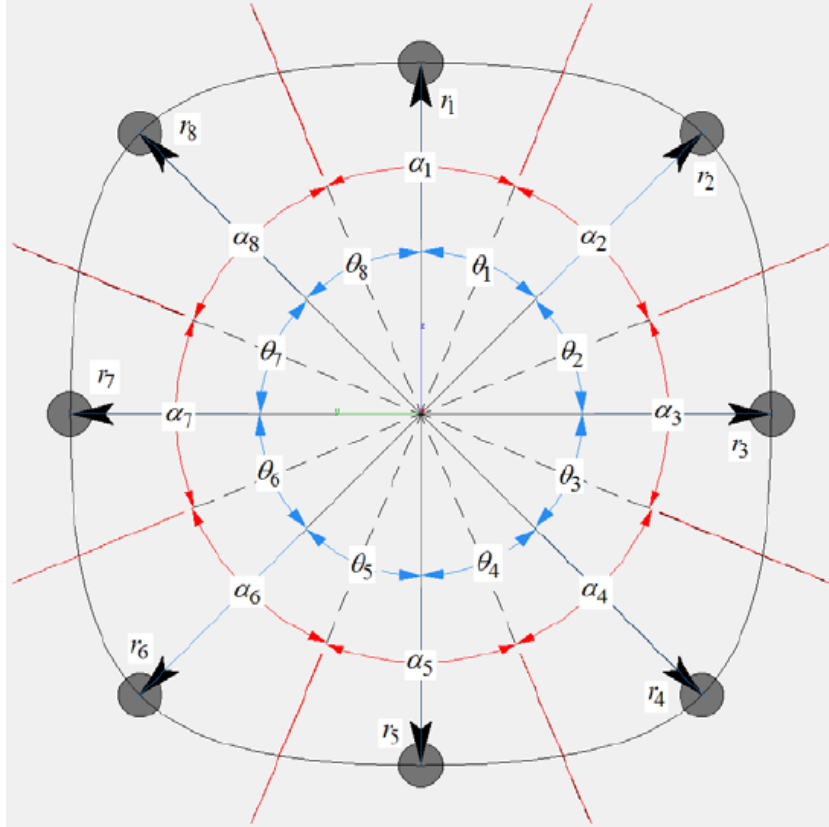


Figure 3.4: Example of cylindrical cross-section with distribution of lumped masses [32]

over 8 lumped masses as shown in Figure 3.4. The weight of these point masses can be estimated by using equation 3.66. The effect of a fuselage floor is incorporated by using a correction factor to concentrate more mass at the bottom lumped mass (mass 5). This correction factor is set to 1 for the nose and tail sections of the fuselage and 2 for the center sections. Obviously, in the case of nacelles no floor is present and thus no correction factor is used. Moreover, the position of these point masses needs to be estimated as well. The position coordinates of these point masses depend on the object's geometry and can be determined with simple trigonometry.

$$W_i = W_f \frac{A_{fus_i}}{\sum A_{fus_i}} \quad (3.65)$$

$$W_j = W_i \frac{S_j}{\sum S_j} \quad (3.66)$$

With the masses and their geometrical coordinates known, the moments of inertia for each point mass can be estimated by using equations 3.67 to 3.70. As shown by these equations, it is assumed that lumped masses' mass moment of inertia around their centre of gravity is zero, which is a valid assumption provided that the fuselage is divided in a large amount of lumped masses. Finally, the moments of inertia should be added for all point masses to obtain cross-sectional moments of inertia, which in its turn should be summed to obtain the fuselage's and nacelles' moments of inertia contributions.

$$I_{xx_j} = W_j \left[ (y_{cg_j} - Y_{cg})^2 + (z_{cg_j} - Z_{cg})^2 \right] \quad (3.67)$$

$$I_{yy_j} = W_j \left[ (z_{cg_j} - Z_{cg})^2 + (x_{cg_j} - X_{cg})^2 \right] \quad (3.68)$$

$$I_{zz_j} = W_j \left[ (x_{cg_j} - X_{cg})^2 + (y_{cg_j} - Y_{cg})^2 \right] \quad (3.69)$$

$$I_{xz_j} = W_j \left[ (x_{cg_j} - X_{cg})(z_{cg_j} - Z_{cg}) \right] \quad (3.70)$$

### 3.4.2. LIFTING SURFACES

Two approaches are used to estimate the moments of inertia contributions of the lifting surfaces. The main wing's inertia tensor is estimated with the method as described in reference [33]. This approach requires knowledge on the wing's geometry as well as the distribution of masses for key components in the main wing such as the skins and spars. In order to obtain the distribution of these masses, the results of the Initiator's *EMWETWeight*-module are used.

Now, the main issue with EMWET, is that it estimates the wing weight by sizing the wingbox for the given input loads first and then applies a correction factor in order to estimate the weight of secondary components. Note that in the Initiator, the input loads for EMWET are determined using AVL. This correction factor has only been validated for main wings and therefore, EMWET may only be used to estimate the weight of wings and not that of horizontal and vertical tailplane's. Therefore, another approach is required to estimate the inertia tensor of these lifting surfaces and to this purpose section 8.1 of the DATCOM method is used [34].

### MAIN WING

As stated before, the approach to estimate the main wing's contribution to the aircraft mass moment of inertia tensor has been taken from reference [33]. Now, in analogy with the method used for cylindrical objects, the wing mass is first divided over a number of span-wise stations. For convenience, the number of spanwise stations is set equal to the amount of span-wise stations from EMWET. Next, the mass at the wing stations, is spread over the aerofoil in 5 lumped masses as shown in Figure 3.5. The area of the aerofoil and its segments is then calculated by integrating the thickness chord-wise, for which equation 3.71 may be used. Note that this equation should be integrated over the segments to obtain the areas of those respective segments.

$$A_{aerofoil_i} = 10C_{\eta_i}^2 (t/c) \left( 0.197933x^3 - 0.063x^2 - 0.1172x^3 + 0.071075x^4 - 0.0203x^5 \right)_0^1 \quad (3.71)$$

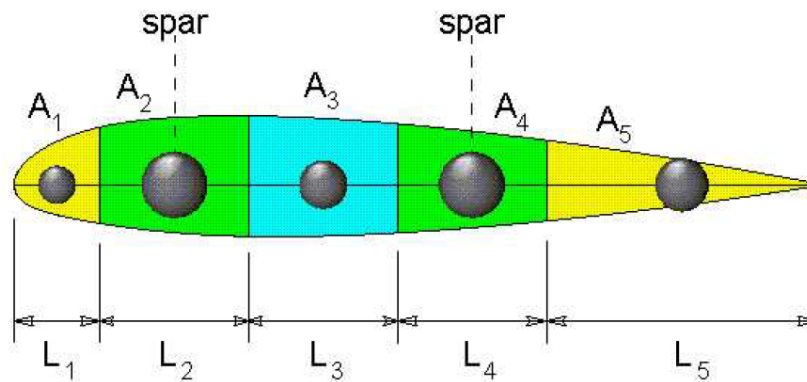


Figure 3.5: Example of aerofoil cross-section with distribution of lumped masses [33]

Next, the intermediate parameter ( $m$ ) has to be calculated for which equation 3.75 can be used. The parameters A1 and B1 can be determined from equations 3.73 and 3.74, while the C1-term in these equations can be determined with equation 3.72. Finally, note that the slope in these equations should be varied until the half-wing's centre of gravity lies on the mean geometrical chord.

$$C_1 = \frac{\left(W - \frac{b^2}{2} \text{slope}\right)}{b} \quad (3.72)$$

$$A_1 = C_1 \left(\frac{b}{N_{st}}\right) + \left(\frac{\text{slope}}{2}\right) \frac{b^2}{N_{st}^2} \quad (3.73)$$

$$B_1 = C_1 \left(\frac{b}{N_{st}}\right) + \left(\frac{3\text{slope}}{2}\right) \frac{b^2}{N_{st}^2} \quad (3.74)$$

$$m = B_1 - A_1 \quad (3.75)$$

Finally, the weight distribution at the aerofoil cross-sections is determined by using equations 3.77 to 3.81. The fractions of the skin ( $F_{skin}$ ), the ribs ( $F_{ribs}$ ) and the spars ( $F_{fs}, F_{ms}$  or  $F_{skin}$ ) to the total wing weight are determined from EMWET. Note that EMWET only provides the thickness of these elements, hence first the trapezoidal volume of the skin and spars is estimated based on EMWET's thickness and the Initiator's wing geometry. After which, the obtained volume is multiplied by the material density to obtain the weight of these elements. The rib weight may be estimated using equation 3.76 [41]. Note that the  $k_r$ -factor is assumed to be  $0.5 \cdot 10^{-3}$  [41]. Observe that this approach has been validated by comparing the original EMWET wing weight to the weight obtained based on the EMWET thicknesses and it was observed that

$$m_{rib} = k_r \rho S_w \left(1 + \frac{(t/c)_r + (t/c)_t}{2}\right) \quad (3.76)$$

$$W_{1_i} = \left(S_1 F_{skin} + \left(\frac{A_{airfoilsegment1_i}}{A_{airfoil_i}}\right) F_{ribs}\right) (A_1 + m(i-1)) \quad (3.77)$$

$$W_{2_i} = \left((S_2 - S_1) F_{skin} + \left(\frac{A_{airfoilsegment2_i}}{A_{airfoil_i}}\right) F_{ribs} + F_{fs}\right) (A_1 + m(i-1)) \quad (3.78)$$

$$W_{3_i} = \left((S_3 - S_2) F_{skin} + \left(\frac{A_{airfoilsegment3_i}}{A_{airfoil_i}}\right) F_{ribs} + F_{ms}\right) (A_1 + m(i-1)) \quad (3.79)$$

$$W_{4_i} = \left((S_4 - S_3) F_{skin} + \left(\frac{A_{airfoilsegment4_i}}{A_{airfoil_i}}\right) F_{ribs} + F_{rs}\right) (A_1 + m(i-1)) \quad (3.80)$$

$$W_{5_i} = \left((1 - S_4) F_{skin} + \left(\frac{A_{airfoilsegment5_i}}{A_{airfoil_i}}\right) F_{ribs}\right) (A_1 + m(i-1)) \quad (3.81)$$

The position of each aerofoil section can be determined with equations 3.82 to 3.84. Note that equation 3.84 only shows how to calculate the apex point of each aerofoil. Hence, to determine the x-coordinate for each aerofoil segment, one still needs to add half the distance of that segment and the total distance of the preceding segments.

$$Y_{cg_i} = \frac{i}{N_{stw}} \frac{b_w}{2} - \frac{1}{2} \frac{b_w}{N_{stw}} \quad (3.82)$$

$$Z_{cg_i} = Z_{apex_w} + Y_{cg_i} \tan \Gamma \quad (3.83)$$

$$X_{apex_{w_i}} = X_{apex_w} + Y_{cg_i} \tan \Lambda_{LE_w} \quad (3.84)$$

$$(3.85)$$

Finally, the main wing's inertia tensor can be obtained by summing the separate contributions first over the segments, then over the aerofoils and finally over the entire wing, by using equations 3.67 to 3.70. Again, it should be stressed that it is assumed that each segment's moment of inertia around its own centroid is zero, which is a valid assumption provided that the wing is divided into sufficient stations.

### OTHER LIFTING SURFACES

The approach used to estimate the main wing's inertia cannot be applied to other lifting surfaces such as the empennage, because of the lack of information concerning the mass distribution of these surfaces' main

components. Therefore, section 8.1 of the DATCOM method is used to estimate the inertia contributions of these lifting surfaces. Unlike the previously discussed methods, in this method the empennage is not divided into point masses. As such, the empennage's moment of inertia around its centroid is determined first, after which the Steiner-contributions are added [34].

Now, to estimate the empennage's moment of inertia around its centroid, the mass distribution of the horizontal and vertical tailplane have to be determined first. In the DATCOM-method, it is assumed that the mass distribution of any wing, consists of three connected linear functions as shown in Figure 3.6 [34]. It is also shown in this figure how the slope of these functions depends on the wing's planform and can be estimated by determining the parameters  $c_a$ ,  $c_b$  and  $c_c$ . These parameters are respectively the largest, intermediate and smallest value of  $c_x$  in equations 3.86 to 3.88. Also, with these parameters the ratio of weight to chord ( $\rho$ ) can be calculated, using equation 3.89.

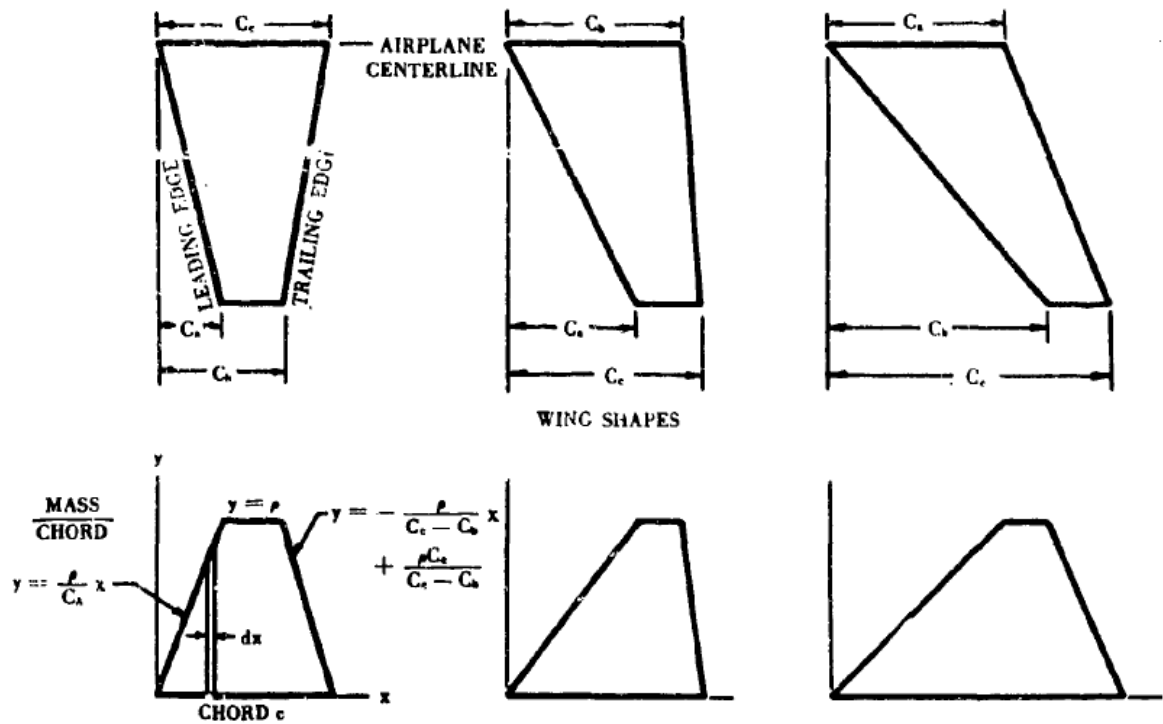


Figure 3.6: Chord-wise mass distribution of lifting surfaces [34]

$$c_x = c_r \quad (3.86)$$

$$c_x = \frac{b \tan \Lambda_{LE}}{2} \quad (3.87)$$

$$c_x = c_t + \frac{b \tan \Lambda_{LE}}{2} \quad (3.88)$$

$$\rho = \frac{W}{0.5(-c_a + c_b + c_c)} \quad (3.89)$$

$$(3.90)$$

According to the DATCOM-method, the pitching moment of inertia for any type of lifting surface around its own centroid can be estimated with equation 3.93. The parameters in this equation are determined from equations 3.92 to 3.93. Note that the  $K_0$ -factor as shown here is only applicable to horizontal and vertical tails.

$$I_0 = K_0 \left[ I - \frac{(\sum mx)^2}{m} \right] \quad (3.91)$$

In which,

$$K_0 = 0.771 \quad (3.92)$$

$$I = \frac{\rho}{12} (-c_a^3 + c_b^3 + c_c^2 c_b + c_c c_b^2 + c_b^3) \quad (3.93)$$

$$\sum mx = \frac{\rho}{6} (-c_a^2 + c_b^2 + c_c c_b + c_c^2) \quad (3.94)$$

Now, in the case of the horizontal tail, the rolling moment of inertia around its centroid ( $I_{ox_{HT}}$ ) is estimated by substituting its geometrical parameters into equation 3.95. The  $K_4$ -factor is determined from Figure B.1a in Appendix B. Next, the pitching moment of inertia around the horizontal tail's centroid ( $I_{oy_{HT}}$ ) is estimated from equation 3.93. Finally the stabilizer's yawing moment of inertia ( $I_{oz_{HT}}$ ) is simply the sum of the horizontal tail's pitching and rolling moment of inertia.

$$I_{ox_{HT}} = \frac{W_{HT} b_{HT}^2 K_4}{24} \left( \frac{c_{r_{HT}} + 3c_{t_{HT}}}{c_{r_{HT}} + c_{t_{HT}}} \right) \quad (3.95)$$

The procedure for estimating the vertical tail's inertia around its centroid, is similar to that of the horizontal tail. First, the rolling moment of inertia around the vertical tail's centroid ( $I_{ox_{VT}}$ ) is determined with equation 3.96. The  $K_5$ -factor is determined from Figure B.1b in Appendix B. Next, the yawing moment of inertia ( $I_{oz_{VT}}$ ) is estimated by substituting the vertical tail's parameters into equation 3.92. Finally the vertical tail's pitching moment of inertia around its centroid ( $I_{oy_{VT}}$ ) is obtained by summing its rolling and yawing moments of inertia.

$$I_{ox_{VT}} = \frac{W_{VT} b_{VT}^2 K_5}{18} \left( 1 + \frac{2c_{r_{VT}} c_{t_{VT}}}{(c_{r_{VT}} + c_{t_{VT}})^2} \right) \quad (3.96)$$

With the inertia tensor around the empennage's centroid estimated, the inertia tensor around aircraft's centre of gravity can be estimated using equations 3.97 to 3.100. Note that the centre of gravity locations of the tail surfaces in these equations are directly taken from the horizontal and vertical tail object in the Initiator. Finally, note that in the DATCOM method, the  $I_{xz}$ -tensor is the only asymmetrical inertia tensor taken into account, which is a valid assumption since the xz-plane is the plane of symmetry for most conventional aircraft.

$$I_{xx} = I_{o_x} + m_{stab} \left( (y_{cg_{stab}} - Y_{cg})^2 + (z_{cg_{stab}} - Z_{cg})^2 \right) \quad (3.97)$$

$$I_{yy} = I_{o_y} + m_{stab} \left( (x_{cg_{stab}} - X_{cg})^2 + (z_{cg_{stab}} - Z_{cg})^2 \right) \quad (3.98)$$

$$I_{zz} = I_{o_z} + m_{stab} \left( (x_{cg_{stab}} - X_{cg})^2 + (y_{cg_{stab}} - Y_{cg})^2 \right) \quad (3.99)$$

$$I_{xz} = m_{stab} \left( (x_{cg_{stab}} - X_{cg})^2 + (z_{cg_{stab}} - Z_{cg})^2 \right) \quad (3.100)$$

### 3.4.3. OTHER AIRCRAFT PARTS

The general method to estimate the mass moment of inertia contributions of the remaining aircraft parts, is to assume that these are point-masses and thus substituting their mass and centre of gravity locations directly into equations 3.67 to 3.70. This straight forward approach is used to estimate the inertia contributions of the following parts:

- Landing gear
- Engines (with starters & controls)
- Aircraft systems & furnishing
- Payload

Until now, only the approach used for estimating the inertia contributions of the empty aircraft have been discussed. To obtain the overall aircraft mass moment of inertia tensor however, it is necessary to estimate the contributions of the payload and fuel as well. Now, to estimate the fuel's contribution to the aircraft's inertia tensor, it is assumed that all fuel is stored in the main wing tanks and is equally divided over the left and right wing halves. Because of this assumption, the suggested approach may not be used to estimate the

inertia tensors of aircraft with belly or trim tanks. Furthermore, the effect of fuel slushing around during flight on the centre of gravity and the inertia tensor are considered to be outside the scope of this research.

Keeping these assumptions in mind, the wing is divided into 80 span-wise stations of equal length, that is 40 in each wing-half. For each of these stations, it is assumed that the area between the front and the rear spar is available for the the storage of fuel. Hence, if the local thickness ratio and spar locations are known, the volume available for fuel storage may be estimated. To this purpose, first the area of the aerofoils adjacent to each station and available for fuel storage is calculated by integrating the local chord thickness from the front spar to the rear spar with equation 3.71. The spar locations are a setting within the Initiator and are thus easily obtained. The local thickness ratio is assumed to vary linearly over the wing in the case of a straight wing. In the case of a wing with kink, it is assumed that the thickness ratio varies linearly from root to kink and again from kink to tip.

With the area available for fuel storage at the adjacent aerofoils of each station known, the available fuel volume in the stations and the total fuel volume is determined by integrating the area over the wing/station-span. Next, the ratio between the available fuel volume at each station and the total fuel volume is calculated and then multiplied by the total fuel mass, in order to obtain a realistic distribution of the fuel mass over the stations. Next, the centre of gravity locations for each station is determined from equations 3.82 to 3.83. Note that for the x-coordinate it is assumed that it lies exactly in the middle between the two spars. With the mass and centre of gravity known for each station, the inertia contributions per station may be obtained, by assuming the the fuel at each station is a point mass. As such these contributions can be estimated by applying equations 3.67 to 3.68 and adding the inertia contributions per station to the total fuel inertia tensor.

# 4

## TECHNICAL IMPLEMENTATION OF METHODOLOGY

In the previous chapter, the methods used to estimate the aircraft (component) weight, stability & control derivatives as well as the inertia tensor were discussed. In this chapter, it is explained how these methods were implemented within the Initiator framework. Note that in this chapter the focus is put on the general work flow within the adjusted modules and that for detailed function descriptions Appendices C to E should be consulted.

### 4.1. CLASS II WEIGHT ESTIMATION

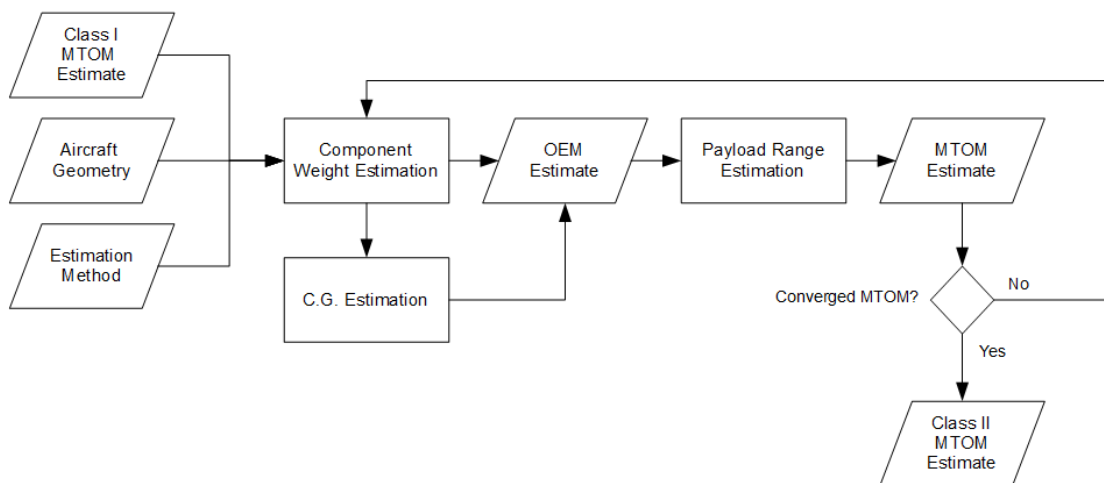


Figure 4.1: Flow Diagram for the Class 2 Weight Estimation Module

The flow diagram of the Initiator's updated Class II weight estimation, which has been implemented in a single module, is shown in Figure 4.1. As indicated by the figure, this module requires three main inputs being the aircraft geometry, the method to be used (Raymer, GD or Torenbeek) and a MTOM estimate. Note that the depending on where the module is called in the Design Convergence, the MTOM estimate is either obtained from the Class I weight estimation or a previous Initiator iteration. Now, with these inputs the module will estimate the weight of all aircraft components with the methodology as described in section 3.2 and as such a new estimate for the OEM is obtained. The component weight estimation also calculates a first estimate for the centre of gravity of major components. As indicated by the second line in Figure 4.1, these estimates are then send to a separate function, which estimates the empty aircraft's centre of gravity more accurately by using a lumped-mass method.

Next, the mission analysis is run, which is responsible for estimating the fuel fraction and drawing the payload range diagram. Note that this mission analysis should not be confused with the separate mission analysis module, which simulates an entire aircraft mission and is run after a converged Class II weight estimate is obtained. Now, with these results a new MTOM estimate is obtained, which is compared to the initial estimate. As soon as these estimates converge within a 0.5% error-margin, the results are stored back in the Initiator's controller. Recall that as mentioned in chapter 2, the controller is used to store the results of completed modules and to control the program flow within the Initiator.

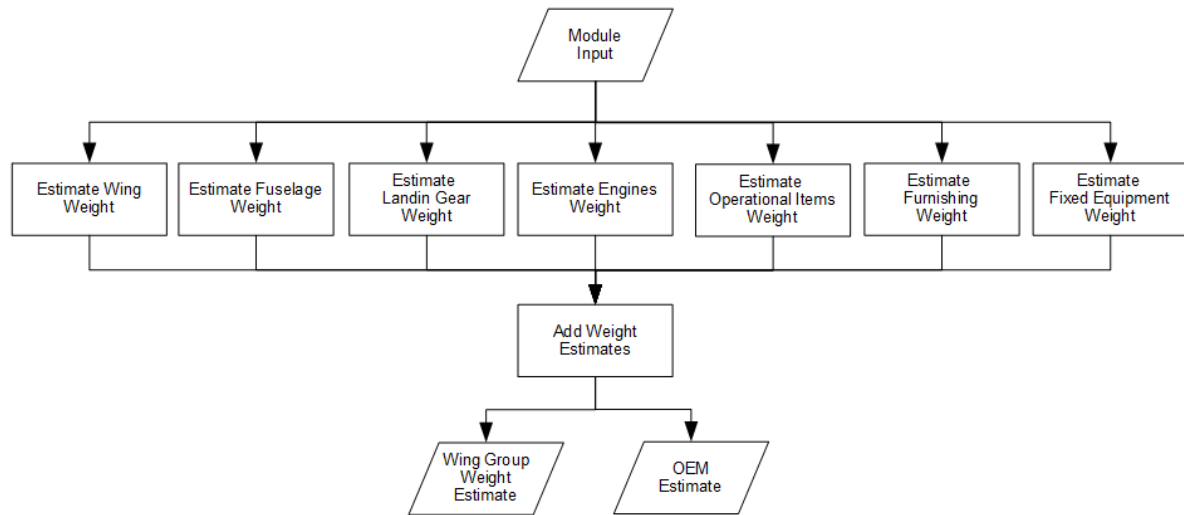


Figure 4.2: Flow Diagram for the component weight estimation

Now, in Figure 4.2 the flow diagram of the component weight estimation is shown. As shown in the top of the figure, the module input consists of the Class I weight estimate, aircraft geometry and the weight estimation method. These inputs are then fed to the functions responsible for estimating the weight of the separate aircraft components as indicated in the second line of the flow diagram. Note that in the Class II weight estimation module, a loop is made running through the aircraft parts of the input geometry. As such it is assured that the module will only compute the weight of parts present in the aircraft geometry. Note that although parts such as winglets and dorsal fins may be present in the aircraft geometry, their weight is not accounted for in the chosen weight estimation methods and therefore neglected in the Initiator. For future work it is recommended to increase the Class II weight estimation module's accuracy by implementing suitable weight estimations methods for these parts as well.

The results of the component weight estimation functions are first stored in local variables. Next, as shown on the third line in Figure 4.2, the weight of all parts is added to obtain a OEM estimate as well as an estimate for the wing group weight. The wing group weight is required for instance in the modules dealing with the sizing of the horizontal tail and the longitudinal stability. Note that these modules also require an estimate for the fuselage's group weight, which is simply obtained by subtracting the wing group weight from the OEM estimate. Finally, note that to obtain the wing group weight, the module will use the aircraft geometry to check the location of landing gear and nacelles to determine whether these contribute the wing group weight.

## 4.2. STABILITY & CONTROL DERIVATIVE ESTIMATION

Figure 4.3, shows the flow diagram of the updated stability and control derivative estimation module. Recall that in this module the method described by Roskam in [20] is used to estimate the stability & control derivatives relevant to this research. Also, recall that this method is purely empirical and in essence a simplified version of the DATCOM method as described in [34]. Furthermore, note that this method was mainly chosen as it provides a quick way to estimate the derivatives: between 4 to 5 seconds in updated module. Now, as shown on the top line of Figure 4.3, the main inputs for the module are the MTOM (estimated with the Class II weight estimation module), the aircraft geometry and the top level requirements. Note that the module directly takes these inputs from the Initiator Controller.

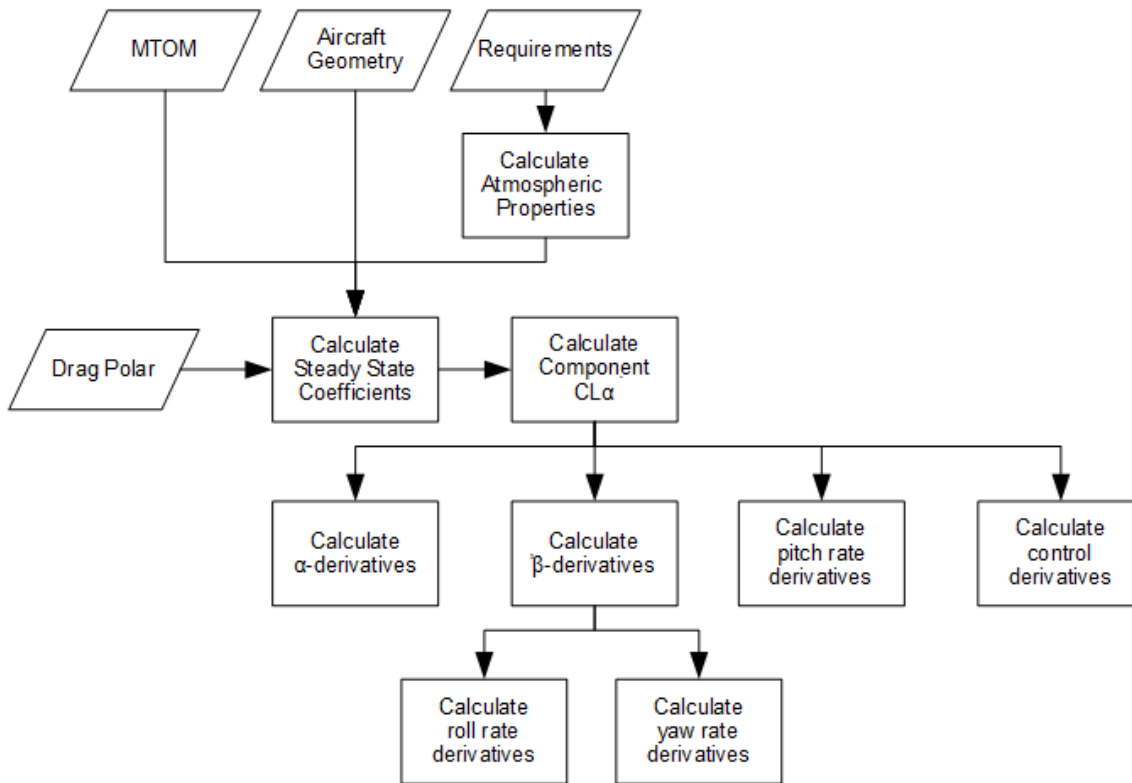


Figure 4.3: Flow Diagram for the Stability and Control Derivative Estimation Module

Now, the first step in this module, as indicated on the second line of Figure 4.3, is to estimate the atmospheric properties at the cruise altitude, for which the ISA-function build in the Initiator is used. Next, based on these conditions and the MTOM, the steady state coefficients are estimated ( $C_{L_1}$  &  $C_{D_1}$ ). The steady state lift coefficient is estimated first, after which the steady state drag coefficient is directly obtained from the drag polar. This drag polar is created by a separate Initiator module and uses the drag prediction method as described by Torenbeek [6]. Next, from the inputs and the estimates for the steady state coefficients, the lift gradients of all lifting surfaces is calculated. Again, as for the Class II weight estimation module, the module will check the aircraft geometry and will only calculate the lift gradients of those surfaces present on the aircraft. Finally, the stability and control derivatives are calculated with the approach described in section 3.3. As can be observed in Figure 4.3, for each motion a different function has been created. Furthermore, observe that the roll rate derivatives and the pitch rate derivatives depend on the vertical tail's contribution to the sideforce-due-to-sideslip derivative ( $C_{y_{\beta_v}}$ ), which is an output of the function used to calculate the angle-of-sideslip derivatives.

Explaining the detailed workflow of each separate function within the stability and control derivative estimation module is outside the scope of this chapter. For more detailed information on this subject Appendix D may be consulted. As an example however, it will be explained in the following paragraphs how the angle-of-attack derivatives ( $C_{L_\alpha}$ ,  $C_{D_\alpha}$  &  $C_{m_\alpha}$ ) are estimated by the Initiator. Now, in the top diagram shown in Figure 4.4 the flow diagram to estimate  $C_{L_\alpha}$  is shown. On the left hand side of this diagram it is shown that to calculate this derivative, the required inputs are the aircraft geometry & weight, the atmospheric conditions, the steady state coefficients and the lifting surfaces' lift gradients. Next, the estimation function will go through the aircraft parts in the geometry and calculate the correction factors as described in section 3.3 to estimate the contributions of the wing-fuselage combination, horizontal tail and canard after which these contributions are added in order to obtain the aircraft's  $C_{L_\alpha}$ . Finally, recall that  $C_{D_\alpha}$  can be directly estimated from  $C_{L_\alpha}$ , by using equation 3.42 as shown in section 3.3.

Finally, in the lower flow diagram of Figure 4.4 it is shown how  $C_{m_\alpha}$  is estimated by the updated module. Observe that the same inputs are required as for the lift-due-to-angle-of-attack derivative. Moreover, to estimate this derivative, the function will run through the various aircraft parts to estimate their contributions to the shift in the aircraft's aerodynamic centre. As shown in the flow diagram there is a maximum of three parts that may cause a shift in the aircraft's aerodynamic centre, being the fuselage, the horizontal tail and the canard. Recall that aerodynamic centre of the wing-fuselage is calculated as a single contribution and that the shift due to the fuselage is determined with equation 3.45. Next, the aircraft's centre of gravity is called from the Initiator controller, which allows to calculate  $C_{m_\alpha}$  with equation 3.44.

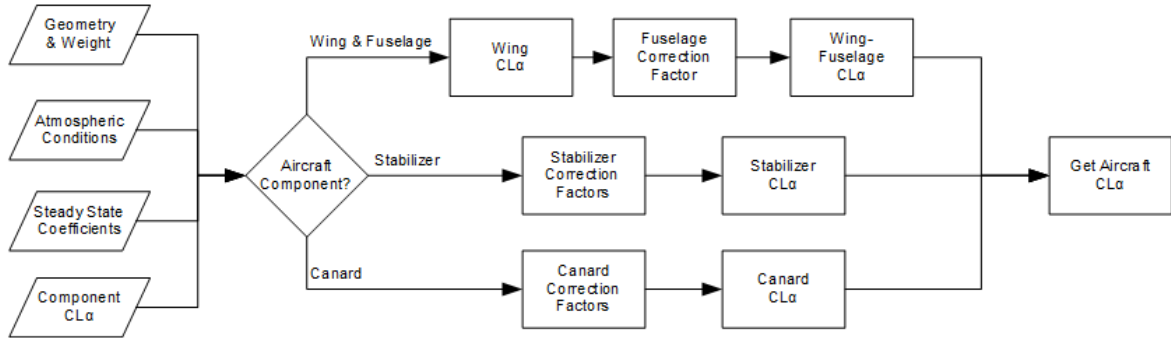
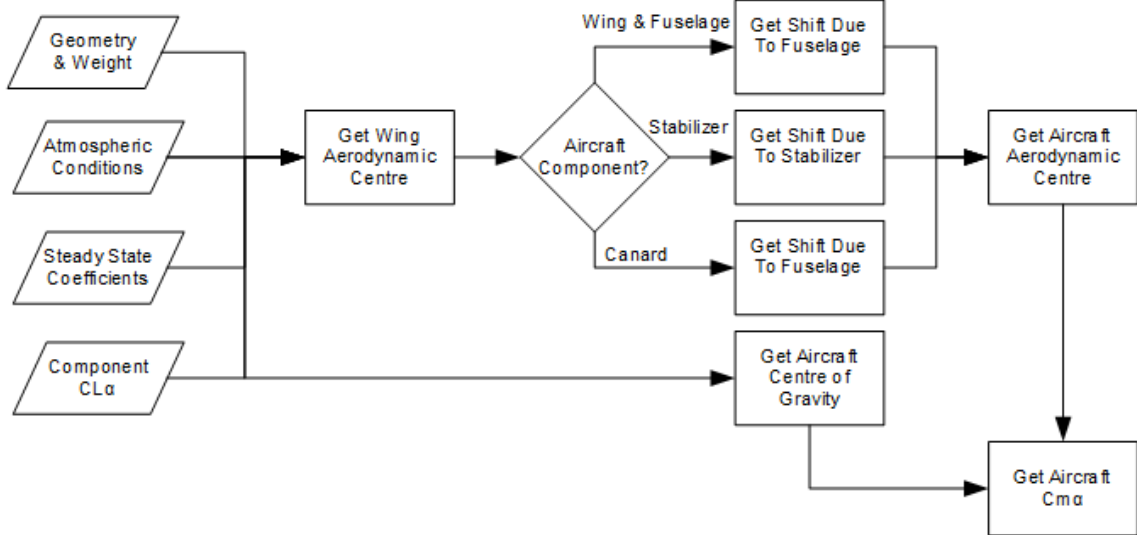
(a) Flow Diagram to estimate  $C_{L_\alpha}$ (b) Flow Diagram to estimate  $C_{m_\alpha}$ 

Figure 4.4: Flow Diagrams to estimate the angle-of-attack derivatives

### 4.3. INERTIA ESTIMATION

In Figure 4.5 the flow diagram of the updated Inertia estimation module is shown. As indicated on the top of this flow diagram, the module requires the following inputs: the aircraft geometry, the aircraft & component weight and the aircraft & component c.g. positions. Like any other Initiator module, the inertia estimation module gets these inputs directly from the Initiator controller. From these inputs, the module calls the aircraft geometry first and checks which parts are present. Based on the encountered parts, it sends the respective component weight and c.g. position together with the aircraft's c.g. position of the to separate functions, as shown in the second line of Figure 4.5.

It is worth mentioning that the specific components contributing to the systems and operational items weight and thus inertia, depend on the method used for the Class II weight estimation. Therefore, the functions re-

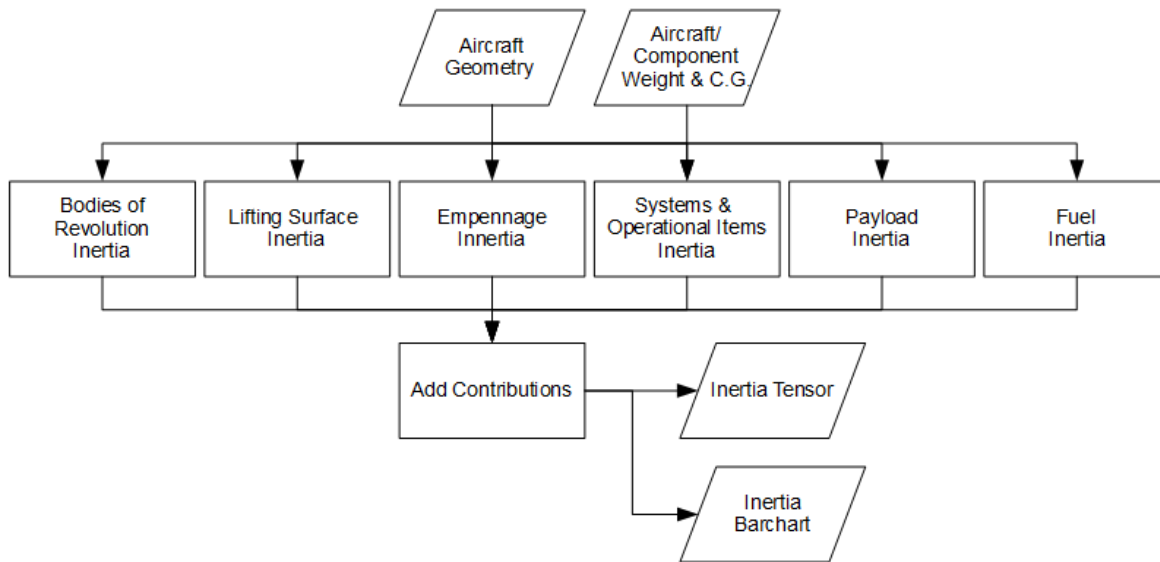


Figure 4.5: Flow Diagram for the Inertia Estimation Module

sponsible for estimating these inertia contributions have been set-up such that they call the weight estimation method used from the Initiator controller before estimating the inertia contributions. For more detailed descriptions of other functions Appendix E may be consulted.

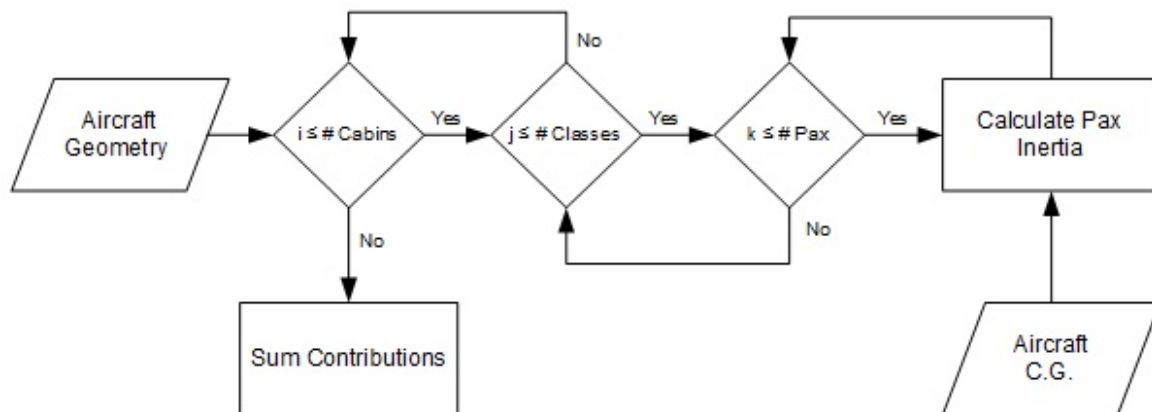


Figure 4.6: Flow Diagram to estimate the passenger inertia

Now, as an example of the workflow of the functions used to estimate the various contributions to the inertia tensor, consider the workflow diagram of the payload inertia function as shown in Figure 4.6. As shown on the left side of the diagram, this function requires the aircraft geometry and the passenger mass as inputs. Note that the passenger mass in the Initiator is a setting, which can thus be changed per aircraft upon user’s request. In this research however, it is assumed that each passenger weighs 80kg in accordance with reference [17].

Next, the module goes through three loops in order to locate and estimate the contribution of each passenger as that of a single point mass. As shown in Figure 4.6 the module first loops through the cabins, next through the classes in that cabin and finally trough each passenger in that class. The advantage of this procedure is that also the inertia contributions of aircraft with multiple cabins can be estimated. It should also be mentioned here that the Initiator’s cabin uses a local coordinate system and therefore, the cabin position coordinate is added to each passenger/cargo coordinate, in order to obtain the correct passenger positions.

Finally note that the contribution of the cargo to the inertia tensor is calculated in a similar way. In this case, the module loops first through the cargo bays and then through the cargo containers, if containers are used. When the cargo is stored in containers, the mass is equally divided over these containers. The contribution of each container is then assumed to be a single point mass with the centre of gravity at the container's geometric centre. When the cargo is stored as bulk however, it is assumed that the cargo consist of single point mass per cargo bay, with the centre of gravity at the cargo bay's geometric centre.

# 5

## VALIDATION OF METHODOLOGY

In this chapter it is explained how the methodology described in the previous chapters was validated. First, the updates made to the Initiator's Class I sizing modules are validated in section 5.1, followed by the validation of the Class II Weight module in section 5.2. Next, in section 5.3 it is described how the estimation of the stability and control derivatives has been validated. This chapter concludes with describing the validation of the inertia estimation in section 5.4.

### 5.1. VALIDATION OF CLASS I WEIGHT ESTIMATION AND SIZING

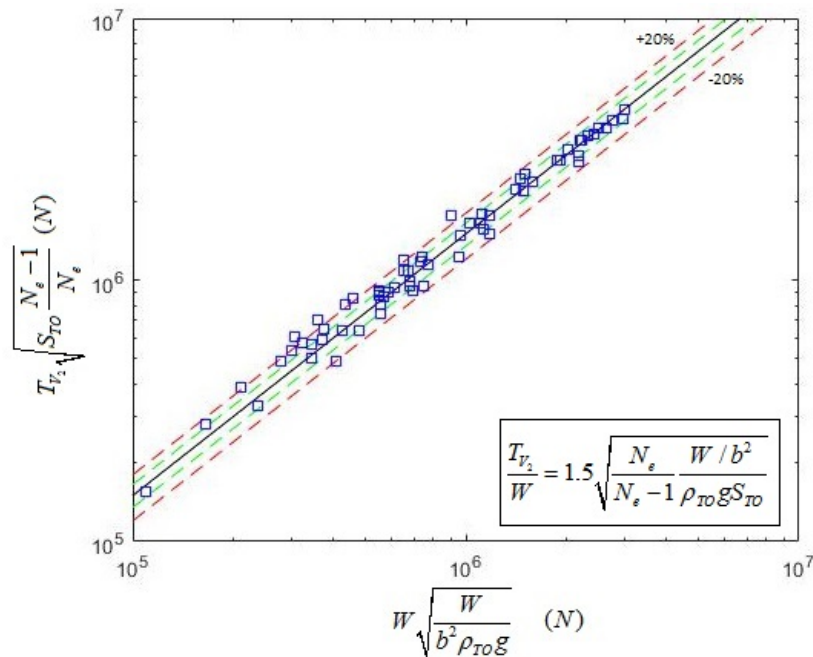


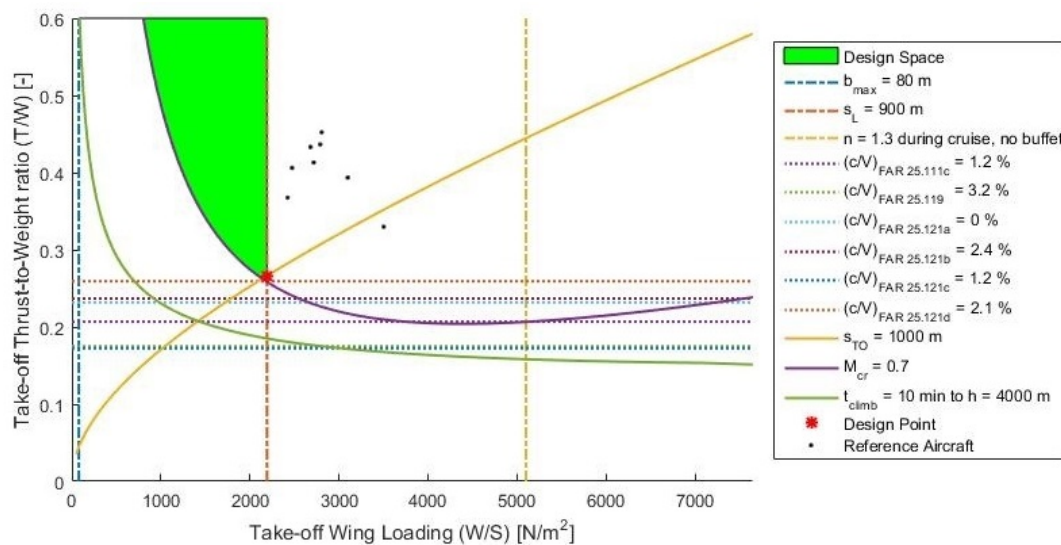
Figure 5.1: Validation of take-off constraint in Weight and Thrust Loading Diagram

Recall that the *WingThrustLoading*-module was updated because of its tendency to underestimate the thrust loading of business jet aircraft. To solve the issue, a new relation (equation 3.2) was derived to estimate business jet's take-off distance constraint more accurately. Now, in Figure 5.1 the new relation is shown with the black solid line as a function of the normalized weight (see the x-axis). The blue squares indicate the 70 reference business jet aircraft, for which this new relation was set-up. Furthermore, the 10% and 20% error margin are indicated by the green and red dotted lines respectively. As shown in this figure, the updated relation still has a relatively large error margin of around 20%, which is considerably higher than equation 3.1 had for conventional commercial aircraft (around 10%) [23]. If one would use the original constraint relation however,

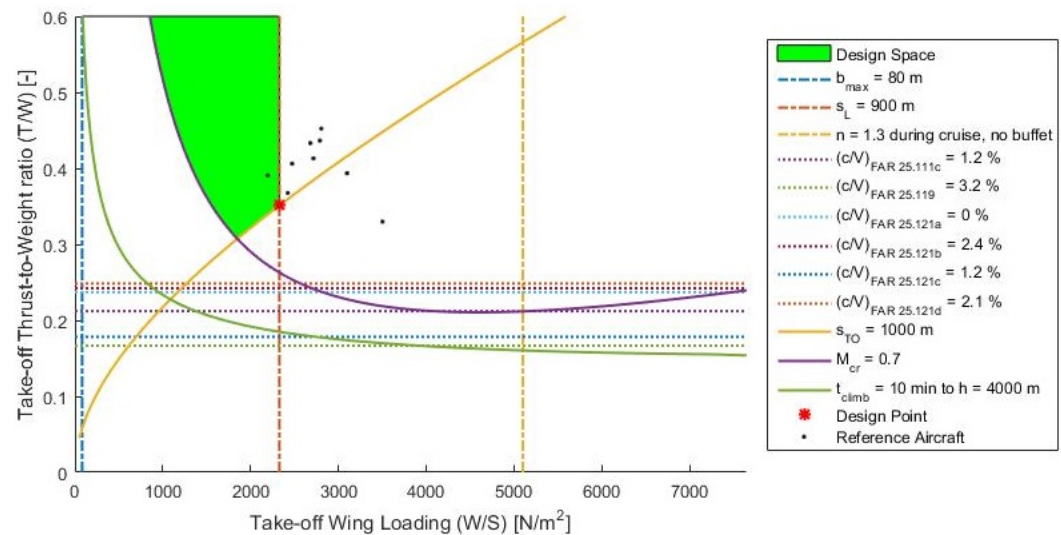
the error margin remains the same, but the old relation underestimates the required thrust loading on average by almost 30%. Therefore it may be concluded that the new relation is a considerable improvement over the old.

Even though the updated relation improves the estimated thrust loading, still care should be taken due to the large scatter. A possible explanation for this scatter is the huge variety in requirements imposed on business jet aircraft. For instance, the range of the reference aircraft, varies from 1800km to 12964km, whereas the payload ranges from 3238kg to 227kg and the take-off distance between 492m and 1974m. Therefore it is anticipated that a further improvement to estimate the take-off thrust loading constraint may be obtained by deriving different equations for multiple types of business jet categories.

Finally, in Figure 5.2 the original and the updated thrust and wing loading diagrams of the Cessna Citation II are shown. Again it can be observed that for both diagram's the the take-off and landing constraints are active. Furthermore it can be seen that as expected the thrust loading of the aircraft in the updated diagram is considerably higher (around 0.3) and much closer to that of the reference aircraft indicated with the black dots.



(a) Original Wing Thrust Loading diagram for the Cessna Citation II



(b) Updated Wing Thrust Loading diagram for the Cessna Citation II

Figure 5.2: Comparison of the original and the updated wing loading diagram for the Cessna Citation II

## 5.2. VALIDATION OF THE CLASS II WEIGHT ESTIMATION

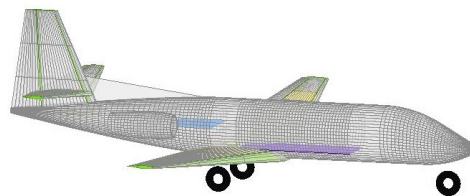
In section 3.2, Torenbeek's and GD's preliminary weight estimation methods as described in reference [18] were explained. Furthermore, in section 4.1, it was explained how these weight estimation methods were implemented in the Initiator's Class II weight estimation module. In this section, it will be investigated how these methods predict the the key masses of several business jets. Recall, that Raymer's Class II weight estimation method was already implemented in the Initiator and will thus also be included in this comparison. Furthermore, since the Initiator is a general preliminary design tool, it will also be investigated how these methods predict the same key masses for two conventional commercial aircraft. The aircraft used in this comparison are:

- Cessna Citation II
- Bombardier Learjet 45
- Embraer Phenom 300
- Gulfstream G650
- Airbus A320-200
- Fokker 100

In Tables 5.1 to 5.6 an overview is shown how Raymer's, Torenbeek's and the GD-method compare when predicting the MTOM, the fuel mass and the EOM of these reference aircraft. The reference data in these tables has been taken directly from the Initiator's aircraft database, which contains data from references [29] and [30]. Furthermore, the Initiator's estimates were obtained with a design convergence that is slightly different then as described in section 2.7. In this design convergence, the Initiator only runs through the Class II and Mission Analysis loops, thus excluding the Class II.V loop. It was specifically chosen to include the Mission Analysis in this convergence, because it predicts the fuel mass more accurately than the Class II weight estimation module itself. The decision to exclude the Class II.V loop was made in order to purely assess the validity of the Class II weight estimation methods. Also, note that the fuselage length and diameter highly influence the OEM estimate and thus it should be aimed at creating a fuselage in the Initiator with a length and width similar to those of the reference aircraft. Now, in the Initiator the fuselage is sized with the *Fuselage-Configurator*-module, which sizes the fuselage around the required cabin space. Therefore the seat spacing, seat width and aisle width were adjusted for each aircraft separately to obtain accurate weight results.



(a) Cessna Citation II



(b) Initiator Cessna Citation II

Figure 5.3: Comparison in geometry of the Cessna Citation II

In Figure 5.3, a comparison is made between the actual Cessna Citation II<sup>1</sup> and the geometry created by the Initiator. Furthermore, in Table 5.1 the weight predicted according to Torenbeek's, Raymer's and the GD-method are shown. Now, in the case of the Citation II, the GD-method predicts the MTOM with the smallest error. When comparing the predictions for the OEM however, it can be seen that the GD-method actually predicts the OEM with the largest error. Furthermore, in Table 5.1, it can be seen that predicted fuel mass with all methods is off by a considerable margin, which explains that although the estimate for the MTOM is reasonable for a preliminary design method, the OEM is quite far off.

<sup>1</sup>CC-BY-SA TU Delft

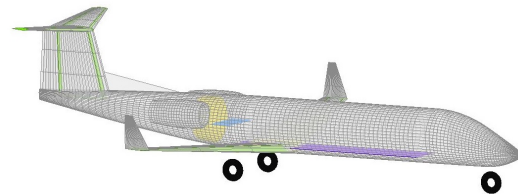
Table 5.1: Comparison of the weight estimates for the Cessna Citation II

Parameter	Cessna Citation II	Torenbeek	Error [%]	Raymer	Error [%]	GD	Error [%]
MTOM [ $kg$ ]	6713	7065	5.2	7582	12.9	6523	-2.8
FM [ $kg$ ]	2118	1659	-21.7	1912	-9.7	1563	-26.2
Payload [ $kg$ ]	522	522	0.0	522	0.0	522	0.0
EOM [ $kg$ ]	4073	4884	19.9	5148	26.4	4960	21.8
W/S [ $N/m^2$ ]	2195	2328	6.0	2364	7.7	2336	6.4
T/W [-]	0.3906	0.3501	-10.4	0.3543	-9.3	0.3516	-10.0

Furthermore, in the last two rows of Table 5.1 the wing and thrust loading of the actual aircraft is compared to those estimated by the Initiator based on the input requirements. First, it can be observed that even though the requirements for all aircraft are the same, the Initiator will estimate these parameters with a small difference. This can be explained by the fact that the Initiator runs again through the wing thrust loading estimation module each iteration. Because the aircraft have a different mass and thus a different geometry for each method, a slightly different wing and thrust loading may be expected. Also, it should be observed that the predicted wing loading is slightly larger than the reference wing loading. As a consequence, the wing will be relatively smaller and thus the predicted results are expected to be slightly higher if an identical wing loading were to be used. Finally, it can also be observed that the thrust loading is still slightly underestimated with the new thrust loading requirement relation, which is a consequence of the large scatter in the reference data as shown in Figure 5.1.



(a) Bombardier Learjet 45



(b) Initiator Bombardier Learjet 45

Figure 5.4: Comparison in geometry of the Bombardier Learjet 45

Table 5.2: Comparison of the weight estimates for the Bombardier Learjet 45

Parameter	Bombardier Learjet 45	Torenbeek	Error [%]	Raymer	Error [%]	GD	Error [%]
MTOM [ $kg$ ]	9752	8598	-11.8	7676	-21.3	6698	-31.3
FM [ $kg$ ]	2495	2259	-9.4	2158	-13.5	1886	-24.4
Payload [ $kg$ ]	850	850	0.0	850	0.0	850	0.0
EOM [ $kg$ ]	6407	5488	-14.3	4668	-27.1	3962	-38.2
W/S [ $N/m^2$ ]	3305	3220	-2.6	3281	-0.7	3283	-0.7
T/W [-]	0.3389	0.3890	14.8	0.3933	16.1	0.3933	16.1

The same comparison can also be made for the Bombardier Learjet 45 and in Figure 5.4 the actual aircraft<sup>2</sup> is compared to the geometry predicted by the Initiator. Also, in Table 5.2 the same comparison as for the Cessna Citation II is made. Now, in the case of the Learjet 45, it can be seen that the convergence with Torenbeek's method produces the most accurate results, both in terms of MTOM as well as for the fuel mass and

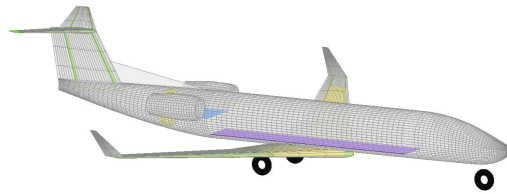
<sup>2</sup>CC-BY-SA O. Milborne

the EOM. Furthermore it can be seen that the predicted wing loading is quite close to the actual wing loading, be it slightly underestimated. As a consequence, it may be expected that with the proper wing loading, the predicted weights will decrease, increasing the error. Finally, it may also be observed that in this case, the thrust loading is over predicted by a considerable margin of around 15%.

Also, in Figure 5.4 it may be observed that apparently the available fuel volume in the main wing of Learjet 45 is not sufficient to store the required fuel. As a consequence the Initiator will create an additional fuel tank in the fuselage, directly behind the rear cargo bay and between the nacelles. This additional fuel tank is indicated by the yellow cylinder in the Initiator geometry. Interestingly enough, this is also the case in the actual aircraft, where bladder tanks are installed behind the cabin to accommodate for the fuel that does not fit in the wings [29]. Also, observe that in the Initiator geometry, the fuselage tank is placed behind the rear cargo bay. In reality the fuselage tank is placed directly behind the cabin, with the rear cargo bay behind it. The reason for this is twofold. First, by placing the tank closer to the wing, the shift in centre of gravity is reduced. Secondly, the nacelles do not interfere with the positioning of the rear cargo door. Therefore, for future work it is recommended to change the design logic in the Initiator.



(a) Embraer Phenom 300



(b) Initiator Embraer Phenom 300

Figure 5.5: Comparison in geometry of the Embraer Phenom 300

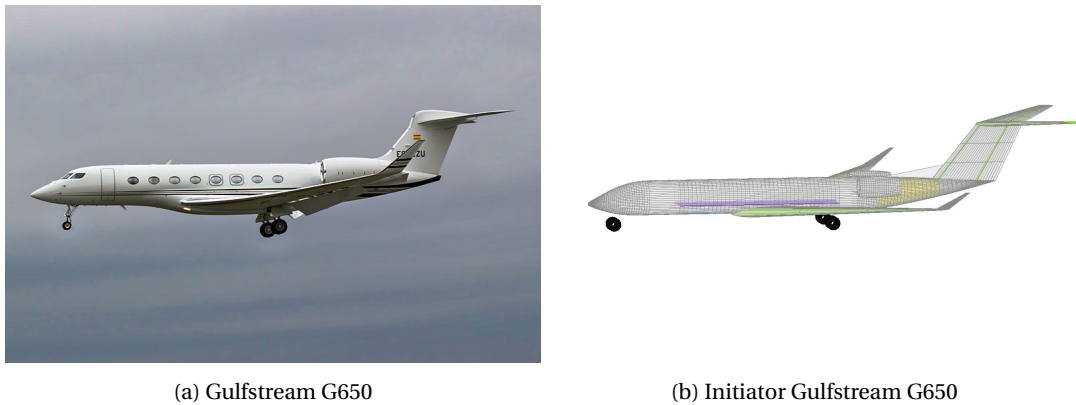
Table 5.3: Comparison of the weight estimates for the Embraer Phenom 300

Parameter	Embraer Phenom 300	Torenbeek	Error [%]	Raymer	Error [%]	GD	Error [%]
MTOM [kg]	8150	8374	2.8	7388	-9.3	6620	-18.8
FM [kg]	2200	1842	-16.3	1667	-24.2	1515	-31.1
Payload [kg]	1096	1096	0.0	1096	0.0	1096	0.0
EOM [kg]	6350	5436	-14.4	4625	-27.2	4009	-36.9
W/S [ $N/m^2$ ]	2805	2884	2.8	2899	3.4	2909	3.7
T/W [-]	0.3740	0.3620	-3.2	0.3633	-2.9	0.3640	-2.7

The same comparison was also made for the Embraer Phenom 300. The actual aircraft<sup>3</sup> and the by the Initiator predicted geometry are shown in Figure 5.5. Furthermore, an overview of the different weights predicted with Torenbeek's, Raymer's and the GD-method is shown in Table 5.3. In the case of the Phenom 300, Torenbeek's method provides the highest accuracy for predicting the MTOM, followed by Raymer's method. Again, just as was the case for the Cessna Citation II, it may be deduced from Table 5.3 that the prediction in the MTOM is actually slightly compensated by the error in fuel mass, i.e. due to the high lift-to-drag ratio, the fuel weight is underpredicted, which balances the error in the EOM. Finally, in the last two rows in Table 5.3, it can be seen that for the Phenom 300, the wing and thrust loading are estimated with a reasonable level of accuracy (between 3.7% and -3.2% respectively).

The last business jet for which this comparison was made, is the Gulfstream G650. In Figure 5.6 the actual aircraft<sup>4</sup> is compared with the geometry predicted by the Initiator and in Table 5.4 the weights predicted by

<sup>3</sup>CC-BY-SA J. Payne<sup>4</sup>CC-BY-SA B. Riobó



(a) Gulfstream G650

(b) Initiator Gulfstream G650

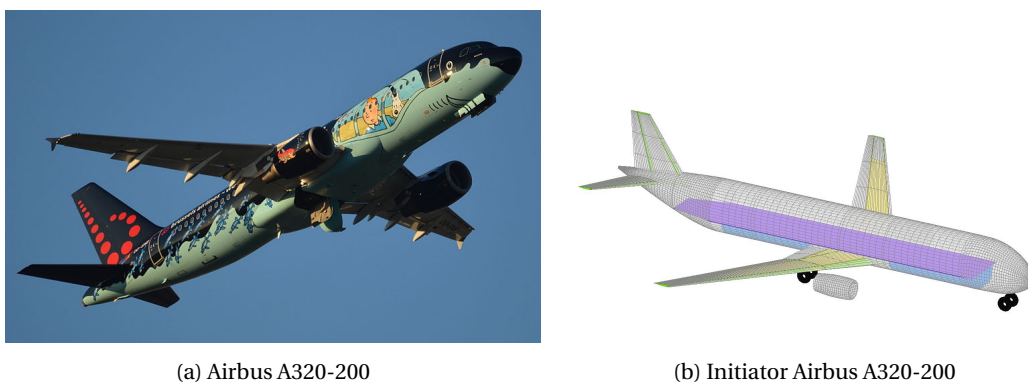
Figure 5.6: Comparison in geometry of the Gulfstream G650

Table 5.4: Comparison of the weight estimates for the Gulfstream G650

Parameter	Gulfstream G650	Torenbeek	Error [%]	Raymer	Error [%]
MTOM [kg]	45180	42335	-6.3	25880	-42.7
FM [kg]	17738	18739	5.6	12033	-32.2
Payload [kg]	2948	2948	0.0	2948	0.0
EOM [kg]	24494	20648	-15.7	10899	-55.5
W/S [ $N/m^2$ ]	3718	4095	10.1	4211	13.3
T/W [-]	0.3389	0.2999	-11.5	0.3051	-10.0

the Initiator are compared with the reference data. First, observe that unlike the other business jet aircraft described in this section, no results were obtained for the GD-method. The reason is that the Initiator was unable to complete a design convergence, as it encountered an error within the *AVL* module. Very likely this error is caused by the fact that the weight predicted with the GD-method was so low, such that the Initiator was unable to generate proper wing and tail surfaces to feed into the *AVL* module, causing the design convergence to crash.

Next, in Table 5.4 it can be seen that in the case of the G650, Torenbeek's method is the only approach resulting in a reasonable estimate of the MTOM. The fuel mass is predicted to be around 5% higher than the actual fuel mass, while the EOM is considerably under predicted. When comparing the wing loading, it can be observed that the Initiator overestimates the wing-loading, resulting in a smaller wing. As a consequence, it is anticipated that if the wing loading can be lowered to the actual wing loading a more accurate result in terms of MTOM and EOM can be obtained for the G650. Finally, it should be noticed that the thrust loading is underpredicted by around 10%.



(a) Airbus A320-200

(b) Initiator Airbus A320-200

Figure 5.7: Comparison in geometry of the Airbus A320-200

Table 5.5: Comparison of the weight estimates for the Airbus A320-200

Parameter	Airbus A320-200	Torenbeek	Error [%]	Raymer	Error [%]	GD	Error [%]
MTOM [kg]	73500	74267	1.0	55283	-24.8	56840	-22.7
FM [kg]	13000	13171	1.3	9818	-24.5	10050	-22.7
Payload [kg]	20767	20767	0.0	20767	0.0	20767	0.0
EOM [kg]	39733	40329	1.5	24698	-37.8	26023	-34.5
W/S [ $N/m^2$ ]	5889	6289	6.8	6291	6.8	6287	6.8
T/W [-]	0.3100	0.3094	-0.2	0.3094	-0.2	0.3093	-0.2

Since the Initiator is a general preliminary design tool, it makes sense to also validate the changes made to the Class 2 Weight Estimation for a set of conventional aircraft. The first aircraft for which this has been done is the Airbus A320-200 and a comparison between the A320-200<sup>5</sup> and its Initiator counterpart is shown in Figure 5.7. Furthermore, the comparison in predicted weights per approach is shown in Table 5.5. Also for this aircraft it can be observed that the results obtained with Torenbeek's method are the most accurate and that the error margin's on the results obtained with the other two approaches is very high (up to almost 40% in the EOM). Also, from Table 5.5 it can be deduced that the error in MTOM, is very likely caused by a too high wing loading, resulting in an under prediction of the wing weight. Finally, the thrust loading is predicted with a very high accuracy over all the methods.

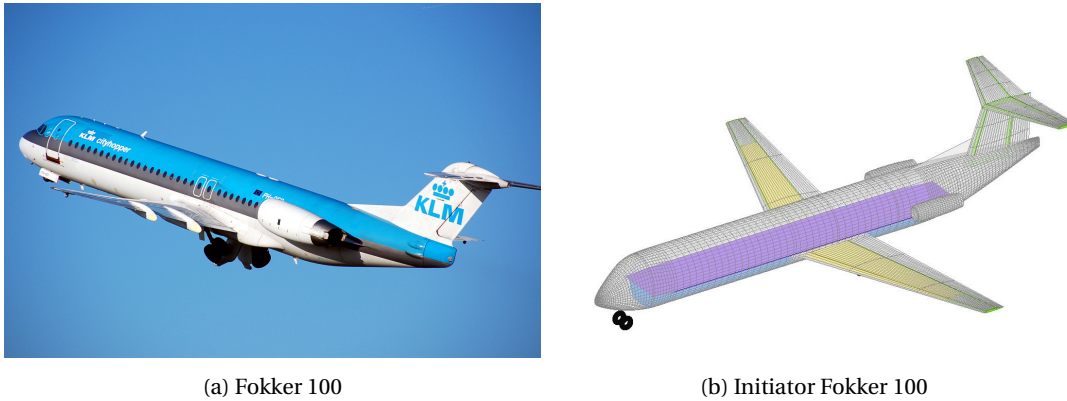


Figure 5.8: Comparison in geometry of the Fokker 100

Table 5.6: Comparison of the weight estimates for the Fokker 100

Parameter	Fokker 100	Torenbeek	Error [%]	Raymer	Error [%]	GD	Error [%]
MTOM [kg]	44450	45434	2.2	34000	-23.5	33006	-25.7
FM [kg]	7710	7282	-5.5	6003	-22.1	5819	-24.5
Payload [kg]	11240	11240	0.0	11240	0.0	11240	0.0
EOM [kg]	25500	26912	5.5	16757	-34.3	15947	-37.5
W/S [ $N/m^2$ ]	4664	4116	-11.7	4179	-10.4	4178	-10.4
T/W [-]	0.2800	0.2714	-3.1	0.2755	-1.6	0.2758	-1.5

The last aircraft for which the weight estimates over the various methods has been compared is the Fokker 100<sup>6</sup>, as shown in Figure 5.8, together with the geometry estimated by the Initiator. Also in the case of this aircraft, it was observed that Torenbeek's method provides the most accurate results as is shown in Table 5.6. It should be noted here that the wing loading is underpredicted by 10%, which is anticipated to decrease the accuracy of the presented results if brought closer to the reference aircraft.

<sup>5</sup>CC-BY-SA S. Mortier<sup>6</sup>CC-BY Arpingstone

Now, from this discussion it can be concluded that overall Torenbeek's method delivers the most consistent results. Furthermore, it was also observed that this method has the tendency to slightly overestimate the MTOM and EOM of commercial aircraft and to underestimate these weights for business jet aircraft. That being said the margin of error is around 5% which is what may be expected from a general preliminary design tool. Furthermore, these results should be reviewed with care, because the Initiator produces the design of an aircraft based on the requirements of reference aircraft and will thus always be slightly different.

Furthermore, it was observed that the GD-method and Raymer's methods consistently under predict the MTOM by a considerable margin. Now, with the exception of the estimation of the APU weight nothing was changed in Raymer's method except for the implementation of the iteration loop. This loop is not mentioned by Raymer in reference [8], hence it is possible that by implementing this loop, the methodology is unable to predict the MTOM with the desired level of accuracy. Another possible explanation, is of course that there are still some bugs left within the code, causing both the GD-method and Raymer's method to consistently underpredict the MTOM and EOM. Finally, because of these results, it was decided that all further predictions made with respect to changes in aircraft and component weight shall be estimated with Torenbeek's method in the Initiator design convergence.

### 5.3. VALIDATION OF THE STABILITY AND CONTROL DERIVATIVE ESTIMATION

To validate the stability and control derivative estimation module, the module was made stand-alone from the Initiator and separate input files were created for the Learjet 24 and the Boeing 747-100 at various conditions as shown in Table 5.7 and 5.8. These files define the main geometrical parameters as well as the conditions at which the derivatives are to be calculated. The input files are written in MS Excel format and each consists of five tabs. The first tab contains geometrical data of the lifting surfaces (wing, horizontal tail, vertical tail, canard). In the second tab the overall geometrical aircraft- and fuselage data are stored, while the third tab contains the geometrical data of all control surfaces (ailerons, flaps, elevators, rudders, ). The fourth tab contains data corresponding to atmospheric conditions at which the derivatives are determined, e.g.: steady-state angle of attack/sideslip, altitude, Mach Number, Reynolds number, etc. Finally in the last tab the fuselage is divided into 13 stations, as shown by Figure 5.9.

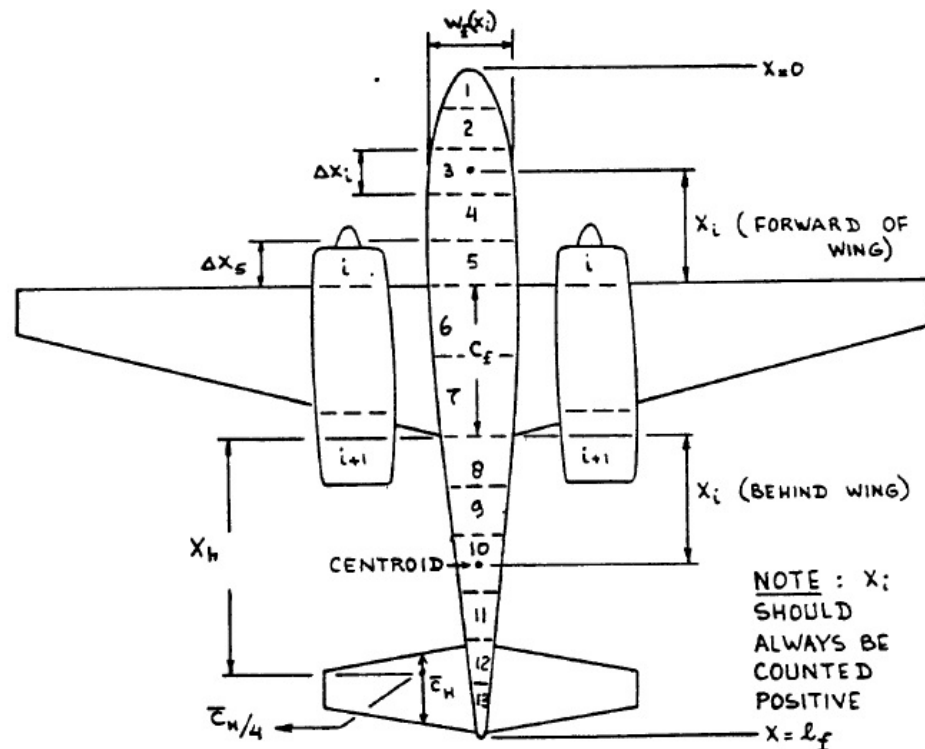


Figure 5.9: Definition of Fuselage Stations [20]

The conditions at which the derivatives were estimated are summarized in Table 5.7 for the Learjet 24 and in Table 5.8 for the Boeing 747-100. As can be seen in these tables, the Learjet 24's derivatives were calculated in three conditions. First, during a cruise flight at FL400 at MTOM and secondly during a cruise flight at identical conditions with the exception of a lower mass. Finally, also the derivatives of the Learjet 24 during an approach at MTOM were estimated. In the case of the Boeing 747-100, also 3 conditions were evaluated. Again first the derivatives were estimated for a cruise flight at maximum cruise speed at FL400 and MTOM and secondly for cruise flight at the same weight, but at FL200. Finally, also the 747-100's derivatives during approach at MLM were estimated. The reference data used for the validation of these derivatives was retrieved from Chapter 11 in reference [20].

Table 5.7: Conditions used for validating stability and control derivatives (Learjet 24)

Learjet 24	Cruise (High Mass)	Cruise (Low Mass)	Approach
Altitude [-]	FL400	FL400	Sealevel
Mach Number [-]	0.7	0.7	0.15
Reynolds Number [-]	$1.07 \cdot 10^7$	$1.07 \cdot 10^7$	$8.29 \cdot 10^6$
Flap Deflection [deg]	0	0	40
Center of gravity ( $\bar{x}_{cg}$ )	0.32	0.32	0.32
Mass [kg]	5,897	9,000	5,897
Initial Attitude ( $\alpha$ ) [deg]	2.7	1.5	1.8
$C_{L_1}$ [-]	0.41	0.28	1.64

Table 5.8: Conditions used for validating stability and control derivatives (Boeing 747-100)

Boeing 747-100	Cruise (High Altitude)	Cruise (Low Altitude)	Approach
Altitude [-]	FL400	FL200	Sealevel
Mach Number [-]	0.9	0.65	0.2
Reynolds Number [-]	$5.48 \cdot 10^7$	$8.18 \cdot 10^7$	$1.39 \cdot 10^6$
Flap Deflection [deg]	0	0	30
Center of gravity ( $\bar{x}_{cg}$ )	0.25	0.25	0.25
Mass [kg]	288,773	288,773	255,826
Initial Attitude ( $\alpha$ ) [deg]	2.4	2.5	8.4
$C_{L_1}$ [-]	0.52	0.4	1.676

The most relevant stability and control derivatives calculated for the Learjet 24 are compared with the reference data in Table 5.9. The derivatives shown here, either directly influence the longitudinal aircraft behaviour or are directly dependent on contributions from the horizontal tail. As can be seen in this table, the angle of attack derivatives are generally estimated with a high accuracy. The drag-due-to-angle-of-attack derivative is spot on, whereas the lift-due-to-angle-of-attack derivative is slightly overestimated. The pitching moment derivative with angle of attack is slightly underestimated in the cruise conditions, but the error becomes larger in approach conditions with a flap deflection of 40 degrees. The only derivative with respect to angle of sideslip affected by the horizontal tail is the lift-due-to-sideslip derivative and as can be seen, overall this derivative is predicted rather well in the case of the Learjet 24. Next, when considering the pitch rate derivatives, it may be observed that although the module predicts the moment-due-to-pitch-rate derivative rather well, it has the tendency to overestimate the lift-due-to-pitch-rate derivative by almost a factor of two. Furthermore, it may also be deduced from this table that the elevator control derivatives are estimated rather well, with a general tendency to overestimate. Finally, observe that although the reference assumes the drag from the elevator to be zero. From these results however it may be deduced that although small, there is definitely an effect.

The same comparison was also made for the Boeing 747-100 and the results are summarized in Table 5.10. As for the Learjet 24, the methodology predicts the angle of attack derivatives reasonably well. Again it may be observed that the module has the tendency to slightly overestimate the longitudinal stability ( $C_{m_\alpha}$ ). The lift-due-to-sideslip is predicted reasonably well in cruise conditions, however as can be seen in this table the

Table 5.9: Validation of the Learjet 24's most important derivatives

Derivative	High Mass		Low Mass		Approach	
	Reference	Calculated	Reference	Calculated	Reference	Calculated
$C_{D\alpha}$	0.3	0.31	0.22	0.22	1.06	1.06
$C_{L\alpha}$	5.84	6.08	5.84	6.08	5.04	5.05
$C_{m\alpha}$	-0.64	-0.43	-0.64	-0.43	-0.66	-0.33
$C_{l\beta}$	-0.11	-0.17	-0.10	-0.10	-0.17	-0.16
$C_{Dq}$	0	0	0	0	0	0
$C_{Lq}$	4.70	8.79	4.70	8.79	4.10	7.06
$C_{mq}$	-15.50	-16.39	-15.50	-16.39	-13.5	-13.39
$C_{D\delta_e}$	0	0.06	0	0.04	0	0.230
$C_{L\delta_e}$	0.46	0.57	0.46	0.57	0.40	0.57
$C_{m\delta_e}$	-1.24	-1.41	-1.24	-1.41	-0.98	-1.41

prediction in approach conditions is very far off. Now, during the approach, the aircraft's lift coefficient is rather high and this is believed to result in the module's tendency to overestimate the wing-fuselage contribution to lift-due-to-sideslip derivative. Moving on in Table 5.10, it may be observed that the module has the tendency the same tendency as for the Learjet 24 to overestimate the lift-due-to-pitch-rate derivatives and to quite accurately predict the moment-due-to-pitch-rate is reasonably well predicted. The trends found for the Learjet 24's elevator control derivatives can also be observed for the Boeing 747-100. It can be seen that a small drag-due-elevator deflection is obtained, which is too high in case of the approach. The lift- and moment-due-to-elevator-deflection are again slightly overestimated.

Table 5.10: Validation of the Boeing 747-100's most important derivatives

Derivative	FL400		FL200		Approach	
	Reference	Calculated	Reference	Calculated	Reference	Calculated
$C_{D\alpha}$	0.5	0.29	0.2	0.19	1.13	1.08
$C_{L\alpha}$	5.5	5.79	4.4	5.01	5.67	4.51
$C_{m\alpha}$	-1.6	-1.9	-1	-1.65	-1.45	-1.46
$C_{l\beta}$	-0.095	-0.14	-0.16	-0.10	-0.28	-1.19
$C_{Dq}$	0	0	0	0	0	0
$C_{Lq}$	7.8	10.20	6.6	8.79	5.65	7.06
$C_{mq}$	-25.5	-26.01	-20.5	-22.64	-21.4	-20.64
$C_{D\delta_e}$	0	0.07	0	0.05	0	0.89
$C_{L\delta_e}$	0.3	0.44	0.32	0.44	0.40	0.43
$C_{m\delta_e}$	-1.2	-1.44	-1.3	-1.44	-1.4	-1.44

From the foregoing discussion it may be concluded that for the majority of the stability and control derivatives impacting the aircraft's longitudinal behaviour, the separated stability and control estimation module does a reasonable well job at predicting these. There are however some sources of error that require some further explanation. First, it should be noted that the approach used, has been developed for a large set of aircraft types, ranging from general aviation aircraft such as the Cessna 172 to large commercial aircraft such as the Boeing 747. In reference [20] it is even suggested that the stability and control derivatives of fighter aircraft, such as the McDonnell Douglas Phantom F4 could be calculated with this approach. As a consequence the methodology contains a large number of empirical factors that will cause derivatives to deviate from the given data for a specific aircraft.

Furthermore the results calculated for the aircraft in approach configuration should be reviewed with care, because within the module only the effects of plain flaps has been implemented. Reference [20] does include how other flap types are to be implemented, however it was chosen to leave this to future development as most reference business jet aircraft make use of plain flaps. In the case of the Boeing 747 however, this is horribly wrong assumption, as this aircraft has triple slotted fowler flaps. Finally, observe in Tables 5.7 and

5.8, only the centre of gravity's x-position is given, which is generally speaking sufficient to accurately estimate the longitudinal stability and control derivatives. However, to estimate the lateral/directional derivatives it is important to also have an accurate estimate for the c.g.'s y- and z-coordinate. The lack thereof in the separated module has been observed to cause relatively large errors with respect to these derivatives.

#### 5.4. VALIDATION OF THE INERTIA ESTIMATION

To validate the approach used to estimate the inertia tensor, the results obtained with the Initiator were compared to reference data for the Fokker 100 from reference [42]. This reference provides Inertia data for the aircraft in a fully equipped, empty condition (EOW). Furthermore the relations are given to estimate the changes to the aircraft centre of gravity and the Inertia tensor, due to loading the aircraft with passengers and fuel. A simple Matlab tool called *Fokker Inertia* was written, in which these relations were implemented and this tool is described in more detail in Appendix F. Note that reference [42] also provides the relations for the effect of fuel slushing, but these have not been implemented in the the tool as these effects are also not included in the Initiator.

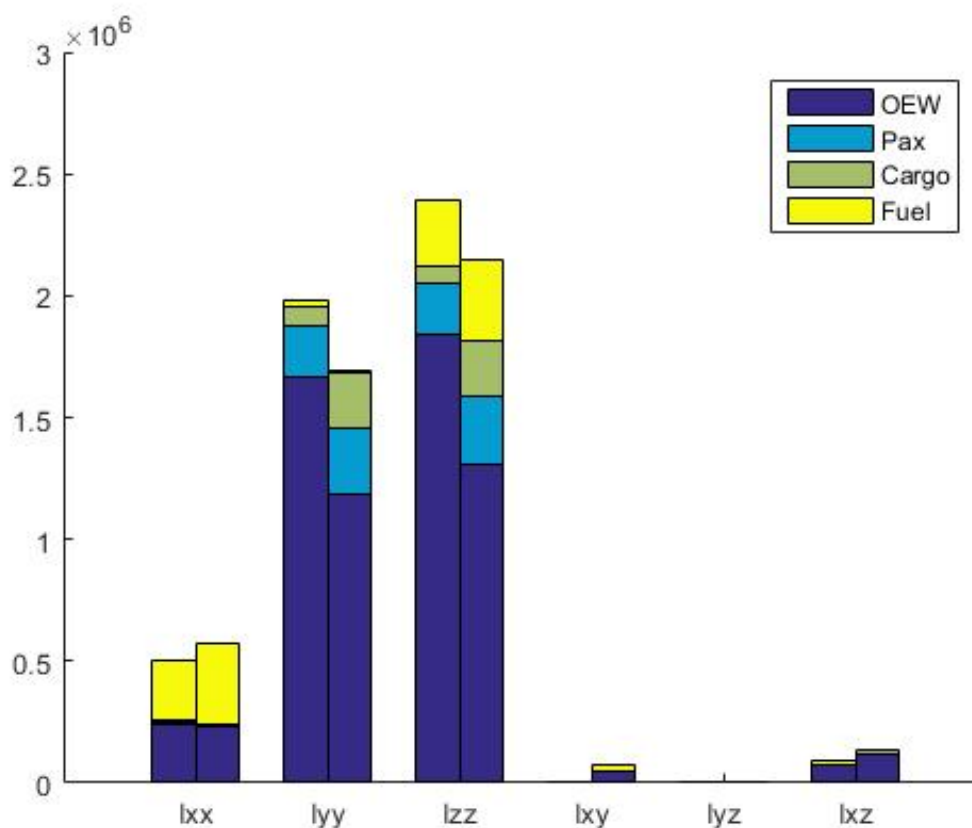


Figure 5.10: Inertia tensors calculated for the Fokker 100 (left) the Initiator Fokker 100 (right)

Now, in Figure 5.10 two sets of inertia tensors are shown. The left bars represent the reference Inertia tensors for a fully loaded Fokker 100, while the right bars represent those obtained for a fully loaded Fokker 100-like aircraft created by the Initiator. In Table 5.11 a comparison is made between the main geometrical and mass parameters of the Fokker 100 and the Initiator Fokker 100. As can be seen from this table the majority of these parameters are quite close, with a maximum error around 10% as can be expected from any preliminary sizing tool. Hence, from this data a valid comparison of the Inertia tensors of both aircraft can be made.

When comparing the Inertia tensors in Figure 5.10, it can be observed that the Initiator does a reasonable job at predicting the total Inertia tensors of the aircraft, with a slight tendency to under predict the symmetrical

Table 5.11: Comparison of the Fokker 100 and the Initiator-Fokker 100 most relevant parameters

Parameter	Fokker 100	Initiator-Fokker 100
MTOM [kg]	43090	44942
EOM [kg]	24375	26536
PLM [kg]	11242	11108
FM [kg]	8332	7299
Fuselage Length [m]	32.5	30.6
Fuselage Height [m]	3.3	3.71
Fuselage Width [m]	3.3	3.68
Wing Area [m <sup>2</sup> ]	93.5	106.9
Wing Span [m]	28.8	30
Wing Sweep [deg]	17.45	17.43
Wing MAC [m]	3.8	4.1
Horizontal Tail Area [m <sup>2</sup> ]	21.72	24.1
Horizontal Tail Span [m]	10.0	11.0
Horizontal Tail Sweep [deg]	26.0	26.2
Horizontal Tail MAC [m]	0.39	0.35
Vertical Tail Area [m <sup>2</sup> ]	12.3	17.2
Vertical Tail Height [m]	3.3	4.1
Vertical Tail Sweep [deg]	41.0	41.3
I <sub>xx</sub> [kg · m <sup>2</sup> ]	5.12 · 10 <sup>5</sup>	5.81 · 10 <sup>5</sup>
I <sub>yy</sub> [kg · m <sup>2</sup> ]	1.97 · 10 <sup>6</sup>	1.68 · 10 <sup>6</sup>
I <sub>zz</sub> [kg · m <sup>2</sup> ]	2.38 · 10 <sup>6</sup>	2.14 · 10 <sup>6</sup>
I <sub>xz</sub> [kg · m <sup>2</sup> ]	-7.54 · 10 <sup>3</sup>	1.35 · 10 <sup>5</sup>
I <sub>xy</sub> [kg · m <sup>2</sup> ]	6 · 10 <sup>1</sup>	8.6 · 10 <sup>4</sup>
I <sub>yz</sub> [kg · m <sup>2</sup> ]	7.64 · 10 <sup>4</sup>	-5.21 · 10 <sup>3</sup>

tensors ( $I_{xx}$ ,  $I_{yy}$ ,  $I_{zz}$ ). Also, it can be seen that the Initiator's inertia estimation module mainly has the tendency to under predict the empty aircraft's contributions. Furthermore, based on the fact that the Initiator-Fokker 100 is slightly larger than the actual Fokker 100, one would actually expect an over prediction of the Inertia tensor. Additionally, it may be observed that the contributions of the cargo seem to be over predicted and thus have a correcting effect on the overall results. Finally, it can also be observed that the contributions to the Inertia tensor caused by passengers and fuel are fairly similar for the Fokker 100 and the Fokker 100 like aircraft.

The aforementioned errors can be attributed to a variety of sources, but differences between the centre of gravity of the actual and the initiator aircraft are believed to be the major source of error. Now, it can be observed in Figure 5.10, that the  $I_{xx}$  component tensor is the symmetrical inertia component tensor predicted with the highest level of accuracy. This is expected, since the  $I_{xx}$  tensor (as shown by equation 3.67) only depends on the mass and distances between the y and z component of the aircraft's and its component's centres of gravity, which are fairly easy to predict. Furthermore it can be observed that the new module has the tendency to slightly over-estimate the fuel's contribution to the  $I_{xx}$  tensor. This can be explained by the fact that in the *getFuelInertia*-function, fuel is spread over the entire wing based on the theoretically available fuel volume between the spars and from root to tip. In reality however, the fuel tanks do not extend fully to the wing tip. As a consequence, the *getFuelInertia*-function stores more fuel mass further away from the centre of gravity, resulting in an over-prediction of the fuel's  $I_{xx}$  contribution.

Finally, it should be stressed that finding reference data that provides accurate estimates for the Inertia tensor, including the effect of loading the aircraft, is quite difficult. Therefore in this research, the *InertiaEstimation*-module is only validated for one aircraft, which is rather limited. Therefore, it is highly recommended for future work, to validate the module for more aircraft if accurate data can be found.

## 5.5. CONCLUSIONS

In this chapter, the updates made to the Initiator were validated. First, it was shown that the new derived relation for the take-off thrust loading constraint (equation 3.28) provided a much more accurate estimate albeit with a error margin around 20%. Furthermore it was shown by comparing the weight estimates obtained for several business jet and conventional aircraft with the Raymer's, Torenbeek's and GD's Class II weight estimation methods, that Torenbeek's method provided the most reliable result for both types of aircraft. As a consequence, the results that will be discussed in chapter 6 will be obtained with Torenbeek's method. Next, it was shown by separating the stability & control derivative estimation module from the Initiator and by comparing the estimates with reference data for the Boeing 747 and the Learjet 24, that the module is capable of predicting the longitudinal stability & control derivatives with a level of accuracy as may be expected from a preliminary design tool. Finally, also the updated inertia estimation module was validated by comparing the estimated tensor with data for the Fokker 100 and it was shown that the updated module has the tendency to slightly underestimate the inertia tensor. Now, from the foregoing discussion it may be concluded that the Initiator at this point may be used to investigate the effects of relaxed static stability on a business jet in the preliminary design phase.



# 6

## RESULTS & DISCUSSION

In this chapter the effects of relaxed static stability on the preliminary design of business jet aircraft are discussed. First in section 6.1 the baseline aircraft used to determine these effects is introduced. Next, the procedure used to decrease the static margin is explained in section 6.2. Finally, in section 6.3 it is discussed how changing the static margin affects the overall aircraft design in terms of weight, inertia tensor and stability and control derivatives.

### 6.1. BASELINE AIRCRAFT

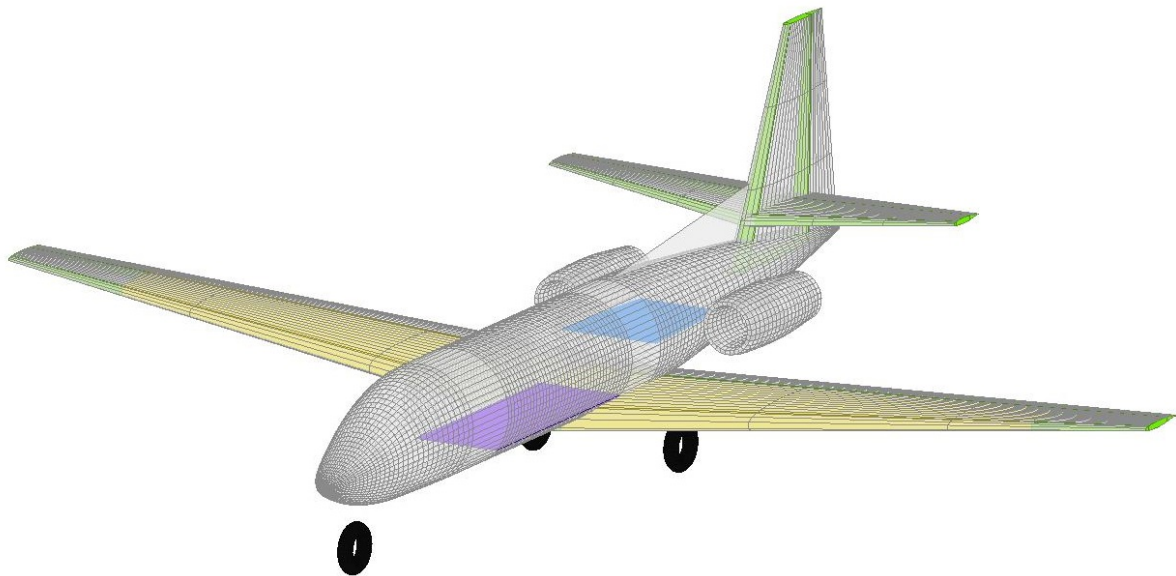


Figure 6.1: The Initiator-Citation

To assess the effects of relaxed static stability on the aircraft design, as well as on the handling qualities a reference business jet aircraft was created with the Initiator, based on the requirements of the Cessna Citation II. To create this baseline business jet aircraft, the Initiator's design convergence as explained in section 2.7 was slightly updated. In this updated design convergence the fuselage weight estimation module, which updates the fuselage weight in the Class 2.5 loop, is not used. Reason for excluding this module is that it overestimated the fuselage weight of business jets by a considerable margin. Moreover, this module estimated that the windows and doors are by far the largest contribution to the fuselage weight, each accounting for approximately one third of the total fuselage weight. Also, note that in this convergence, the convergence tolerance was set to 0.1% on the Class 2 Weight Estimation loop and a to 0.5% for the Mission Analysis and the Class 2.5 loops.

Now, in Figure 6.1 the geometry of the aircraft created by the Initiator with the Cessna Citation II's requirements is shown. To keep the difference with the actual Cessna Citation II clear, the aircraft created by the Initiator with the Cessna Citation's requirements will be referred to as the Initiator-Citation from this point on. Also, in Table 6.1 a comparison is made between the actual Citation II and the Initiator-Citation's most relevant parameters. The reference data in this table for the actual aircraft has been obtained from reference [30]. As can be observed from this table, the Initiator estimates the MTOM of the Initiator-Citation slightly higher than that of the actual aircraft. This can partially be attributed to the fact that the input payload is about 5% larger, causing the Initiator to overestimate the empty and fuel mass as well. Furthermore, in Table 6.1 it is shown that the fuselage of the Initiator Citation is slightly longer than the Citation II's fuselage. Furthermore, it may be observed that fuselage diameter is also slightly larger. This is caused by the fact the Initiator-Citation's fuselage is estimated with an inside-out approach, based on requirements for seat width, pitch and aisle width. Also, the data obtained from reference [30] actually shows the cabin width and height and thus a small margin should be added to obtain the fuselage's width and height.

Table 6.1: Comparison of the Citation and the Initiator-Citation's most relevant parameters

Parameter	Citation II	Initiator-Citation
MTOM [ $kg$ ]	6713	7470
ZFM [ $kg$ ]	5125	5652
Payload Mass [ $kg$ ]	1133	1200
Fuselage Length [ $m$ ]	13.39	13.11
Fuselage Height [ $m$ ]	1.47	1.54
Fuselage Width [ $m$ ]	1.47	1.54
Wing Area [ $m^2$ ]	30	33.27
Wing Span [ $m$ ]	15.75	16.74
Wing Sweep (1/4 Chord) [ $deg$ ]	0	0.9
Horizontal Tail Area [ $m^2$ ]	6.48	7.10
Horizontal Tail Span [ $m$ ]	5.79	5.96
Horizontal Tail Sweep (1/4 Chord) [ $deg$ ]	0	0
Vertical Tail Area [ $m^2$ ]	4.73	5.45
Vertical Tail Span [ $m$ ]	2.64	2.95
Vertical Tail Sweep (1/4 Chord) [ $deg$ ]	33	17.7

In Table 6.1 the most relevant properties of the Initiator-Citation's lifting surfaces are shown as well. As indicated in this table, the wing area is about  $3 m^2$  larger than the actual aircraft's wing area. This is caused by the fact that both aircraft have an identical wing loading, but since the MTOM of the Initiator-Citation is larger, its wing is also slightly larger than the actual wing. Furthermore, it can be seen that also the area of the horizontal and vertical tail are larger compared to those the Citation II. Now, these surfaces were sized based on the volume coefficient of the Citation II, which can be obtained from tables 8.5a and 8.5b in [19]. Moreover, from the data presented in in Table 6.1 it can also be deduced that the ratio of the horizontal tail area over the wing area ( $S_H/S$ ) is 0.216 for the actual Cessna Citation II, whereas that of the Initiator-Citation is 0.213. The same observation can be made for the vertical tail, with  $S_V/S$  equal to 0.158 for the Citation II and 0.163 for the Initiator-Citation. These ratios confirm the proper implementation of the tail volume coefficients along with the correct positioning of wing and tail surfaces.

In Figure 6.2 the most relevant changing parameters during the design convergence of the Initiator-Citation is shown. The top left plot in this figure shows how the error in MTOM converges over each iteration. In this particular case, the error between the Class I and Class II weight estimates requires five iterations to converge. This can also be seen in the top right figure, showing that both methods converge after five iterations at a MTOM of approximately 7 tonnes. Next, the mission analysis module is run for the first time, which simulates an entire aircraft mission from take-off to landing (including a divergence) and provides the Initiator with a new fuel fraction. The new fuel fraction is slightly higher than the one calculated with the Class II weight estimation. This can also be observed in the bottom left figure, where it is shown that the fuel fraction increases from around 0.22 to 0.24. Next on the top left plot it is shown that the Initiator needs another two runs of the Class II weight estimation in order to arrive at a new converged MTOM with the updated fuel

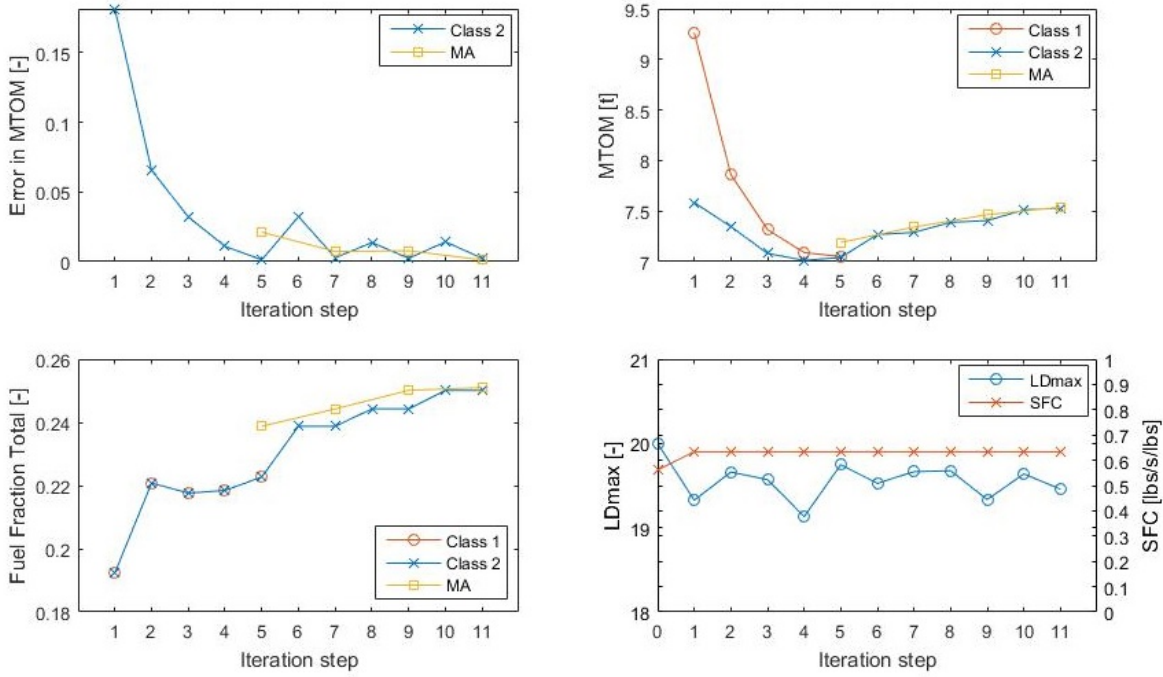


Figure 6.2: Overview of the design convergence for the Citation-Initiator

fraction. With the new converged MTOM, the mission analysis is run again to obtain a new estimate for the fuel fraction and this loop continues until the MTOM estimate converges at a MTOM around 7.5 tonnes. Finally, in the top right figure it is shown how the maximum lift-over-drag ratio and specific fuel consumption change per iteration of the design convergence. Observe that although the specific fuel consumption remains nearly constant, the maximum lift-over-drag ratio shows relatively large fluctuations throughout the design convergence. Up to this point no plausible explanation for these fluctuations has found and therefore it is recommended to further investigate this issue in future research with the Initiator.

## 6.2. PROCEDURE FOR RELAXED STATIC STABILITY

The approach used to obtain relaxed static stability in this research is to bring the aerodynamic centre closer to the centre of gravity by shifting the wing forwards by a percentage of the mean aerodynamic chord (see equation 6.1) as shown in Figure 6.3. Note that by moving the wing forward, the aircraft's centre of gravity moves forward as well, be it at a slower rate than the aerodynamic centre. As a consequence the static margin decreases. The wing shift however, should not be confused with the change static margin. Next, the horizontal and vertical tail are both sized with the volume coefficient of the Cessna Citation II as obtained from tables 8.5a and 8.5b in reference [19]. It is assumed that with this approach, the horizontal tail meets the stability and control requirements, such as control during take-off and landing. However, the horizontal stability estimation module as described in [11] would need be updated such that this assumption can be verified.

$$Shift = \frac{\Delta x}{MAC} \quad (6.1)$$

Furthermore, note that in order to obtain a fair comparison with respect to the effects of relaxed static stability, it was decided to keep the wing loading of the Initiator-Citation fixed throughout the Business Jet Convergence and equal to the wing loading of the original Citation II ( $W/S = 2202.5 \text{ N/m}^2$ ). The rationale behind this choice is that in the Initiator Design Convergence and thus also in the Business Jet Design Convergence, the thrust-wing-loading-diagram is updated each iteration. As a consequence, the chosen design point is also slightly different in each iteration, which affects the wing size and thus the weight estimate. Therefore it was decided to fix the wing and thrust loading and it was confirmed that the chosen design point lied in the available design space, be it not in the most optimal position.

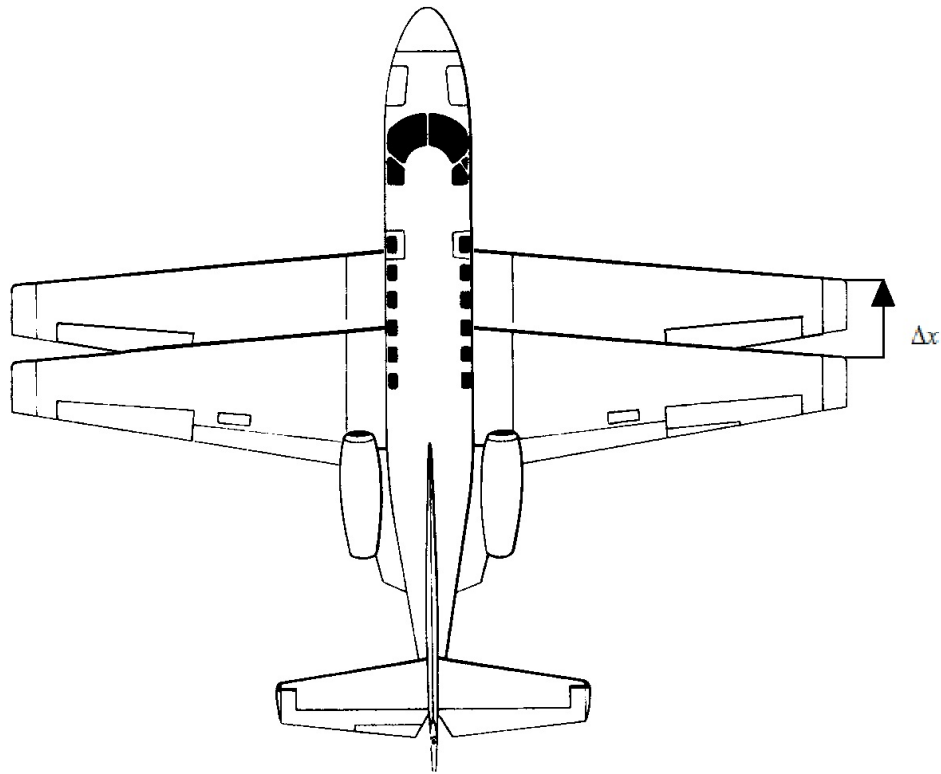


Figure 6.3: Definition of the wing shift

Moreover, it should be mentioned that there are a couple of different approaches to investigate relaxed static stability, which were discarded on purpose in this research. A first possibility would have been to use the *HorizontalStabilityEstimation*-module as described in reference [11], which sizes the horizontal tail based on Torenbeek's x-plot approach, which was shortly described in section 2.5. The module has indeed been used in this research, but while doing so, it was observed that it was not suited to achieve the research goals as formulated in section 2.8, for a couple of reasons of which the most important ones will be discussed here.

First of all, the *HorizontalStabilityEstimation*-module has the tendency to over-estimate the stabilizing effect of the engines during take-off. As a consequence the take-off control constraint shifts to the right in the x-plot diagram and becomes the active constraint by a considerable margin. A similar right shift was also observed for the stability requirements and as a consequence, the Initiator will shift the wing forward. As a consequence it was found that some aircraft were designed with a  $S_h/S$  of 0.3 or higher and with a centre of gravity shift ranging between 60 and 80% on the mean aerodynamic chord. For these reasons it was concluded that at this point the *HorizontalStabilityEstimation*-module is not suited for investigating relaxed static stability and therefore a different approach was chosen.

Finally, relaxed static stability could also have been achieved by keeping the wing position constant. In that case a frequently used approach is to shift the centre of gravity with one or more trim tanks [11]. Currently however, the Initiator is limited to one tank per part and therefore this type of relaxed static stability is not considered.

### 6.3. EFFECTS OF RELAXED STATIC STABILITY

A first anticipated effect of relaxed static stability is a decrease in horizontal and vertical tail area as their tail arm increases. In Figure 6.4, the change in area for the wing, horizontal and vertical tail area as a function of wing shift is shown. Observe that because the aircraft's MTOM reduces while the wing loading is maintained constant (see Figure 6.5), the wing area decreases as well. Consequently the horizontal and vertical tail area

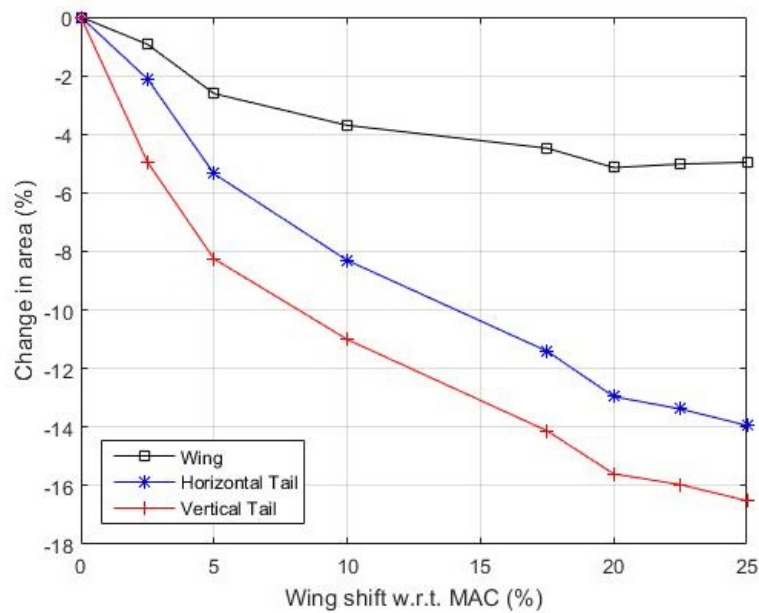


Figure 6.4: Change in wing, horizontal and vertical tail area as function of wing shift

decrease is due to the combination of increase in tail arm and decrease in wing area. Furthermore, it can be observed in this figure that a maximum wing area decrease of around 5% with respect to the baseline is obtained at a wing shift of 20%. Finally, a horizontal and vertical tail reduction of respectively 14% and 16% may be anticipated for a wing shift of 25%.

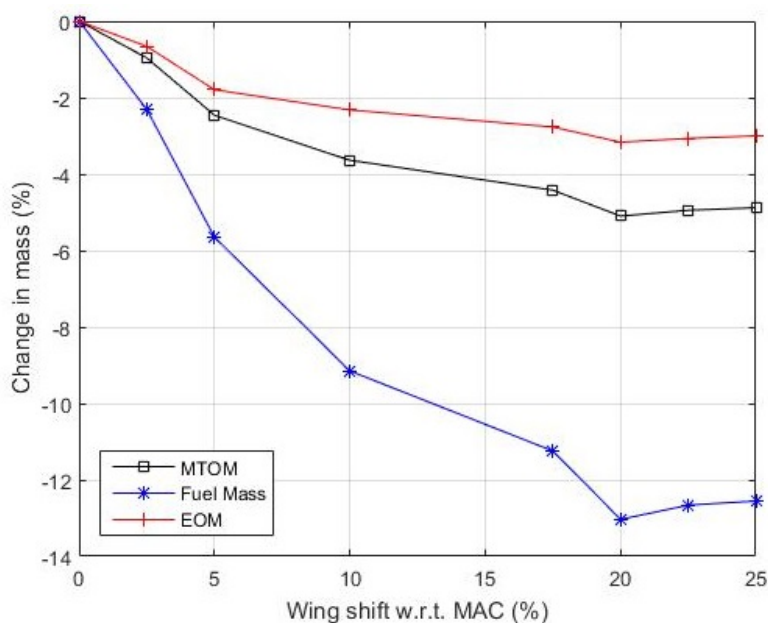


Figure 6.5: Change in MTOM, EOM and fuel mass as function of wing shift

A second anticipated effect of relaxed static stability is an overall reduction in the aircraft's MTOM, which has two primary causes. First there is the effect of reducing the horizontal and vertical tail size snowballing through the design. This means that since the components become smaller, the overall aircraft becomes lighter which allows for a smaller and thus lighter wing. Furthermore since the aircraft becomes lighter, the fuel required to fly the same mission reduces as well. As a consequence the anticipated weight loss is larger than simply the sum of the weight gains for the horizontal and vertical tail. Secondly, by reducing the static

margin, the stabilizer will produce less trim drag and thus an increase in lift-over-drag ratio may be expected. As a consequence, it is expected that a further reduction in fuel mass may be achieved, which will again have a snowball effect on the entire aircraft.

Now, in Figure 6.5 the effect of the wing shift on the maximum take-off mass, empty operative mass and fuel mass is shown for the Initiator-Citation. As can be observed in this figure, the general trend follows the expectations formulated in the previous paragraph. Also observe that the largest gain in terms of MTOM reduction actually is obtained by the decrease in fuel mass, rather than the decrease in EOM. Furthermore it may be observed that instead of steadily decreasing, the fuel mass decreases but at a fluctuating rate. This is believed to be caused by the fluctuation of the maximum lift-over-drag ratio during the Initiator's Design Convergence as was shown in the bottom left plot in Figure 6.2. Now, from Figure 6.5 it may be deduced that in case of the Citation-Initiator a maximum reduction around 5% in MTOM is achieved at 20% wing shift. For the same wing shift, the corresponding decrease in EOM of 3% may be achieved whereas a maximum reduction of 14% in fuel mass may be anticipated. As stated before the reduction in fuel mass is partially due to the reduction in aircraft mass, but also due to decrease in drag. This is can also be seen in Figure 6.6, which shows the change of the lift-over-drag ratio as function of the wing shift. Observe that at around 20% wing shift a kink in the curve appears. It will later be shown that this point also coincided with the change of sign in the aircraft's longitudinal stability.

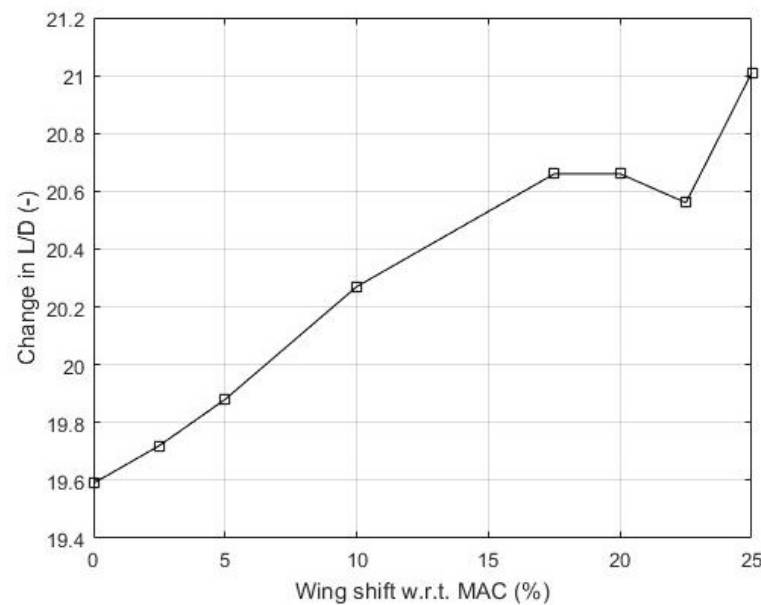


Figure 6.6: Change in lift-over-drag ratio as function of wing shift

Next, in Figure 6.7, the same comparison as in Figure 6.5 is made, however now the change in the mass of key components such as the wing, fuselage, horizontal and vertical tail is shown. As can be observed in this figure, the overall trend is a decrease in component mass, with the fuselage being a notable exception. The increase in fuselage mass can be explained when considering equation 3.12, which shows that in Torenbeek's method, the fuselage mass is amongst other variables also dependent on the tail arm. From a structural perspective this makes sense, because by increasing the tail arm, the moment caused by the horizontal and vertical tail on the fuselage increases as well. As a consequence, the fuselage needs to be reinforced to maintain the same structural stiffness and strength, thus becoming heavier. It is expected that if relaxed static stability were achieved by for instance by making use of a trim tank, the fuselage mass may be decreased as well.

Now, since it was observed that the largest gain with respect to MTOM and fuel mass was achieved at a wing shift of 20%, a top view of both aircraft has been plotted next to each-other in Figure 6.8. The most obvious change that may be observed in this figure is the forward shift in wing position. Furthermore, it can also be seen that the horizontal tail area and wing area have decreased albeit slightly harder to observe than the wing shift.

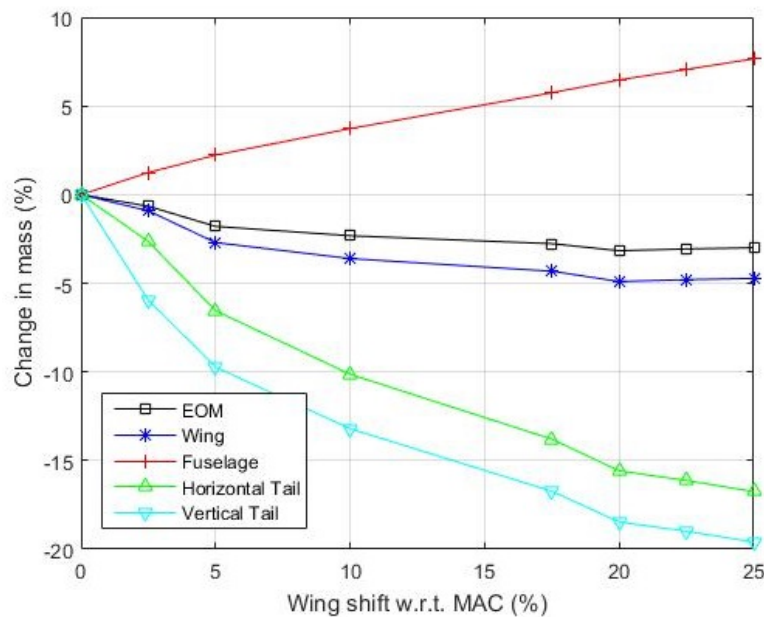


Figure 6.7: Change in MTOM, EOM and fuel mass as function of wing shift

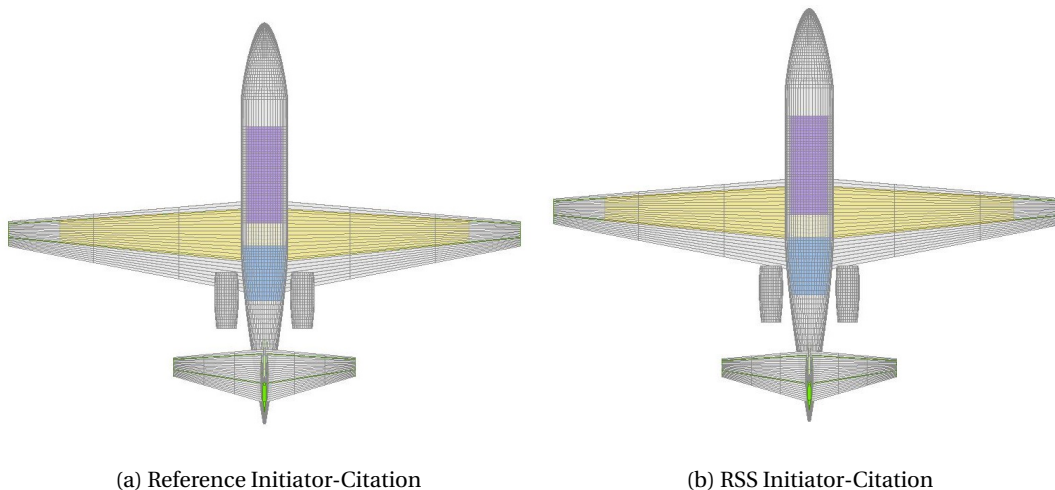


Figure 6.8: Comparison in geometry of Cessna Citation II with or without RSS

In Table 6.2, the change in angle of attack derivatives as a function of the wing shift is shown. Now, a first observation is that the drag-due-to-angle-of-attack derivative remains constant and that the lift-due-to-angle-of-attack decreases very slightly. Furthermore as expected, by shifting the wing and reducing the static margin, the longitudinal stability decreases considerably as may be observed in the last column in Table 6.2. Additionally, it can be observed that the aircraft becomes longitudinal unstable at wing shift slightly larger than 20%, which is also the point where the largest reduction in MTOM was achieved.

As can be observed in Table 6.3, the pitch rate derivatives have a tendency to decrease or even become more negative. Now in the case of the lift-due-to-pitch-rate derivative this may be explained by the fact the wing's contribution becomes smaller, which is a direct consequence of decreasing the static margin. Due to the fact that the tail volume is maintained constant in this comparison, the horizontal tail's contribution to this derivative remains nearly constant as well, note that there is a small change in  $C_{L_{\dot{\alpha}_h}}$  due to the reduction in tail size. In the case of the moment-due-to-pitch-rate derivative, the decrease is mainly caused by a larger

Table 6.2: Change in angle of attack derivatives versus wing shift

Derivative	0	5	10	15	20	25
$C_{D\alpha}$	0.195	0.195	0.195	0.194	0.195	0.195
$C_{L\alpha}$	6.104	6.102	6.100	6.099	6.095	6.093
$C_{m\alpha}$	-0.518	-0.434	-0.313	-0.129	-0.036	0.121

Table 6.3: Change in pitch rate derivatives versus wing shift

Derivative	0	5	10	15	20	25
$C_{lq}$	7.697	7.424	7.057	6.536	6.236	5.784
$C_{mq}$	-8.941	-9.441	-9.663	-9.473	-9.932	-9.998

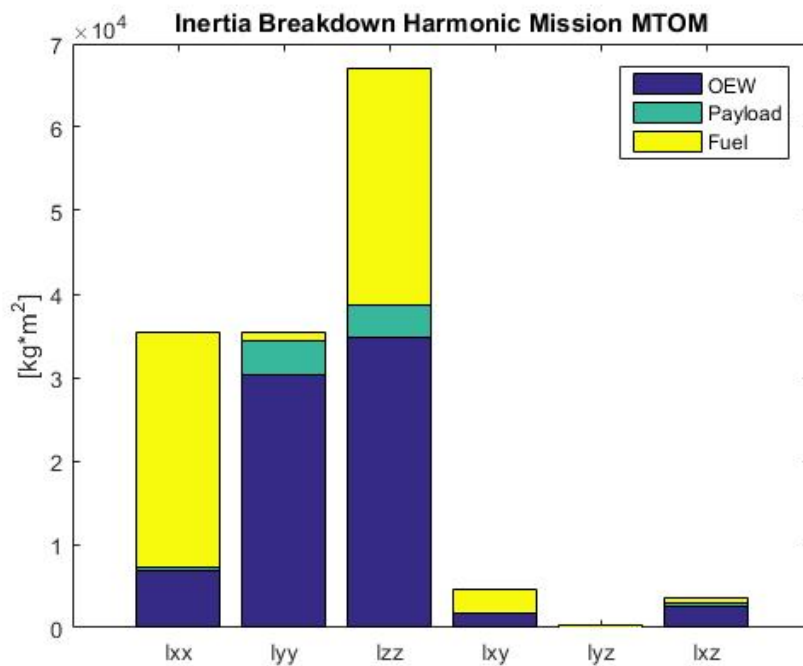
negative horizontal tail contribution, which can be explained by the fact that the tail arm becomes larger. The change in the wing's contribution to this derivative is minimal.

Table 6.4: Change in elevator control derivatives versus wing shift

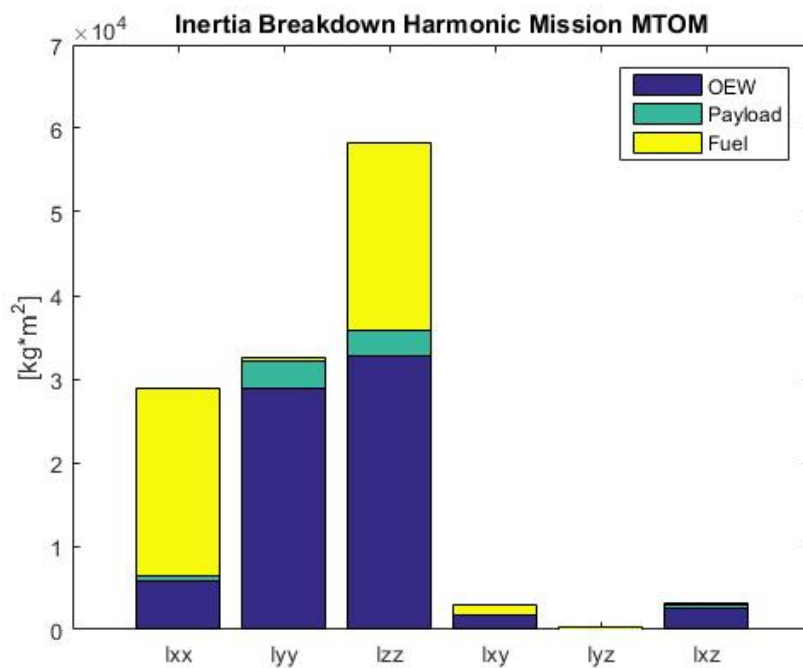
Derivative	0	5	10	15	20	25
$C_{D_e}$	0.021	0.021	0.020	0.020	0.020	0.019
$C_{L_e}$	0.672	0.652	0.639	0.634	0.616	0.608
$C_{m_e}$	-1.362	-1.388	-1.393	-1.379	-1.395	-1.390

In Table 6.4 the change in elevator control derivatives as a function of the wing shift is shown. Before discussing this result, it should be mentioned that in the Initiator the control surfaces are sized based on fractions of the wing and horizontal tail. For instance, in the case of the Initiator-Citation, the elevator is assumed to run over the entire horizontal tail's span and to have a chord of 0.3 times the horizontal tail's chord. Now, from Table 6.4 it can first of all be observed that although very small, the drag-due-to-elevator is not equal to zero, as is often assumed [20]. Furthermore it can also be seen that this derivative decreases with increasing wing shift, which is expected as the elevator decreases due to the decreasing horizontal tail area as shown in Figure 6.4. A similar observation can be made for the lift-due-elevator control derivative. Finally, the elevator control power actually increases for an increasing wing shift, which is believed to be caused by the fact that the increase in moment arm overcompensates for the decrease in elevator power due to the reduction in elevator size. To conclude this section, similar observations may also be made for the rudder control derivatives and the aileron control derivatives. Note that aileron control power will actually decrease, which is caused by a decrease in wing span and a decrease in aileron size.

Finally, in Figure 6.9 the inertia tensor of the reference Initiator-Citation is compared to the inertia tensor obtained for Initiator-Citation with a 20% wing shift. First, it may be observed that analogue to the Fokker 100 as discussed in section 5.4, the most relevant inertia contributions are those around the symmetrical axes. Furthermore, it may be observed that the fuel contribution to the Initiator-Citation's inertia tensor is relatively large. This makes sense because the fuel mass contributes more than 25% percent to the aircraft's MTOM when it is fully loaded. Moreover, since the fuel is stored in the wing it makes sense that fuel's contribution around the aircraft's body x and z-axis is relatively large, which may also be observed in Figure 6.9. Also, notice that the fuel contribution to the moment of inertia around the y-axis is minimal. This is caused by the fact that the fuel tank is very closely located to the y-coordinate of the aircraft's centre of gravity. Now, when comparing the inertia tensor of the original to that of the RSS aircraft, the expected decrease can be observed. From this figure it may be deduced that a maximal decrease around 15%, 11% and 13% may be obtained for respectively the  $I_{xx}$ ,  $I_{yy}$  and the  $I_{zz}$  components of the Inertia tensor.



(a) Reference Initiator-Citation's Inertia Tensor



(b) RSS Initiator-Citation's Inertia Tensor

Figure 6.9: Comparison of the Inertia Tensors



# 7

## CONCLUSIONS & RECOMMENDATIONS

In this final chapter, the major conclusions drawn and recommendations to be made from this research are summarized. The conclusions are discussed in section 7.1, while the recommendations can be found in section 7.2

### 7.1. CONCLUSIONS

At the beginning of this report, the following goals were formulated for the research into the effects of relaxed static stability on business jet aircraft:

1. Update the Initiator such that it can design a business jet aircraft with a preliminary level of accuracy
2. Quantify the effect of relaxed static stability on the business jet's preliminary design
3. Assess the effect of relaxed static stability on the dynamic behaviour of a business jet

In order to achieve these goals, the preliminary design tool called the Initiator has been used. Since this tool was set-up for large conventional commercial aircraft, the capabilities of the Initiator were extended as part of this research, such that it can also be used to analyse the preliminary design of business jet aircraft. First, the empirical weight estimation methods of Torenbeek and General Dynamics were added to Class 2 weight estimation. This was a necessary step for business jet aircraft, as the original Initiator uses Raymer's method, which is set-up for large cargo aircraft. Furthermore it was shown how the weight estimation modules were updated to account for the use of composites in modern aircraft and that an iterative MTOM-estimating loop was implemented. Based on the validation made for these updates, it may be concluded that at this point the Initiator is capable of predicting the MTOM of business jet aircraft with an average error margin around 5% if Torenbeek's weight estimation method is used. Furthermore, it was shown that a similar error margin may be obtained for conventional commercial aircraft, thus validating the usage of the updated Initiator as a preliminary design tool for both conventional and business jet aircraft.

Moreover, as part of this research, also the modules responsible for estimating the stability and control derivatives as well as the inertia tensor received numerous updates. The stability and control derivative estimation module was updated by implementing the empirical approach of Roskam, which is a simplified version of the DATCOM method. Furthermore, it was shown by validating the module with reference data for the Learjet 24 and the Boeing 747, that the updated module does a reasonable well job at predicting the longitudinal stability derivatives as well as the control derivatives. Finally, the inertia estimation module was updated with the lumped mass methods of Anemaat and DATCOM to estimate the empty aircraft's inertia tensor and a new lumped mass method was developed to estimate the contributions of the payload and fuel. This module was validated with reference data of the Fokker 100 and it was shown that the module could be used for preliminary design purposes although it has the tendency to slightly underestimate  $I_{yy}$  and  $I_{zz}$  inertia components.

Next, to assess the effect of relaxed static stability on business jet aircraft, a baseline aircraft called the Citation-Initiator was created and it was observed that a 5% decrease in MTOM may be achieved when reducing the Static Margin from the reference to zero. The anticipated decrease in EOM is slightly smaller at around 3%. By far the largest reduction in MTOM can be attributed to the reduction in required fuel mass, which is around

12% in the case of the Initiator-Citation. This reduction is a direct consequence of reducing the aircraft's MTOM, but also by decreasing the trim drag. This is also reflected in the fact that an increase around 5% for Initiator-Citation's maximum lift-to-drag-ratio was obtained.

Now, when looking at the effect of RSS on various aircraft components some remarkable conclusions can be made. First, although it was observed that the EOM decreases by 3%, the weight of the fuselage actually increases by around 7%. This is caused by the fact that in this research, RSS is obtained by shifting the wing forward. As a consequence the tail arm increases, but this also results in a heavier fuselage weight because the bending moment on the fuselage increases. Therefore it is anticipated that a further reduction in MTOM may be achieved if RSS would for instance be obtained by making use of a trim tank. Furthermore it was observed that RSS results to a reduction in wing, horizontal and vertical tail area, which also reflects in a reduction of their component weights. The reduction in wing size is direct consequence of the reduction in MTOM and keeping the wing-loading constant, hence a wing weight reduction of 5% was obtained. The increased tail arm is responsible for reducing the horizontal tail and vertical tail weight by 14% and 16% respectively.

The most noticeable effect of RSS on the stability derivatives, was the change of the Initiator-Citation's  $C_{m_\alpha}$  from -0.518 for the reference aircraft to -0.036 for the aircraft with a 20% wing shift. Which effectively means that for this wing shift, the aircraft is still longitudinal stable, but only just. Furthermore, a steady decrease in the pitch rate derivatives was observed for an increase in wing shift. Also, it was rather surprisingly observed that although the elevator's size decreases, the elevator control power is almost unaffected by relaxed static stability. This can again be attributed to the fact that the tail/elevator-arm increases. Note that if a trim tank would be used, a more noticeable effect on the elevator control derivative would be expected. Finally, as anticipated the drag and lift due to elevator deflection slightly decreased, which can be attributed to the fact that the elevator size decreases in accordance with the decrease in horizontal tail size.

## 7.2. RECOMMENDATIONS

With respect to the weight estimation three major recommendations can be made. First, as indicated in chapter 6.3, there are still some relatively large fluctuations in maximum lift-to-drag-ratio per iteration in the Initiator's Design Convergence. Now, because these fluctuations result in a large uncertainty bound on the fuel estimate, they are a major source of error in the results. Therefore, for future work it is recommended to further investigate, what causes these fluctuations. Furthermore, when estimating the weight of the systems, the effect of adding a fly-by-wire system to deal with negative longitudinal stability has not been incorporated. When negative stability would be investigated in future work, it is highly recommended to implement this effect, as otherwise overly optimistic results may be expected. Finally, the equations used to estimate the instruments weight in the Class 2 Weight Estimation, rather conservatively assume that conventional analogue instrument are used. Modern (business jet) aircraft frequently make use of a so-called "glass cockpit" and thus an improvement in the predicted systems weight and MTOM may be expected if more accurate relations for this type of instruments would be implemented.

Next, as shown in section 5.3, the estimation of some of directional and lateral stability derivatives is still quite rough. Therefore it is suggested to expand the current approach with results from AVL and/or DATCOM. Do note that the current module has one major advantage over AVL, which is that it also takes the effects of fuselage and nacelles into account, whereas AVL only considers the effects of the lifting surfaces. Finally note that the stability & control derivatives obtained with the module should only be used as a first estimate and that more accurate methods such as CFD methods or wind tunnel tests should be used to obtain more reliable estimates.

As mentioned in section 6.2, relaxed static stability in this research is achieved by shifting the wing forward. The horizontal and vertical tail are then sized with the volume coefficient of the reference aircraft. Another approach would be to estimate the horizontal tail size with the Initiator's horizontal stability estimation module. In this research the module has been discarded, because of its tendency to move the wing too much forward leading to unreliable results. If this issue could be solved however, it is recommended to use this module and expand its capabilities such that it can also put a constraints on the horizontal tail size for instance for take off or the landing flare. Furthermore, it is anticipated that an improvement in accuracy can be achieved, if the Initiator's directional stability estimation module would be used to size the vertical tail, instead of using the

vertical tail volume coefficients. As stated before, this module is currently not used, because of its tendency to maximize the tail arm, by increasing the vertical tail's sweep.

There are also a couple of recommendations to be made for future expansions within the Initiator. Currently the cargo bay of aircraft with a low cabin floor are placed directly behind the cabin. Next, it is checked whether the fuel required for the harmonic mission fits in the wing and if this is not the case a fuel tank is placed behind the cargo bay. This obviously has a large effect on the c.g. range during cruise and therefore it is recommend to change the design logic in the future, such that the cargo bay is shifted to the rear if a fuselage tank is required. Furthermore, some business jet aircraft such as the Cessna Citation II have a cargo bay in the nose, this is currently not possible with the Initiator. Also, at the moment EMWET is only used to estimate the weight of the main wing's wingbox, which is then used to estimate the main wing's contribution to inertia tensor. To make the inertia estimation method more consistent it is suggested to use EMWET to estimate the horizontal tail's weight as well. The limiting factor at the moment is that EMWET estimates the wingbox weight first based on the input load and then uses a correction factor to account for the secondary structure's weight. Hence, to use EMWET on the horizontal tail this correction factor for horizontal tails should be estimated first.

Finally, as mentioned in the conclusions, relaxed static stability in this research was obtained by shifting the wing forward. For future work however, it may be interesting to investigate how RSS affects the aircraft design if other methods are used. For instance trim tanks could be used, and when this approach is used it is anticipated that gains in the fuselage weight could be made at the cost of elevator effectiveness. Furthermore, for this type of relaxes static stability, it would also be necessary to estimate the added weight to the control and fuel system required for automatically moving fuel around during flight. To quantify these statements further research would be required and this would also require a major update to the Initiator, because currently only one tank per aircraft part can be created.



# A

## CLASS II WEIGHT ESTIMATION: ASSUMPTIONS

The Class II Weight Estimation methods have been developed for conventional aircraft types (wing-fuselage-tail combinations). As such within the *Class2WeightEstimation*-module a conventional aircraft configuration is assumed and care should be taken when using it to estimate the weight of non-conventional aircraft (e.g. BWB's, Prandtl planes, etc.). Furthermore, when implementing Torenbeek's and the GD-method in the module, some additional assumptions were made, which will be explained in the following paragraphs.

First, the furnishing and operational items weight highly depends on the design range of the aircraft. Therefore four design range categories are assumed, each with corresponding correction factors. The design categories with their respective ranges are:

- **Regional/short range:** assumed to have a design range below 1500 nmi (2778 km).
- **Medium range:** assumed to have a design range between 1500 nmi (2778 km) and 2500 nmi (4630 km).
- **Long range:** assumed to have a design range between 2500 (4630 km) and 5000 nmi (9260 km).
- **Ultra long range:** assumed to have a design range over 5000 nmi (9260 km).

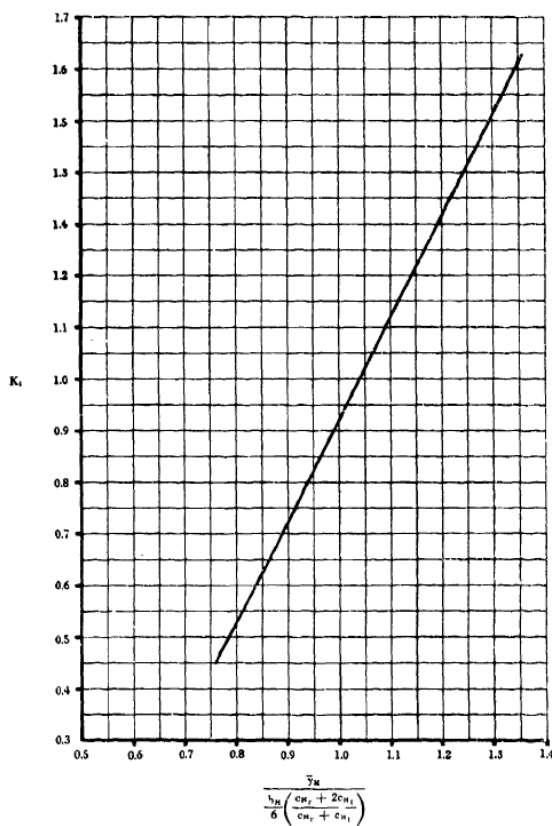
Next, the following assumptions have been made with respect to estimating empty weight ( $W_E$ ):

- **Wing:**
  - The main wing is assumed to have lift-dumping surfaces or spoilers mounted on it's upper surface.
  - It is assumed that flaps are installed, which can be of any type except for the fowler flap type.
- **Fuselage:**
  - It assumed that the fuselage is pressurized up to a maximum differential pressure of 8.6 psi.
  - The number of (belly) cargo doors is settable in the setting files. In case it is not specified, a standard of 2 cargo doors is assumed.
- **Empennage:**
  - The horizontal tail is assumed to be fixed ( $K_h = 1$ ).
  - It's assumed that the elevator takes up approximately 20 percent of the horizontal tail area.
- **Nacelles/Engines:**
  - Fuselage buried nacelles are not considered: nacelles are assumed to be mounted on either the wing or the fuselage ( $K_{intl} = 1$ ).
  - The pylon is assumed to be 85% of the nacelle length.
  - The nacelle diameter is assumed to be 110% of the engine diameter.
  - The nacelle lip is assumed to be 15% of the nacelle length.
  - The maximum static pressure typically ranges between 15 and 50 psi, for this method the average of 32.5 psi is assumed.
  - It is assumed that no afterburner is installed.

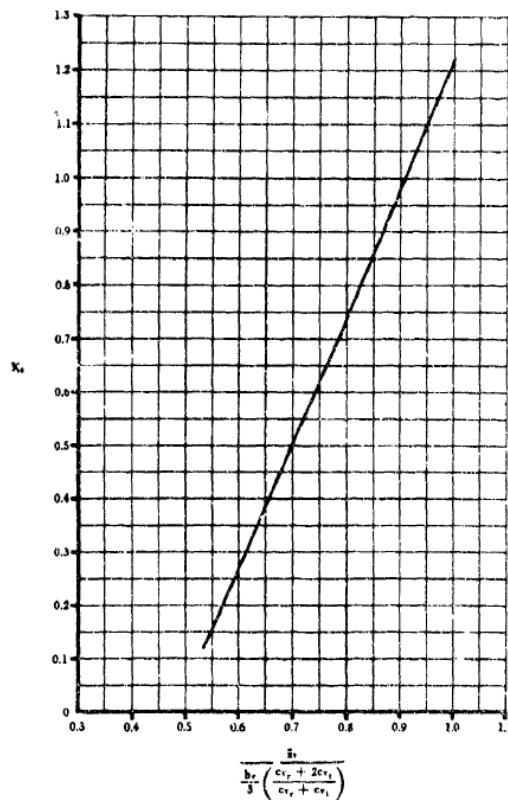
- It is assumed that engines with a bypass ratio higher than 3 can be considered high bypass ratio engines.
- The installed engine mass is assumed to be 1.3 times the dry engine weight [8].
- **Systems and fixed equipment:**
  - The control system is assumed to be (electrically) powered.
  - The number of functions performed by the control ranges typically between 4 and 7 [8], the average of 5.5 is assumed.
  - The number of mechanical functions performed by the controls typically range between 0 and 2 [8], the average of 1 is assumed.
  - It is assumed that wing mounted control surfaces use 10% of the wing area.
  - The systems electrical rating typically ranges between 40 to 60 kVA for commercial transport aircraft [8], the average of 50 kVA is assumed.
  - It is assumed that Jet A-1 with a density of 6.84 lbs/gal is used.
  - Integral fuel tanks or a so-called wet wing is assumed.
  - Reciprocation engines are not considered, i.e. the engines are of type turbojet, turbofan or turbo-prop.
  - For conventional transport aircraft, it is assumed that the cabin takes up to 40% of the fuselage volume, while for business jets this fraction goes up to 70%.
  - The APU is assumed to weigh approximately 0.8% of the MTOW [18].
  - The uninstalled avionics weight typically ranges between 800 to 1400 lbs [8], the average 1100 lbs is assumed.
  - Paint is assumed to weigh 0.45% of the MTOW [18].
  - It is assumed that flight crew consists of 2 pilots.
  - At least one flight attendant per 50 passengers is assumed.

# B

## DATCOM FIGURES



(a) Horizontal Tail Rolling  $K_4$ -factor



(b) Vertical Tail Rolling  $K_5$ -factor

Figure B.1: Empennage rolling  $K$ -factor

In section 3.4, it was described how the inertia tensors for the horizontal and vertical tail plane are to be estimated, using the method as described in Section 8.1 of DATCOM [34]. To determine the horizontal tail's rolling moment of inertia around it's centroid, equation B.1 is used and the  $K_4$ -factor can be determined from Figure B.1a[34].

$$I_{Ox_{HT}} = \frac{W_{HT} b_{HT}^2 K_4}{24} \left( \frac{c_{r_{HT}} + 3c_{t_{HT}}}{c_{r_{HT}} + c_{t_{HT}}} \right) \quad (B.1)$$

A similar procedure is used to estimate the vertical tail's rolling moment of inertia around its centroid (see equation B.2). The  $K_5$ -factor in this equation can be determined from Figure B.2.

$$I_{ox_{VT}} = \frac{W_{VT} b_{VT}^2 K_5}{18} \left( 1 + \frac{2c_{r_{VT}} c_{t_{VT}}}{(c_{r_{VT}} + c_{t_{VT}})^2} \right) \quad (\text{B.2})$$

# C

## CLASS2WEIGHTESTIMATION-MODULE

In chapter 4, the general work flow of the *Class2WeightEstimation*-module has been described. In this appendix a more detailed description of this module's main functions and their respective in- and outputs is given.

### GETMAINWINGWEIGHT

The *getMainWingWeight*-function estimates the mass and centre of gravity of the aircraft's main wing. This function has three inputs: the Initiator controller, a wing-object and an input-string indicating which method of the three available methods (Raymer, Torenbeek or GD) should be used. The function also checks whether the mass-estimate has to be corrected for the use of composites. Recall that this correction is based on the correction factors described in section 3.1. Furthermore, the methodology as described in chapter 3.2 is unable to estimate the wing weight of a wing with a kink, therefore the *equivalentWing*-function is called to transform the wing into the equivalent wing. Finally, note that the *getMainWingWeight*-function can be used to estimate the weight of a boxwings as well, the function is then simply called twice: once for the front/lower wing and a final time for the rear/upper wing.

### GETFUSELAGEWEIGHT

The *getFuselageWeight*-function is used to estimate the aircraft's fuselage weight and centre of gravity. The function has three inputs: the Initiator controller, the fuselage-object and the method-string. Just like the *getMainWingWeight*-function, this function also checks and corrects the fuselage mass-estimate for the use of composites. Furthermore, note that if Raymer's approach is used, a correction factor ( $K_{ws}$ ) dependent on the main wing geometry needs to be estimated. Therefore, the wing-object is called from the controller in this case and transformed into the equivalent wing with the *equivalentWing*-function, after which this correction factor may be determined.

### GETWINGWEIGHT

The *getWingWeight*-function estimates the mass and centre of gravity of all lifting surfaces, excluding the main wing. This function has also three inputs: the aircraft-object, the lifting surface-object and the method-string. Within the function two separate cases have been implemented: one to estimate the weight of the horizontal tail or the canard (or both in case of a three-surface aircraft) and another to estimate the vertical tail's weight. Note that the current *getWingWeight*-function cannot be used to estimate the weight of unconventional tail types such as a V-tails or Y-tails.

### GETENGINEWEIGHT

The *getEngineWeight*-function estimates the mass and centre of gravity of the dry engine as well as other parts of the propulsion system. Note that in case of turboprop aircraft, this function, can only be used to estimate the dry engine mass. The *getEngineWeight*-function has as input-arguments the Initiator controller, a single engine-object and the method-string. The dry-engine mass is estimated from the engine database within the Initiator and is assumed to be simple function dependent on the static thrust. Finally, note that the assumptions made when implementing the *getEngineWeight* can be found in Appendix A.

#### GETFIXEDEQUIPMENTWEIGHT

Depending on the selected methodology, the *getFixedEquipmentWeight* accounts for the mass contributions of the fuel system, flight controls, instrumentation, electrical system, airconditioning system, APU, etc. This function has two inputs, being the Initiator controller and the method-string. All assumptions made when creating this function can be found in Appendix A.

#### GETFURNISHINGWEIGHT

The *getFixedEquipmentWeight*-function is used to estimate the mass and centre of gravity of the furnishing. What is meant by furnishing highly depends on the selected methodology, but in general it contains contributions of seats, lavatories, galleys, etc. Just as the *getFixedEquipmentWeight*-function, it has the Initiator controller and the method-string as inputs.

#### GETOPERATIONALITEMS

The operational items account for the crew provisions, the cabin supplies, the potable water and the toilet chemicals, safety equipment and residual fuel. In order to estimate the mass and the centre of gravity of these items, the *getOperationalItems*-function is used. Since only Torenbeek's methodology takes these items into account [6], the function has a single input argument, being the Initiator controller.

#### GETLANDINGGEARWEIGHT

The *getLandingGearWeight*-function is a simplified version of the module developed by N.C. Heerens in reference [37]. The function only takes the Initiator controller and first estimates the number of wheels on the landing gear based on the aircraft database. By imposing lateral and longitudinal limits on the gear, the landing gear is completely designed, after which the weight can be estimated by adding the weight of its components.

#### MISSIONESTIMATIONCLASSII

The estimate for the fuel mass made with the *Class1WeightEstimation*-module is updated with *MissionEstimationClassII*-function. This function has the Initiator controller and the OEM (determined by adding the contributions of the aforementioned functions) as inputs. Based on these inputs, the *MissionEstimationClassII* runs through a variety of missions (ferry, harmonic, etc.) and updates the estimate for the fuel mass. Furthermore, it checks whether the calculated fuel volume fits within the aircraft's tanks and draws the corresponding payload range diagrams.

# D

## STABILITY AND CONTROL DERIVATIVES ESTIMATION FUNCTIONS

In chapter 4, the general work flow of the *ControlStabilityDerivativeEstimation*-module has been described. In this appendix a more detailed description of the module's main functions and their respective in- and outputs is given.

### IMPERIAL

As mentioned before the stability and control derivatives are estimated with the approach described in Airplane Design part VI [20]. This method uses the imperial system, while in the Initiator the metric unit system is used. Therefore the *imperial*-function was written to convert all relevant parameters into the imperial unit system. The function takes the Initiator controller as input and outputs two structure arrays, called *aero* and *obji*. The *aero*-array contains all relevant aerodynamic properties (air density, dynamic viscosity, Mach number, etc.). All parameters related to the geometry of the aircraft are stored in the *obji*-array. Finally, note that this function also handles the conversion from the actual aircraft wing into the equivalent wing (in imperial system).

### GETSTEADYSTATE

This function takes the Initiator controller and the *aero*-array as inputs and calculates the steady state lift and drag coefficient. First, the steady state lift coefficient is calculated with equation 3.38. Next, the drag polar is called from the Initiator controller, from which then the steady state drag coefficient can be determined. Finally, the results are returned to the main run-file in a structure array called *SS*.

### CALCULATEANGLEOFATTACKDERIVATIVES

*CalculateAngleofAttackDerivatives* is used to calculate the stability derivatives with respect to angle of attack ( $C_{L_\alpha}, C_{D_\alpha}$  &  $C_{M_\alpha}$ ) and rate of angle of attack ( $C_{D_{\dot{\alpha}}}, C_{L_{\dot{\alpha}}}$  &  $C_{M_{\dot{\alpha}}}$ ). Recall that these derivatives are estimated with the method as described in Chapter 10.2 of Airplane Design Part VI [20]. The function takes the Initiator controller and the *imp* and *aero* structures as input and stores its results in a single structure array called *AOAD*.

### CALCULATEANGLEOFSIDESLIPDERIVATIVES

The *CalculateAngleofSideslipDerivatives*-function is used to calculate the stability derivatives with respect to angle of sideslip ( $C_{y_\beta}, C_{l_\beta}$  &  $C_{n_\beta}$ ). Just like the *CalculateAngleofAttackDerivatives*-function, this function takes the Initiator controller and the *imp* and *aero* structures as input and stores its results in a single structure array called *AOSD*.

### CALCULATEROLLRATEDERIVATIVES

*CalculateAngleofSideslipDerivatives* estimates the stability derivatives with respect to roll rate ( $C_{y_p}, C_{l_p}$  &  $C_{n_p}$ ). This function takes the Initiator controller, the vertical tail's contribution to the sideforce-due-to-sideslip-derivative ( $C_{y_{\beta_v}}$ ) and the *imp* and *aero* structures as input and stores the results in the structure array called

*RRD*. Note that for the estimating the yawing-moment-due-to-roll-rate derivative ( $C_{n_p}$ ), only the effect of deflecting plain flaps is taken into account. For future work, it is recommended to expand the current function to account for the deflection of other flap types as well, by using the methodology as described in Chapter 8 of reference [20].

#### CALCULATEPITCHRATEDERIVATIVES

The *CalculatePitchRateDerivatives*-function is used to estimate the stability derivatives with respect to pitch rate ( $C_{D_q}, C_{l_q}$  &  $C_{m_q}$ ). This function takes the Initiator controller and the *imp* and *aero* structures as input and stores the results in the structure array called *PRD*

#### CALCULATEYAWRATEDERIVATIVES

The *CalculateYawRateDerivatives*-function is used to determine the derivatives with respect to pitch rate ( $C_{y_r}, C_{l_r}$  &  $C_{n_r}$ ). Just like the *CalculateAngleofSideslipDerivatives*, this function uses the Initiator controller, the vertical tail's contribution to the sideforce-due-to-sideslip-derivative ( $C_{y_{\beta v}}$ ) and the *imp* and *aero* structures as input. Its results are stored in a structure array called *YRD*

#### CALCULATEAILERONCONTROLDERIVATIVES

In the *CalculateAileronControlDerivatives*-function, the control derivatives with respect to aileron deflection are estimated ( $C_{y_a}, C_{l_a}$  &  $C_{n_a}$ ). The function takes the initiator controller and the *imp* & *aero* structures as input and estimates the control derivatives with the methodology from reference [20]. Finally, it stores the results in a structure array called *AileronDerivatives*. Note that for all control derivatives, it is assumed that the deflection of the surface is the same as deflecting a plane flap

#### CALCULATEELEVATORCONTROLDERIVATIVES

The *CalculateElevatorControlDerivatives*-function is used to estimate the control derivatives with respect to elevator deflection ( $C_{D_e}, C_{L_e}$  &  $C_{m_e}$ ). The function takes the initiator controller and the *imp* & *aero* structures as inputs and estimates and stores the results in a structure array called *ElevatorDerivatives*.

#### CALCULATERUDDERCONTROLDERIVATIVES

The *CalculateRudderControlDerivatives*-function is used to estimate the control derivatives with respect to rudder deflection ( $C_{y_r}, C_{l_r}$  &  $C_{n_r}$ ). The function takes the initiator controller and the *imp* & *aero* structures as inputs and estimates and stores the results in a structure array called *RudderDerivatives*. Note that this function is only capable of calculating the rudder derivatives of aircraft with a single vertical tail! Furthermore it is not possible to estimate the rudder derivatives of a split rudder's parts.

# E

## DETAILED INERTIA ESTIMATION FUNCTIONS

In chapter 4, the general work flow of the *InertiaEstimation*-module has been described. In this chapter a more detailed description of this module's main functions and their respective in- and outputs is given.

### BODIESOFREVOLUTIONINNERTIA

The *BodiesOfRevolutionInnertia*-function is used to calculate the inertia contributions of the fuselage and the nacelles (without engines), based on the methodology as described in section 3.4.1. The function has three inputs: that aircraft's the centre of gravity, the cylindrical the part's geometry and its weight. Next, the cylindrical object is divided into lumped masses as explained for which the mass and centre of gravity is determined as explained in section section 3.4.1. Next, the inertia contributions of each lumped mass is calculated with equations 3.67 to 3.70, which are added first in a loop over the cross-section and then in a loop over the entire part, in order to obtain the part's inertia contributions. The output of this function is a single 3x3 inertia matrix.

### LIFTINGSURFACESINNERTIA

The *LiftingSurfacesInertia*-function estimates the inertia tensors of the main wing, based on the approach described in section 3.4.2. This function has four inputs, being the Initiator controller, the main wing part, the aircraft's centre of gravity, and the density of the material used in the wing.

From the Initiator controller, the results from the *EMWETWeight*-module are called first, from which the number of stations is called in which the wing should be divided. Next, the weight fractions of skin, ribs, spars is determined using the *CalculateWeightFractions*-function, after which the slope in equations 3.72 to 3.74 is determined. Next, a loop is started over each aerofoil section which first calculates the area of aerofoil segment, with the *AirfoilArea*-function. Next, the A1, B1 and C1 terms in equation 3.73 to 3.72 are determined, after which the centre of gravity and the mass of the lumped mass on that aerofoil segment may be estimated. From these results, the inertia contributions of those lumped masses is estimated with equation 3.67 to 3.70, which are then are then added per aerofoil segment and then over the entire wing.

Once this loop over the entire wing has been completed, the result it multiplied by two to account for the inertia of both the left and right wing-half. Finally, *BodiesOfRevolutionInnertia*-function outputs the results for the main in a single 3x3 inertia matrix.

### CALCULATEWEIGHTFRACTIONS

The *CalculateWeightFractions*-function is called in the *LiftingSurfacesInertia*-function in order to estimate the weight fractions of the major components with respect to the total wing weight. It takes as inputs, the Initiator controller, the wing surface object, the density of the wing material and the locations of the front and rear spar. Based on these inputs, it calls the following functions to calculate the weight of the wing's major components:

- *CalculateSparMass*
- *CalculateSkinMass*
- *CalculateRibMass*

Next, the wing-box weight is calculated from the primary structure weight, after which the fractions of the major components with respect to total wing weight are calculated. Finally, the results are stored in a single structure, called *WeightFraction*

#### CALCULATESPARMASS

The *CalculateSparMass*-function is called by the *CalculateWeightFractions*-function and calculates the spar mass based on the following inputs: the Initiator controller, the spar location, thickness and material density and the wing surface. Based on the number of EMWET stations, the spar is split in an equal amount of stations after which the volume for each spar station is calculated based on the spar and wing thickness. By multiplying the spar volume with the material density and by two for the other wing half, the total spar weight is determined.

#### CALCULATESKINMASS

The *CalculateSkinrMass*-function is called by the *CalculateWeightFractions*-function and calculates the skin mass based on the following inputs: the Initiator Controller, the skin thickness, the wing surface, material density and front and rear spar position. Just as for the *CalculateSparMass*-function, the amount of stations is set equal to the amount of EMWET stations, after which the volume of the skin is calculated and multiplied by the material density and by two to obtain the weight of the skin for the entire wing. Note that this function needs to be called twice, once to calculate the weight of the upper skin and a second time for the weight of the lower skin.

#### CALCULATERIBMASS

The *CalculateRibMass*-function is also called by the *CalculateWeightFractions*-function and calculates the rib mass based on equation 3.76. It takes the MainWing object and the material density as inputs and outputs the rib mass.

#### POINTMASSINERTIA

The *PointMassInertia*-function calculates the inertia matrix for a point mass. It takes the weight of the part, that part's centre of gravity and the aircraft's centre of gravity as inputs and calculates the inertia matrix bases on equations 3.67 to 3.70. The output of this function is a 3x3 inertia matrix.

#### GETSYSTEMINERTIA

The *getSystemInertia*-function calculates the inertia tensors for the aircraft systems. It takes the Initiator controller and the Class 2 Weight Results as input. Based on the method selected for the Class 2 Estimation-module, this function will call the systems incorporated within that method and estimate the inertia tensors with the *PointMassInertia*-function. At the end of this function the inertia contributions are added and outputted in a single 3x3 inertia matrix.

#### GETOPERATIONALITEMSINERTIA

Unlike the systems, the operational items are not specific to the Class 2 Weight Estimation method. Their inertia tensors are estimated with the *getOperationalItemsInertia*-function, which takes the Class 2 Weight results as input and calculates the inertia tensors of all operational items with the *PointMassInertia*-function. The output of this function is a 3x3 inertia matrix.

#### GETFUELINERTIA

The *getFuelInertia*-function takes the Class 2 Weight Estimation results as input and calculates the inertia tensors of the fuel based on the approach described in section 3.4.3. Recall that in this approach, each wing-half is divided into 40 station and that the fuel volume is divided over the wing based on the available fuel volume ratio. Next, the centre of gravity locations of each wing station is calculated and the *PointMassInertia*-function is used to calculate the inertia contributions of each station. Finally, all fuel inertia contributions are added and outputted by *getFuelInertia*-function in a 3x3 inertia matrix for the fuel. Again, it is important to stress that this function cannot be used to estimate the inertia contribution of belly or trim tanks.

#### GETPAYLOADINERTIA

The *getPayloadInertia*-function uses the Class 2 Weight Results and the Initiator controller as inputs. From this controller it will call the aircraft fuselage and make a loop through every cabin and another loop through all the seats within that cabin, to obtain the seat coordinates of the passengers. Next, based on the seat coordinate and the passenger weight (Initiator input) the inertia contribution of each passenger is calculated with the *PointMassInertia*-function and then added to obtain the total inertia contribution of the passengers.

For the cargo a similar procedure is followed, however it is first checked whether the cargo is stored in bulk or in containers. In the case of bulk cargo, the cargo's contributions is immediately obtained with the the *PointMassInertia*-function. If the cargo is stored in containers, the function loops over the cargo bays and then over cargo containers, in order to obtain the mass and centre of gravity location of each container. Also in this case the cargo's inertia tensors are obtained with the *PointMassInertia*-function. Finally, the *getPayloadInertia*-function outputs the two inertia matrices: one for the passengers and cargo separately.



# F

## FOKKER INERTIA TOOL

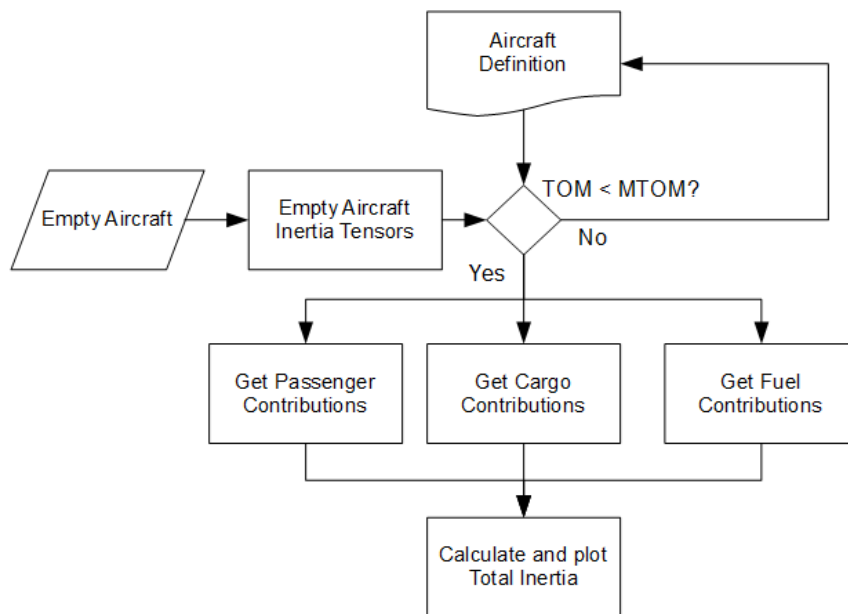


Figure F.1: Flow Diagram for the Fokker Inertia tool

In Figure F.1 the flow diagram of the Fokker Inertia tool is shown. This tool estimates the Inertia tensor for the Fokker 100 based on the approach described in reference [42]. As can be observed in this diagram, first the tensors of the empty aircraft are determined. These tensors depend on the user input for the landing gear position and in Table E.1 the difference between the inertia tensor components depending on the landing gear position is shown.

Table E.1: Overview of empty Fokker 100 Inertia tensor contributions for gear down and up

Inertia Contribution	Gear Down	Gear Up
$I_{xx}[kg \cdot m^2]$	252960	244340
$I_{yy}[kg \cdot m^2]$	1668670	1666400
$I_{zz}[kg \cdot m^2]$	1846990	1845050
$I_{xy}[kg \cdot m^2]$	0	-7000
$I_{yz}[kg \cdot m^2]$	0	60
$I_{xz}[kg \cdot m^2]$	89020	87200

Next, the loading of the aircraft is determined from the aircraft-definition-m.file and it is checked whether the take-off mass exceeds the MTOM. If this is the case, the tool will produce an error and instruct the user to update the aircraft-definition-file. An example of such a aircraft-definition-file is shown in Figure E2

```

4      % Floor [row, number of pax, xrpax(m)] 27
5 -    Cabin.Floor = [1      2      -9.45    28
6          2      5      -8.63    29 -    % YRpax & ZRpax
7          3      5      -7.82    30 -    Cabin.YRpax = 0.1;
8          4      5      -7.01    31 -    Cabin.ZRpax = 0;
9          5      5      -6.2     32
10         6      5      -5.38    33 -    % Cargo [position, volume (m^3), % filled, XRCgcar (m)
11         7      5      -4.57    34         Cargo = [1  1.4 60 -8.357
12         8      5      -3.76    35         2  1.4 60 -7.272
13         9      5      -2.94    36         3  1.4 62 -6.187
14        10      5      -2.13    37         4  1.4 62 -5.102
15        11      5      -1.32    38         5  1.4 62 -4.017
16        12      5      -0.5     39         6  1.4 62 -2.932
17        13      5      0.31     40         7  1.4 62 -1.847
18        14      5      1.13     41         8  1.4 62 3.194
19        15      5      1.94     42         9  1.4 62 4.279
20        16      5      2.75     43        10  1.4 62 5.364
21        17      5      3.56     44        11  1.4 60 6.449
22        18      5      4.38     45        12  1.76 60 8.485];
23        19      5      5.19     46 -    % Fuel [Mass tank left, centre, right]
24        20      5      6        47 -    Fuel = [3855 0 3855];
25        21      5      6.81
26        22      5      7.63];

```

Figure E2: Overview of the aircraft-definition-file

Next, the inertia tensor for the filled aircraft can be estimated. In equation E1 it is shown that the total inertia component consists of the contribution of the EOM, the passengers, cargo and the fuel. Observe that the passenger contribution in this equation is split into the Steiner contributions and the contributions due to the inertia around the passenger's centroid. Note that similar equations have been used to estimate the other inertia tensor components.

$$I_{xx} = I_{xx_{OEW}} + \sum (M_{pax_N} \cdot (y_{pax_N}^2 + z_{pax_N}^2) + N_{pax} \cdot I_{xx_{1pax}} + I_{xx_{car}} + I_{xx_{fuel}} \quad (E.1)$$

# BIBLIOGRAPHY

- [1] P. A. Roberts, R. L. Swaim, D. K. Schmidt, and A. J. Hinsdale, *Effects of Control Laws and Relaxed Static Stability on Vertical Ride Quality of Flexible Aircraft*, (1977), Purdue University, Prepared for NASA.
- [2] R. E. Perez, H. H. T. Liu, and K. Behdinan, *Relaxed Static Stability Aircraft Design via Longitudinal Control-Configured MDO Methodology*, Tech. Rep. (Institute for Aerospace Studies, University of Toronto, 2006).
- [3] E. Obert, *Aerodynamic Design of Transport Aircraft* (Delft University Press, 2009).
- [4] *Certification Specifications for Large Aeroplanes CS-25*, European Aviation Safety Agency (2007), Amendment 3.
- [5] R. Vos, *AE4240 Advanced Aircraft Design I: Lecture Notes*, Delft University, Faculty of Aerospace Engineering (2015).
- [6] E. Torenbeek, *Synthesis of Subsonic Airplane Design* (Delft University Press, Martinus Nijhoff Publishers, 1982).
- [7] J. Duncan, *Pilot's Handbook of Aeronautical Knowledge* (U.S. Department of Transportation, FAA, Oklahoma City, 2016).
- [8] D. P. Raymer, *Aircraft Design: A Conceptual Approach* (American Institute of Aeronautics and Astronautics, Inc, 1992).
- [9] G. La Rocca, *AE3211 Systems Engineering and Aerospace Design: Lecture Notes*, Delft University, Faculty of Aerospace Engineering (2015).
- [10] Anonymous, *MD-11 Commercial Transport*, <http://www.boeing.com/history/products/md-11-commercial-transport.page> (2015), Boeing Commercial Airplanes, [Online accessed August 2015].
- [11] Q. J. M. Jansen, *Relaxed Static Stability Performance Assessment on Conventional and Unconventional Aircraft Configurations*, MSc. Thesis, Delft University Of Technology (2015).
- [12] Anonymous, *The Effect of High Altitude and Center of Gravity on The Handling Characteristics of Swept-wing Commercial Airplanes*, [http://www.boeing.com/commercial/aeromagazine/aero\\_02/textonly/fo01txt.html](http://www.boeing.com/commercial/aeromagazine/aero_02/textonly/fo01txt.html) (2015), Boeing Commercial Airplanes, [Online accessed August 2015].
- [13] Anonymous, *Airport Reference Code and Approach Speeds for Boeing Airplanes*, <http://www.boeing.com/assets/pdf/commercial/airports/faqs/arcandapproachspeeds.pdf> (2011), Boeing Commercial Airplanes, [Online accessed August 2015].
- [14] Anonymous, *Aircraft Accident Report: Abnormal Runway Contact (ARC)*, (2012), The Kingdom of Saudi Arabia: General Authority of Civil Aviation Safety and Economic Regulations Safety Department.
- [15] N. Goto, *Aircraft Accident Report: Crash During Landing Federal Express Corporation N526FE*, (2013), JTSA.
- [16] J. E. Hall, *Aircraft Accident Report: Crash During Landing Federal Express Corporation N611FE*, (2000), NTSB.
- [17] J. Roskam, *Airplane Design Part I: Preliminary Sizing of Airplanes* (DARcorporation, 1985).
- [18] J. Roskam, *Airplane Design Part V: Component Weight Estimation* (DARcorporation, 1985).

- [19] J. Roskam, *Airplane Design Part II: Preliminary Configuration Design and Integration of the Propulsion System* (DARcorporation, 1985).
- [20] J. Roskam, *Airplane Design Part VI: Preliminary Calculation of Aerodynamic, Thrust and Power Calculations* (DARcorporation, 2008).
- [21] J. Roskam, *Airplane Design Part VII: Determination of Stability, Control and Performance Characteristics: FAR and Military Requirements* (DARcorporation, 2008).
- [22] R. J. M. Elmendorp, *Synthesis of Novel Aircraft Concepts for Future Air Travel*, MSc. Thesis, Delft University Of Technology (2014).
- [23] A. Slingerland, *Preliminary Sizing of Conventional and Unconventional Aircraft*, Msc. thesis, Delft University Of Technology (2014).
- [24] T. Langen, *Development of a conceptual design tool for conventional and boxwing aircraft*, MSc. Thesis, Delft University Of Technology (2011).
- [25] F. Vaessen, *Improved aerodynamic analysis to predict wing interaction of high-subsonic three-surface aircraft*, MSc. Thesis, Delft University Of Technology (2013).
- [26] J. Van Dommelen, *Design of a Forward-Swept Blended Wing Body Aircraft*, MSc. Thesis, Delft University Of Technology (2011).
- [27] M. Hoogreef, *The Oval Fuselage*, MSc. Thesis, Delft University Of Technology (2012).
- [28] M. Siggel and T. Stollenwerk, *TIXI: Fast and simple XML interface library*, <https://github.com/DLR-SC/tixi>, [Online accessed April 2015].
- [29] P. Jackson, *Jane's All the World's Aircraft*, <https://www.ihs.com/products/janes-worlds-aircraft-development.html> (2016), IHS, [Online accessed 08-July-2016].
- [30] E. Roux, *Avion civils à réaction: Plan 3 vues et données caractéristiques* (Éditions Élodie Roux, 2007).
- [31] T. Mutluay, *The Development of an Inertia Estimation Method to Support Handling Quality Assessment*, MSc. Thesis, Delft University Of Technology (2015).
- [32] W. A. J. Anemaat and B. Kaushik, *Body Inertia Estimation*, DARcorporation (2012), MEM0934.
- [33] W. A. J. Anemaat and B. Kaushik, *Lifting Surface Inertia Estimation*, DARcorporation (2012), MEM0933.
- [34] R. D. Finck, *USAF Stability and Control DATCOM*, Tech. Rep. (McDonnell Douglas Corporation, Douglas Aircraft Division, Long Beach, California, 1977).
- [35] A. Baker, S. Dutton, and D. Kelly, *Composite Materials for Aircraft Structures, Second Edition* (AIAA, Inc., Reston VA, 2004).
- [36] Anonymous, *Explore the vision jet*, <http://cirrusaircraft.com/aircraft/vision-sf50/>, Cirrus Aircraft, [Online accessed July 2016].
- [37] N. Heerens, *Landing gear design in automated design environment*, MSc. Thesis, Delft University Of Technology (2014).
- [38] P. MacMillin, O. Golovidov, W. Mason, B. Grossman, and R. Haftka, *Trim, Control, and Performance Effects in Variable-Complexity High Speed Civil Transport Design*, Tech. Rep. (Dept. of Aerospace and Ocean Engineering, Virginia Polytechnic Institute and State University, 1996).
- [39] J. Grasmeyer, *Stability and Control Derivative Estimation and Engine-Out Analysis*, Tech. Rep. (Dept. of Aerospace and Ocean Engineering, Virginia Polytechnic Institute and State University, 1998).
- [40] W. Diehl, *The mean aerodynamic chord and the aerodynamic center of a tapered wing*, Tech. Rep. (NASA, 1942).
- [41] W. Liu and W. Anemaat, *A refined method for wing weight estimation and a new method for wing center of gravity estimation*, AIAA, Vol. 4371 (2013).
- [42] A. van Gelder, *Fokker Report*, Tech. Rep. (Fokker B.V., Amsterdam, The Netherlands, 1987).